

ISSN 2186-3644 Online ISSN 2186-361X

IRDR

Intractable & Rare Diseases Research

Volume 7, Number 1
February, 2018



www.irdrjournal.com

IRDR

Intractable & Rare Diseases Research



ISSN: 2186-3644
Online ISSN: 2186-361X
CODEN: IRDRA3
Issues/Year: 4
Language: English
Publisher: IACMHR Co., Ltd.

Intractable & Rare Diseases Research is one of a series of peer-reviewed journals of the International Research and Cooperation Association for Bio & Socio-Sciences Advancement (IRCA-BSSA) Group and is published quarterly by the International Advancement Center for Medicine & Health Research Co., Ltd. (IACMHR Co., Ltd.) and supported by the IRCA-BSSA, Shandong Academy of Medical Sciences, and Shandong Rare Disease Association.

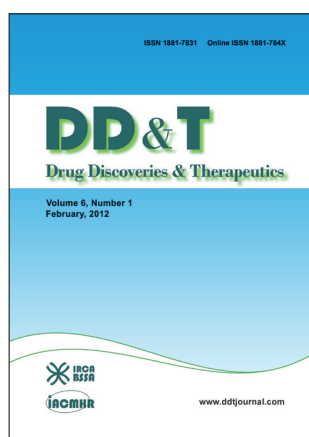
Intractable & Rare Diseases Research devotes to publishing the latest and most significant research in intractable and rare diseases. Articles cover all aspects of intractable and rare diseases research such as molecular biology, genetics, clinical diagnosis, prevention and treatment, epidemiology, health economics, health management, medical care system, and social science in order to encourage cooperation and exchange among scientists and clinical researchers.

Intractable & Rare Diseases Research publishes Original Articles, Brief Reports, Reviews, Policy Forum articles, Case Reports, News, and Letters on all aspects of the field of intractable and rare diseases research. All contributions should seek to promote international collaboration.

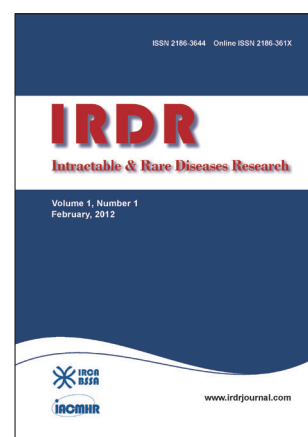
IRCA-BSSA Group Journals



ISSN: 1881-7815
Online ISSN: 1881-7823
CODEN: BTIRCZ
Issues/Year: 6
Language: English
Publisher: IACMHR Co., Ltd.
www.biosciencetrends.com



ISSN: 1881-7831
Online ISSN: 1881-784X
CODEN: DDTRBX
Issues/Year: 6
Language: English
Publisher: IACMHR Co., Ltd.
www.ddtjournal.com



ISSN: 2186-3644
Online ISSN: 2186-361X
CODEN: IRDRA3
Issues/Year: 4
Language: English
Publisher: IACMHR Co., Ltd.
www.irdrjournal.com

Intractable & Rare Diseases Research

Editorial and Head Office

Pearl City Koishikawa 603, 2-4-5 Kasuga, Bunkyo-ku,
Tokyo 112-0003, Japan

Tel: +81-3-5840-9968, Fax: +81-3-5840-9969
E-mail: office@irdrjournal.com
URL: www.irdrjournal.com

Editorial Board

Editor-in-Chief:

Masatoshi MAKUUCHI
Japanese Red Cross Medical Center, Tokyo, Japan

Chief Director & Executive Editor:

Wei TANG
The University of Tokyo, Tokyo, Japan

Co-Editors-in-Chief:

Jinxiang HAN
Shandong Academy of Medical Sciences, Jinan, China

Jose-Alain SAHEL
Pierre and Marie Curie University, Paris, France

Editorial Board Members

Tetsuya ASAKAWA <i>(Hamamatsu, Japan)</i>	Si JIN <i>(Wuhan, China)</i>	Shinichi SATO <i>(Tokyo, Japan)</i>	Yuesi ZHONG <i>(Guangzhou, China)</i>
Karen BRØNDUM-NIELSEN <i>(Glostrup, Denmark)</i>	Yasuhiro KANATANI <i>(Saitama, Japan)</i>	Yasuyuki SETO <i>(Tokyo, Japan)</i>	Jiayi ZHOU <i>(Boston, MA, USA)</i>
Yazhou CUI <i>(Jinan, China)</i>	Mureo KASAHARA <i>(Tokyo, Japan)</i>	Jian SUN <i>(Guangzhou, China)</i>	Wenxia ZHOU <i>(Beijing, China)</i>
John DART <i>(Crowthorne, UK)</i>	Jun-ichi KIRA <i>(Fukuoka, Japan)</i>	Qingfang SUN <i>(Shanghai, China)</i>	Web Editor:
Masahito EBINA <i>(Sendai, Japan)</i>	Toshiro KONISHI <i>(Tokyo, Japan)</i>	ZhiPeng SUN <i>(Beijing, China)</i>	Yu CHEN <i>(Tokyo, Japan)</i>
Clodoveo FERRI <i>(Modena, Italy)</i>	Masato KUSUNOKI <i>(Mie, Japan)</i>	Samia TEMTAMY <i>(Cairo, Egypt)</i>	Proofreaders:
Toshiyuki FUKAO <i>(Gifu, Japan)</i>	Shixiu LIAO <i>(Zhengzhou, China)</i>	Yisha TONG <i>(Heidelberg, Australia)</i>	Curtis BENTLEY <i>(Roswell, GA, USA)</i>
Ruoyan GAI <i>(Jinan, China)</i>	Zhibin LIN <i>(Beijing, China)</i>	Hisanori UMEHARA <i>(Ishikawa, Japan)</i>	Thomas R. LEBON <i>(Los Angeles, CA, USA)</i>
Shiwei GONG <i>(Wuhan, China)</i>	Reymundo LOZANO <i>(New York, NY, USA)</i>	Chenglin WANG <i>(Shenzhen, China)</i>	Office Staff:
Jeff GUO <i>(Cincinnati, OH, USA)</i>	Kuansheng MA <i>(Chongqing, China)</i>	Haibo WANG <i>(Hong Kong, China)</i>	Apolline SONG <i>(Tokyo, Japan)</i>
Toshiro HARA <i>(Fukuoka, Japan)</i>	Katia MARAZOVA <i>(Paris, France)</i>	Huijun WANG <i>(Shanghai, China)</i>	Editorial and Head Office:
Lihui HUANG <i>(Beijing, China)</i>	Chikao MORIMOTO <i>(Tokyo, Japan)</i>	Qinghe XING <i>(Shanghai, China)</i>	Pearl City Koishikawa 603
Reiko HORIKAWA <i>(Tokyo, Japan)</i>	Noboru MOTOMURA <i>(Tokyo, Japan)</i>	Zhenggang XIONG <i>(New Orleans, LA, USA)</i>	2-4-5 Kasuga, Bunkyo-ku
Takahiko HORIUCHI <i>(Fukuoka, Japan)</i>	Masanori NAKAGAWA <i>(Kyoto, Japan)</i>	Toshiyuki YAMAMOTO <i>(Tokyo, Japan)</i>	Tokyo 112-0003, Japan
Yoshinori INAGAKI <i>(Tokyo, Japan)</i>	Jun NAKAJIMA <i>(Tokyo, Japan)</i>	Huijun YUAN <i>(Beijing, China)</i>	Tel: +81-3-5840-9968
Masaru IWASAKI <i>(Yamanashi, Japan)</i>	Takashi NAKAJIMA <i>(Kashiwazaki, Japan)</i>	Wenhong ZHANG <i>(Shanghai, China)</i>	Fax: +81-3-5840-9969
Baoan JI <i>(Houston, TX, USA)</i>	Ming QIU <i>(Shanghai, China)</i>	Xianqin ZHANG <i>(Wuhan, China)</i>	E-mail: office@irdrjournal.com
Xunming JI <i>(Beijing, China)</i>	Phillips ROBBINS <i>(Boston, MA, USA)</i>	Yanjun ZHANG <i>(Cincinnati, OH, USA)</i>	<i>(As of February 2017)</i>
Guosheng JIANG <i>(Jinan, China)</i>	Hironobu SASANO <i>(Sendai, Japan)</i>	Yumin ZHANG <i>(Bethesda, MD, USA)</i>	

Review

- 1 - 6 **Circular RNAs and hereditary bone diseases.**
Naixiang Zhai, Yanqin Lu, Yanzhou Wang, Xiuzhi Ren, Jinxiang Han

Original Article

- 7 - 12 **The natural history of hereditary motor and sensory neuropathy with proximal dominant involvement (HMSN-P) in 97 Japanese patients.**
Natsumi Fujisaki, Shugo Suwazono, Masahito Suehara, Ryo Nakachi, Miwako Kido, Yoshihisa Fujiwara, Saki Oshiro, Takashi Tokashiki, Hiroshi Takashima, Masanori Nakagawa
- 13 - 18 **Comparison of the extraction and determination of serum exosome and miRNA in serum and the detection of miR-27a-3p in serum exosome of ALS patients.**
Qian Xu, Yuying Zhao, Xiaoyan Zhou, Jing Luan, Yazhou Cui, Jinxiang Han
- 19 - 24 **Complex heterozygous *WNT1* mutation in severe recessive osteogenesis imperfecta of a Chinese patient.**
Yanqin Lu, Yunzhang Dai, Yanzhou Wang, Naixiang Zhai, Jian Zhang, Junlong Liu, Xiaoli Yin, Tianyou Li, Xiuzhi Ren, Jinxiang Han
- 25 - 31 **Carotid strain measurement in patients with pseudoxanthoma elasticum – Hint for a different pathomechanism?**
Sebastian Gorgonius Passon, Viviane Küllmar, Anna Katharina Blatzheim, Kristin Solveig Pausewang, Max Jonathan Stumpf, Doris Hendig, Martin Gliem, Simon Pingel, Robert Schueler, Dirk Skowasch, Najib Schahab, Georg Nickenig, Christian Alexander Schaefer

Brief Report

- 32 - 36 **Alzheimer's disease pathology in Nasu-Hakola disease brains.**
Jun-ichi Satoh, Yoshihiro Kino, Motoaki Yanaizu, Yuko Saito
- 37 - 41 **Osteogenesis imperfecta type III/Ehlers-Danlos overlap syndrome in a Chinese man.**
Yanqin Lu, Yanzhou Wang, Frank Rauch, Hu Li, Yao Zhang, Naixiang Zhai, Jian Zhang, Xiuzhi Ren, Jinxiang Han
- 42 - 45 **A *de novo* and novel mutation in the *EYAI* gene in a Chinese child with branchio-oto-renal syndrome.**
Guomin Li, Qian Shen, Li Sun, Haimei Liu, Yu An, Hong Xu
- 46 - 50 **The ratio of urinary α 1-microglobulin to microalbumin can be used as a diagnostic criterion for tubuloproteinuria.**
Hongwen Zhang, Fang Wang, Huijie Xiao, Yong Yao

Case Report

- 51 - 53** **Omental fibromatosis treated by laparoscopic wide surgical resection.**
David Martin, Mirza Muradbegovic, Snezana Andrejevic-Blant, David Petermann, Luca Di Mare
- 54 - 57** **Intracardiac thrombosis in Behçet's Disease successfully treated with immunosuppressive agents: A case of vascular pathergy phenomenon.**
Francisco Galeano-Valle, Pablo Demelo-Rodriguez, Luis Álvarez-Sala-Walther, Blanca Pinilla-Llorente, Miguel Jesús Echenagusia-Boyra, Hugo Rodriguez-Abella, Jorge Del-Toro-Cervera
- 58 - 60** **A case of stent thrombosis presenting as acute myocardial infarction related to right coronary artery originating from the left coronary system.**
Emrah Ermis, Serkan Kahraman, Hakan Ucar, Samir Allahverdiyev
- 61 - 64** **A case of HTLV-1 associated adult T-cell lymphoma presenting with cutaneous lesions and tropical spastic paresis.**
Purva V Sharma, Michael Witteman, Swethika Sundaravel, Tulisa Larocca, Yuanming Zhang, Harry Goldsztajn
- 65 - 68** **Successful ERCP for management of traumatic pancreatic disruption in a patient with situs inversus.**
Vishal Sharma, Sarthak Malik, Harshal S Mandavdhare, Harjeet Singh

Communication

- 69 - 71** **Early electronic screen exposure and autistic-like symptoms.**
Donna Hermawati, Farid Agung Rahmadi, Tanjung Ayu Sumekar, Tri Indah Winarni

Guide for Authors

Copyright

Circular RNAs and hereditary bone diseases

Naixiang Zhai^{1,2}, Yanqin Lu^{1,2}, Yanzhou Wang³, Xiuzhi Ren⁴, Jinxiang Han^{1,2,*}

¹Key Laboratory for Biotech-Drugs Ministry of Health, Key Laboratory for Rare & Uncommon Diseases of Shandong Province, Shandong Medicinal Biotechnology Centre, Shandong Academy of Medical Sciences, Ji'nan, China;

²School of Medicine and Life Sciences, University of Jinan-Shandong Academy of Medical Sciences, Ji'nan, China;

³Department of Paediatric Surgery, Shandong Provincial Hospital, Ji'nan, China;

⁴Department of Orthopaedic Surgery, The People's Hospital of Wuqing District, Tianjin, China.

Summary

Circular RNA (circRNA) is a non-linear form of RNA derived from exonic, intronic, and exon-intron gene regions. circRNAs are characterized by covalent closed loops, highly stable nuclease resistance, and specific expression in species and developmental stages. CircRNA molecules have been identified as playing roles in the regulation of cell transcription, transcriptional expression after translation, interactions with microRNAs, and protein coding. A high stability and tissue- and disease-specific expression allow circRNAs to serve as potential biomarkers both for diseases and prognosis. CircRNAs function in bone remodeling by directly participating in bone-related signaling pathways and by forming the circRNA-miRNA-mRNA axis. Studies have seldom reported on the low incidence of circRNAs in genetic bone disorders. The current study reviews the characteristics of circRNAs and recent research on their role in rare hereditary bone diseases.

Keywords: Circular RNA, biogenesis, hereditary bone diseases, osteoblast, osteoclast

1. Introduction

Circular RNA (circRNA) is a non-linear form of RNA that was first discovered more than 40 years ago (1). As next-generation sequencing has appeared, tens of thousands of circRNAs have been identified (2,3). CircRNAs are predominately expressed in the cytoplasm and highly conserved among different species (3). Great numbers of the functions of circRNAs have been explored, including action as miRNA sponges, to regulate transcription, and protein and peptide coding (4,5). Many studies on circRNAs have involved cancer and other complex diseases, but rare hereditary bone diseases have seldom been reported.

Bone metabolism is related to both osteoblasts, which are responsible for bone formation, and osteoclasts, which are involved in bone resorption. An imbalance in bone homeostasis greatly affects

bone health and induces related bone diseases. Hsa_circ_0019142 and hsa_circ_0005846 have been identified as regulators of osteoblast differentiation and are related to the Wnt signaling pathway. The spectrum of circRNA expression in different stages of osteoclast differentiation in mice has been reported, and this has provided fundamental data for study of the function of circRNAs in bone resorption. Further study of these rare genetic bone disorders would enhance understanding of their underlying mechanisms, potential molecular markers, and cures. Moreover, experience in dealing with these rare bone disorders could increase knowledge of more common bone diseases.

2. Circular RNA and its Features

2.1. The Discovery of circRNA

Noncoding RNA is a functional RNA molecule that is not translated into a protein. It is the main product of eukaryotic transcription, accounting for 95% of the total RNA of eukaryotic cells (6). Noncoding RNAs with regulatory roles are divided into two groups according to their chain length (7,8). Short chain non-coding RNAs are less than 200 nt in length and include

*Address correspondence to:

Dr. Jinxiang Han, Shandong Medicinal Biotechnology Centre, Shandong Academy of Medical Sciences, 18877 Jingshi Road, Ji'nan 250062 China.
E-mail: samshjx@sina.com

small interfering RNAs, microRNAs (miRNAs), and Piwi-interacting RNAs, while long chain non-coding RNAs are longer than 200 nt and include circular RNAs (circRNAs).

CircRNAs were first discovered in RNA viruses during the 1970s (2,3). In the 1980s, they were identified in yeast mitochondria, hepatitis viruses, and humans (9). They are now known to be abundant in eukaryotes and protozoa (10).

The low copy number of circRNAs meant that they were first thought to be wrongly spliced mRNA, RNA processing byproducts, or viruses (1). However, subsequent studies found that endogenous circRNAs are stable, conserved non-random products produced by RNA splicing that play a role in controlling gene expression (11). As high-throughput technology has advanced and corresponding databases such as circBase, deepDase, and starBase have been created in the 21st century, the number of verified circRNAs has increased rapidly, with over 25,000 different types of circRNA being reported in human fibroblasts (12).

2.2. Formation of circulation

Different forms of circRNA have been identified: exon circRNAs, intron circRNAs, and exon–intron circRNAs (13,14). Most circRNAs consist of exons, some of which derive from encoded RNAs in 5' or 3' untranslated regions (UTRs), while others are from non-coded RNAs (11,15). There are two hypotheses for the formation of exon circRNAs. The first involves skipping of precursor RNA over a section of exons during transcription, followed by enzymatic shearing at both ends of this section, and the connection of the ends to form a lariat. The second hypothesis suggests that introns at both ends of the exon carry out base pairing during RNA transcription. The 3' end of the downstream exon connects to the 5' end of the upstream exon to combine two introns, and then the cyclized exon is released as circRNA (16).

RNA polymerase cleaves the intron from pre-mRNA to form an annulus. The circRNA formed in this manner is known as circular intronic RNA (ciRNA) (13). ciRNAs mainly exist in the nucleus and participate in regulating the expression of their parent genes, instead of function as sponges. ciRNAs processing relies on a consensus motif containing a 7-bp 5' end with splice sites rich in guanine and uracil bases, a 7-nt GU-rich element near the 5' splice site, and an cytosine-enriched area near the RNA shear branch sites of 11 bp in length (14).

Many circRNAs in the nucleus contain introns that have not been spliced. These are known as exon–intron circRNAs (EIciRNAs) and are found at many transcription sites. The removal of EIciRNAs reduces the expression of parental mRNA, indicating that they promote parental mRNA transcription (13).

2.3. Characteristics of circRNAs

The difference between circRNA and linear RNA is that the former is a closed annular structure without a 5' cap or a 3' poly A tail, and hence it is not readily degraded by exonuclease. The inherent stability of this structure affords it an important role in internal homeostasis when faced with environmental challenges (17,18).

CircRNAs are found in eukaryotes (11), prokaryotic organisms (10), viruses (19), and Archaea (20). Most circRNAs exist in the cytoplasm of eukaryotic cells, although some are found in the nucleus (1). Their levels of expression are at least 10 times higher than those of their linear isomers (12), although expression varies among different animal tissues, with the highest being reported in the brain and blood (13). RNA samples from whole blood have been analyzed following the removal of ribosome RNA from total RNA, and more than 4,000 specific circRNA molecules have been identified using random primer inversion. These molecules were compared to the ENCODE database, and the expression of circRNAs in the blood was found to be higher than that in the liver and cerebellum (16,21).

In addition to their structural stability and widespread distribution, circRNAs are developmental-stage-specific. An analysis of human oocyte and preimplantation embryo transcription (16) indicated that most circRNAs are developmental-stage-specific (22) and that they are regulated dynamically. In the brain of *Drosophila*, some circRNAs increase with age (23). Nematodes contain thousands of circRNAs that differ in expression depending on the stage of growth or development.

CircRNAs are relatively conserved among species. For example, circRNAs in the human brain are similar to sequences in mice and *Drosophila*. Indeed, of the 1,903 circRNAs identified in mice, 81 are the same as sequences found in humans (24). One study found that 20.2% of pig circRNAs have direct human homologs, while 16.96% of pig circRNAs have direct mouse homologs (25). Another study found a direct homology between 29.4% of pig circRNAs in humans (25), while 1,510 circRNAs (25.45%) in mice and 5,189 circRNAs (87.44%) in humans were homologous to pig circRNAs. Sequential conservation analysis also indicated that circRNAs may have conserved functions in pigs, mice, and humans (26).

2.4. Biological function of circRNAs

CircRNAs contain miRNA binding sites, which make them competitive endogenous RNAs that can be used to isolate miRNA. For example, ciRS-7 with multiple tandem miRNA-7 binding sites can bind to miRS-7 *in vitro*. CircRNAs can also be used as endogenous "miRNA sponges" that inhibit normal miRNA function (27). miRNA sponges play a role in inhibiting miRNA and targeting gene binding. They can also be expressed

at different positions of the genome, so they can serve as an important component of the miRNA-mediated transcriptional regulatory network (28).

CircRNAs can be combined with proteins or used to influence RNA splicing, which indirectly affects protein function (29). For example, EIciRNAs combine with the U1 small nuclear ribonucleoprotein promote RNA polymerase II by interacting with its promoter to enhance gene transcription (30). The expression of mRNA encoded by the host gene was then reduced after removing EIciRNAs, suggesting that nuclear circRNAs have the potential to induce host genes to express themselves. However, not all EIciRNAs are located at transcription sites, so some may also modulate other parts of the genome. Notably, endogenous circRNAs are not associated with ribosome translation. Exogenous circRNAs are translated *in vitro* and *in vivo* through the internal ribosome entry site (IRES) or through the rolling-circle amplification mechanism (31,32), which amplifies short DNA or RNA into a longer strand.

CircRNAs play a similar role in association with mRNAs by combining with the translation initiation site or by destroying the integrity of mature linear RNA to prevent translation. For example, EIciRNAs interact with RNA polymerase and bind U1 snRNP to activate transcription of the parental gene, to inhibit RNA-protein interaction, and to regulate miRNA activity (33).

Recent studies have found that some circRNAs have a coding capability. For instance, Circ-ZNF609 encodes muscle differentiation-related proteins (5) generated from the second exon ring of its host gene with a 753-bp open reading frame. Its UTR elements rely on cis-control elements on the IRES sequence to initiate protein translation from the middle of circRNA (32), albeit at a lower rate than cap translation (5,34,35). CircRNA can also be used after N⁶-methyladenosine modification in non cap-dependent translation (36,37). The N⁶-methyladenosine zone identifies YTHDF3 proteins, binds to circRNA modified sites, and attracts eIF4G2 proteins and other translation initiation factors to drive circRNA translation (38). Some circRNAs also combine with ribosomes to form Rib-circRNA complexes that influence coding; their UTR regions have similar IRES translation-driven functions, but they have translation efficiency (39).

Intracellular circRNAs are secreted extracellularly. Their stability and prevalence in outer secretions and plasma (40,41) makes them suitable as potential disease markers. Compared to healthy individuals, patients with rectal cancer were found to lack 67 types of circRNAs and to possess 257 new forms. Moreover, the level of CircRNA-KLDHC10 expression in this cancer was significantly higher than that in normal serum (42), while the ratio of circRNA to linear RNA in MHCC Lm3-type hepatocellular carcinoma cells was six times higher than that in normal cells (42). Expression of

hsa_circ_0000190 decreased significantly in the plasma and tissue samples of patients with gastric cancer (43), and hsa_circ_0000190 is a potential marker for gastric cancer because it is more sensitive and more specific than two traditional biomarkers, carcinoembryonic antigen (CEA) and CA19-9t. Together, these findings suggest that circRNAs could be used as reliable disease markers with which to diagnose certain cancers (43).

3. CircRNA and Hereditary Bone Disease

3.1. CircRNA in osteoblasts and osteoclasts

Osteoblasts are the main functional cells of bone formation and are responsible for the synthesis, secretion, and mineralization of bone matrix. During bone metabolism, osteoclasts bind to the target area and secrete proteases to dissolve bone minerals, digest bone matrix, and form bone resorption traps. Osteoblasts secrete bone matrix into the trap, and then perform mineralization to form new bone. Therefore, the balance between osteoclasts and osteogenesis is key to maintaining normal bone mass.

Osteoblast differentiation is regulated by a series of hormones, cytokines, and transcription factors (44,45). The transcription factor BMP2 belongs to the transforming growth factor beta superfamily and is one of the most important human cytokines. It induces heterotopic bone and cartilage formation and plays an important role in embryonic growth, cell growth and differentiation, bone development, and fracture repair. MC3T3-E1 cells treated with BMP2 had differential expression of 158 circRNAs, 74 of which were upregulated and 84 of which were downregulated in comparison to control cells. hsa_circ_0005846, hsa_circ_0019142, and hsa_circ_0010042 increased significantly following BMP2 treatment (46). hsa_circ_0005846 and hsa_circ_0019142 interact with 51 and 21 miRNAs, respectively, and both act as a sponge for miR-7067-5p. They are also involved in the FGF, EGF, PDGF, and Wnt signaling pathways, and they participate in cell growth and differentiation (47). BMP2 induces osteogenic differentiation *via* the hsa_circ_0019142/ hsa_circ_0005846 target miRNA-mRNA regulation network (47), in which the level of ALP, SP7, and RUNX2 mRNA expression increases significantly. Moreover, hsa_circ_0019142 interacts with miR-222-3p and miR-7067-5p (48), with the former functioning as an osteoclast inhibitor (49).

The expression of circRNAs is sequential in different stages of osteoclast development in mice. For example, of the 1797 circRNAs identified in mice, 147 were up-regulated in pre-osteoclasts, and 109 were down-regulated. In mature osteoclasts, 78 circRNAs were up-regulated, while 111 circRNAs and 94 miRNAs were up-regulated in activated osteoclasts (50). circRNA-miRNA synergistic regulation plays

an important role in osteoclast formation. miR-103 in the co-regulatory network was up-regulated by hsa_circ_0007873 and down-regulated by hsa_circ_0010763 and hsa_circ_0015622 (51). In addition, miR-335-5p directs the down-regulation of DKK1 (a Wnt inhibitor), it enhances Wnt signaling, and it promotes osteoblast formation and development (52), while miR-29a enhances osteoblast formation by regulating Wnt signaling through a positive feedback loop (53).

3.2. *CircRNA and osteoarthritis*

CircRNA is associated with a variety of diseases such as atherosclerosis and neurological disorders (54,55). However, its role in cartilage and bone and its effects on bone disease are rarely reported.

Osteoarthritis (OA) is a degenerative joint disease caused by cartilage degradation, bone thickening, and spur formation. A circRNA chip revealed differential expression of 71 circRNAs in patients with OA, including the up-regulation of 16 circRNAs such as hsa_circ_0100876 (circRNA-CER), hsa_circ_0101178, hsa_circ_01011914, and hsa_circ_0100086 while a further 55 were down-regulated. circRNA-CER can be up-regulated by cell interleukin-1 and tumor necrosis factor α , and it regulates the expression of MMP13 by endogenously competing with miR-136 to facilitate degradation of the chondrocyte extracellular matrix.

Wnt1 is the pathogenic gene for the autosomal-recessive form of osteogenesis imperfecta. A study that predicted circRNA interaction with miRNAs targeting Wnt1 found that hsa_circ_001042 interacted with miR-21, miR-148, and miR-152, and that it may function in the MAPK signaling pathway. Has_circ00048 and 24 other circRNAs may serve as molecular sponges of miR-148 and miR-152 and may be involved in the focal adhesion pathway (56).

4. Conclusion

In conclusion, circRNAs are diverse, widely distributed molecules with stable structures and complex functions. Little is currently known about the association between circRNAs and hereditary bone disease, but our understanding of the role of miRNAs in hereditary bone disease has progressed considerably. For example, miR-222-3p and miR-7067-5p that are associated with osteoblasts are regulated by circRNA5846 and circRNA19142. Given the extensive interplay that exists between circRNAs and miRNAs, circRNAs are likely to control hereditary bone disease by interacting with miRNA or by their own ability to code protein. Therefore, new studies of circRNA will be crucial to the development of novel treatments. Future work should also examine the function of circRNAs in protein encoding and as miRNA sponges.

Acknowledgement

This project was supported by Grants-in-Aid from the Shandong Government (No. 2016GSF201222, 2016ZDJS07A10).

References

- Cocquerelle C, Mascrez B, Hetuin D, Bailleul B. Mis-splicing yields circular RNA molecules. *FASEB J.* 1993; 7:155-160.
- Cocquerelle C, Daubersies P, Majerus MA, Kerckaert JP, Bailleul B. Splicing with inverted order of exons occurs proximal to large introns. *EMBO J.* 1992; 11:1095-1098.
- Capel B, Swain A, Nicolis S, Hacker A, Walter M, Koopman P, Goodfellow P, Lovell-Badge R. Circular transcripts of the testis-determining gene Sry in adult mouse testis. *Cell.* 1993; 73:1019-1030.
- Peng L, Chen G, Zhu Z, Shen Z, Du C, Zang R, Su Y, Xie H, Li H, Xu X, Xia Y, Tang W. Circular RNA ZNF609 functions as a competitive endogenous RNA to regulate AKT3 expression by sponging miR-150-5p in Hirschsprung's disease. *Oncotarget.* 2017; 8:808-818.
- Legnini I, Di Timoteo G, Rossi F, Morlando M, Briganti F, Sthandier O, Fatica A, Santini T, Andronache A, Wade M, Laneve P, Rajewsky N, Bozzoni I. Circ-ZNF609 Is a Circular RNA that Can Be Translated and Functions in Myogenesis. *Mol Cell.* 2017; 66:22-37.e9.
- Warner JR. The economics of ribosome biosynthesis in yeast. *Trends Biochem Sci.* 1999; 24:437-440.
- Ponting CP, Oliver PL, Reik W. Evolution and functions of long noncoding RNAs. *Cell.* 2009; 136:629-641.
- Zaratiegui M, Irvine DV, Martienssen RA. Noncoding RNAs and gene silencing. *Cell.* 2007; 128:763-776.
- Kos A, Dijkema R, Arnberg AC, van der Meide PH, Schellekens H. The hepatitis delta (delta) virus possesses a circular RNA. *Nature.* 1986; 323:558-560.
- Gao Y, Wang J, Zhao F. CIRI: An efficient and unbiased algorithm for de novo circular RNA identification. *Genome Biol.* 2015; 16:4.
- Memczak S, Jens M, Elefsinioti A, *et al.* Circular RNAs are a large class of animal RNAs with regulatory potency. *Nature.* 2013; 495:333-338.
- Jeck WR, Sorrentino JA, Wang K, Slevin MK, Burd CE, Liu J, Marzluff WF, Sharpless NE. Circular RNAs are abundant, conserved, and associated with ALU repeats. *RNA.* 2013; 19:141-157.
- Li Z, Huang C, Bao C, *et al.* Exon-intron circular RNAs regulate transcription in the nucleus. *Nat Struct Mol Biol.* 2015; 22: 256-264.
- Zhang Y, Zhang XO, Chen T, Xiang JF, Yin QF, Xing YH, Zhu S, Yang L, Chen LL. Circular intronic long noncoding RNAs. *Mol Cell.* 2013; 51:792-806.
- Burd CE, Jeck WR, Liu Y, Sanoff HK, Wang Z, Sharpless NE. Expression of linear and novel circular forms of an INK4/ARF-associated non-coding RNA correlates with atherosclerosis risk. *PLoS Genet.* 2010; 6:e1001233.
- Jeck WR, Sharpless NE. Detecting and characterizing circular RNAs. *Nat Biotechnol.* 2014; 32:453-461.
- Qu S, Zhong Y, Shang R, Zhang X, Song W, Kjems J, Li H. The emerging landscape of circular RNA in life processes. *RNA Biol.* 2017; 14:992-999.

18. Kornienko A E, Guenzl P M, Barlow D P, Pauler FM. Gene regulation by the act of long non-coding RNA transcription. *BMC Biol.* 2013; 11:59.
19. Wu Q, Wang Y, Cao M, Pantaleo V, Burgyan J, Li WX, Ding SW. Homology-independent discovery of replicating pathogenic circular RNAs by deep sequencing and a new computational algorithm. *Proc Natl Acad Sci U S A.* 2012; 109:3938-3943.
20. Danan M, Schwartz S, Edelheit S, Sorek R. Transcriptome-wide discovery of circular RNAs in Archaea. *Nucleic Acids Res.* 2012; 40:3131-3142.
21. Zhang SJ, Chen X, Li CP, Li XM, Liu C, Liu BH, Shan K, Jiang Q, Zhao C, Yan B. Identification and characterization of circular RNAs as a new class of putative biomarkers in diabetes retinopathy. *Invest Ophthalmol Vis Sci.* 2017; 58:6500-6509.
22. Salzman J. Circular RNA Expression: Its Potential Regulation and Function. *Trends Genet.* 2016; 32:309-316.
23. Westholm JO, Miura P, Olson S, Shenker S, Joseph B, Sanfilippo P, Celniker SE, Graveley BR, Lai EC. Genome-wide analysis of drosophila circular RNAs reveals their structural and sequence properties and age-dependent neural accumulation. *Cell Rep.* 2014; 9:1966-1980.
24. Wang PL, Bao Y, Yee MC, Barrett SP, Hogan GJ, Olsen MN, Dinneny JR, Brown PO, Salzman J. Circular RNA is expressed across the eukaryotic tree of life. *Plos One,* 2014; 9:e90859
25. Rybak-Wolf A, Stottmeister C, Glazar P, *et al.* Circular RNAs in the Mammalian Brain Are Highly Abundant, Conserved, and Dynamically Expressed. *Mol Cell.* 2015; 58:870-885.
26. Liang G, Yang Y, Niu G, Tang Z, Li K. Genome-wide profiling of *Sus scrofa* circular RNAs across nine organs and three developmental stages. *DNA Res.* 2017; 24:523-535.
27. Lukiw WJ. Circular RNA (circRNA) in Alzheimer's disease (AD). *Front Genet.* 2013; 4:307.
28. Ghosal S, Das S, Sen R, Basak P, Chakrabarti J. Circ2Traits: A comprehensive database for circular RNA potentially associated with disease and traits. *Front Genet.* 2013; 4:283.
29. Qu S, Yang X, Li X, Wang J, Gao Y, Shang R, Sun W, Dou K, Li H. Circular RNA: A new star of noncoding RNAs. *Cancer Lett.* 2015; 365:141-148.
30. Ashwal-Fluss R, Meyer M, Pamudurti NR, Ivanov A, Bartok O, Hanan M, Evantal N, Memczak S, Rajewsky N, Kadener S. CircRNA biogenesis competes with pre-mRNA splicing. *Mol Cell.* 2014; 56:55-66.
31. Perriman R, Jr A M. Circular mRNA can direct translation of extremely long repeating-sequence proteins *in vivo*. *RNA,* 1998; 4:1047-1054.
32. Wang Y, Wang Z. Efficient backsplicing produces translatable circular mRNAs. *RNA.* 2015; 21:172-179.
33. Chen LL. The biogenesis and emerging roles of circular RNAs. *Nat Rev Mol Cell Biol.* 2016; 17:205-211.
34. Merrick WC. Cap-dependent and cap-independent translation in eukaryotic systems. *Gene.* 2004; 332:1-11.
35. Li S, Mason CE. The pivotal regulatory landscape of RNA modifications. *Annu Rev Genomics Hum Genet.* 2014; 15:127-150.
36. Meyer KD, Saletore Y, Zumbo P, Elemento O, Mason CE, Jaffrey SR. Comprehensive analysis of mRNA methylation reveals enrichment in 3' UTRs and near stop codons. *Cell.* 2012; 149:1635-1646.
37. Yang Y, Fan X, Mao M, Song X, Wu P, Zhang Y, Jin Y, Yang Y, Chen LL, Wang Y, Wong CC, Xiao X, Wang Z. Extensive translation of circular RNAs driven by N6-methyladenosine. *Cell Res.* 2017; 27:626-641.
38. Shi H, Wang X, Lu Z, Zhao BS, Ma H, Hsu PJ, Liu C, He C. YTHDF3 facilitates translation and decay of N6-methyladenosine-modified RNA. *Cell Res.* 2017; 27:315-328.
39. Pamudurti NR, Bartok O, Jens M, *et al.* Translation of CircRNAs. *Mol Cell.* 2017; 66:9-21.e7.
40. Tang M, Wu G, Wang Z, Yang N, Shi H, He Q, Zhu C, Yang Y, Yu G, Wang C, Yuan X, Liu Q, Guan Y, Dong X, Tang Z. Voltage-gated potassium channels involved in regulation of physiological function in MrgprA3-specific itch neurons. *Brain Res.* 2016; 1636:161-171.
41. Wang F, Nazarali AJ, Ji S. Circular RNAs as potential biomarkers for cancer diagnosis and therapy. *Am J Cancer Res.* 2016; 6:1167-1176.
42. Li Y, Zheng Q, Bao C, Li S, Guo W, Zhao J, Chen D, Gu J, He X, Huang S. Circular RNA is enriched and stable in exosomes: A promising biomarker for cancer diagnosis. *Cell Res.* 2015; 25:981-984.
43. Meng S, Zhou H, Feng Z, Xu Z, Ying T, Li P, Wu M. CircRNA: Functions and properties of a novel potential biomarker for cancer. *Mol Cancer.* 2017; 16:94.
44. Yamaguchi A, Komori T, Suda T. Regulation of osteoblast differentiation mediated by bone morphogenetic proteins, hedgehogs, and Cbfa1. *Endocrine Reviews.* 2000; 21:393-411.
45. Komori T. Regulation of osteoblast differentiation by transcription factors. *J Cell Biochem.* 2006; 99:1233-9123.
46. Jiang N, Chen WJ, Zhang JW, Xu C, Zeng XC, Zhang T, Li Y, Wang GY. Downregulation of miR-432 activates Wnt/ β -catenin signaling and promotes human hepatocellular carcinoma proliferation. *Oncotarget.* 2015; 6:7866-7879.
47. Qian DY, Yan GB, Bai B, Chen Y, Zhang SJ, Yao YC, Xia H. Differential circRNA expression profiles during the BMP2-induced osteogenic differentiation of MC3T3-E1 cells. *Biomed Pharmacother.* 2017; 90:492-499.
48. Song J, Li Y. miR-25-3p reverses epithelial-mesenchymal transition *via* targeting Sema4C in cisplatin-resistance cervical cancer cells. *Cancer Sci.* 2017; 108:23-31.
49. Takigawa S, Chen A, Wan Q, Na S, Sudo A, Yokota H, Hamamura K. Role of miR-222-3p in c-Src-Mediated Regulation of Osteoclastogenesis. *Int J Mol Sci.* 2016; 17:240.
50. Jia J, Feng X, Xu W, Yang S, Zhang Q, Liu X, Feng Y, Dai Z. MiR-17-5p modulates osteoblastic differentiation and cell proliferation by targeting SMAD7 in non-traumatic osteonecrosis. *Exp Mol Med.* 2014; 46:e107.
51. Dou C, Cao Z, Yang B, Ding N, Hou T, Luo F, Kang F, Li J, Yang X, Jiang H, Xiang J, Quan H, Xu J, Dong S. Changing expression profiles of lncRNAs, mRNAs, circRNAs and miRNAs during osteoclastogenesis. *Sci Rep.* 2016; 6:21499.
52. Zhang J, Tu Q, Bonewald LF, He X, Stein G, Lian J, Chen J. Effects of miR-335-5p in modulating osteogenic differentiation by specifically downregulating Wnt antagonist DKK1. *J Bone Miner Res.* 2011; 26:1953-1963.
53. Taipaleenmäki H, Bjerre Hokland L, Chen L, Kauppinen

- S, Kassem M. Mechanisms in endocrinology: Micro-RNAs: Targets for enhancing osteoblast differentiation and bone formation. *Eur J Endocrinol.* 2012; 166:359-371.
54. Chen YT, Rettig WJ, Yenamandra AK, Kozak CA, Chaganti RS, Posner JB, Old LJ. Cerebellar degeneration-related antigen: A highly conserved neuroectodermal marker mapped to chromosomes X in human and mouse. *Proc Natl Acad Sci U S A.* 1990; 87:3077-3081.
55. You X, Vlatkovic I, Babic A, *et al.* Neural circular RNAs are derived from synaptic genes and regulated by development and plasticity. *Nat Neurosci.* 2015; 18:603-610.
56. Zhang Y, Ren XZ, Wang YZ, Ma X, Zuo QL, Han JX, Lu YQ. Bioinformatics interaction analysis of Wnt1-targeting miRNAs and their corresponding circRNAs and target genes. *Progress in Biochemistry and Biophysics.* 2016; 43:1094-1101. (in Chinese)

(Received January 31, 2018; Revised February 26, 2018; Accepted February 27, 2018)

The natural history of hereditary motor and sensory neuropathy with proximal dominant involvement (HMSN-P) in 97 Japanese patients

Natsumi Fujisaki¹, Shugo Suwazono^{1,2,*}, Masahito Suehara³, Ryo Nakachi¹, Miwako Kido¹, Yoshihisa Fujiwara¹, Saki Oshiro¹, Takashi Tokashiki¹, Hiroshi Takashima⁴, Masanori Nakagawa⁵

¹Department of Neurology, National Hospital Organization Okinawa National Hospital, Ginowan, Japan;

²Center for Clinical Neuroscience, National Hospital Organization Okinawa National Hospital, Ginowan, Japan;

³Department of Neurology, Fujimoto General Hospital/Fujimoto Medical System, Miyakonojou, Japan;

⁴Department of Neurology and Geriatrics, Kagoshima University, Graduate School of Medical and Dental Sciences, Kagoshima, Japan;

⁵North Medical Center, Kyoto Prefectural University of Medicine, Kyoto, Japan.

Summary

Hereditary motor and sensory neuropathy with proximal dominant involvement (HMSN-P) is a motor and sensory neuronopathy with autosomal dominant inheritance, adult onset, slowly progressive course, and is associated with *TRK-fused gene* (TFG) mutation. At advanced stages, respiratory failure and dysphagia becomes life-threatening, and patients typically die by their 70s. Although there is currently no evidence for effective treatment, a therapy may be found by elucidation of the function of TFG. Recently its pathomechanism has been proposed to be associated with abnormalities in protein transfer from the endoplasmic reticulum. Such pathomechanisms might involve a similar process in amyotrophic lateral sclerosis; thus, its pathomechanisms and treatment strategy might make it a good model for neurodegenerative disorders. It is of great value to clarify the natural history of HMSN-P, in order to judge the treatment effect. By evaluating 97 patients (79 out of 97 were examined and all confirmed with p.Pro 285 Leu mutation) in this study, it was confirmed that this disease follows a uniform course in the earlier stages, and there are individual differences in the onset between 20 and 30 years. Such uniformity might be due to the proposed single gene abnormality. At advanced stages, there are larger individual differences in the progression, but the reasons for these are unknown. Longer survival might be achieved with a better care for respiratory failure and dysphagia if such cares were undertaken at appropriate times.

Keywords: HMSN Okinawa type, natural history, TRK-fused gene

1. Introduction

Hereditary motor and sensory neuropathy with proximal dominant involvement (HMSN Okinawa type; HMSNO, OMIM # 604484, or HMSN-P used in the first detailed report (1), and this report uses the

term HMSN-P) is a slowly progressive disease with autosomal dominant inheritance and adult onset. It is fatal and leads to a condition requiring support for swallowing/respiration in the 50s, which is more than 20 years after the first symptomatic painful muscle spasm. When patients present initial symptoms at around their late 30s, they have often had children. Thus, the disease passed to the next generation very easily.

Symptoms usually start with painful muscle cramping of limbs/trunk in the patients' 30s to 40s, followed by muscle weakness dominated by limb proximal muscles, and accompanied by elevated creatine kinase (CK) values (2). After their 50s,

Released online in J-STAGE as advance publication February 26, 2018.

*Address correspondence to:

Dr. Shugo Suwazono, National Hospital Organization Okinawa Hospital, 3-20-14, Ganeko, Ginowan, Okinawa 901-2214, Japan.

E-mail: zvb10512@nifty.ne.jp

swallowing/respiratory dysfunction could be a life-threatening problem (2). Although HMSN-P is often compared with familial amyotrophic lateral sclerosis (ALS) and spinal muscular atrophy (SMA), there are features that differ from ALS or SMA, such as disappearance of the deep tendon reflex and obvious electrophysiological abnormalities of sensory nerve action potentials from early stages of the disease (1,2). Clinical diagnosis of HMSN-P has been conducted based on such characteristic clinical findings, detailed family history, and laboratory findings including blood examination and electrophysiological tests.

Since TRK-fused gene (TFG) was identified as a gene related to the cause of HMSN-P in 2012 (3), HMSN-P patients having the same mutation have been reported in several regions of the world (4-6), but the disease with the TFG p.Pro 285 Leu mutation is documented only in patients with HMSN-P. On the other hand, another TFG mutation, that is different from the mutation found in HMSN-P, has been reported in ALS patients (7). The relationship between TFG and motor neuron degeneration has been discussed, and the possibility of treating motor neuron disease has been suggested (7), drawing attention widely from the neurodegeneration research field. In 2016, p.Gly269Val was reported as a second genetic mutation of HMSN-P (8), which is identical to the mutation found in autosomal dominant Charcot-Marie-Tooth disease Type 2 (CMT2) families (9). Careful consideration and further examination will be needed to determine whether the phenotype differs between two different mutations within a gene.

Recent studies on TFG abnormalities involved in the pathomechanisms of HMSN-P have suggested impaired protein transfer from the endoplasmic reticulum (ER) to the Golgi body due to the localization of the product protein. Although induced pluripotent stem cells have also been prepared and proteasome disorders were also described (10), detailed mechanism that specifically causes nerve cell degeneration is still unclear. There are many diseases that may be involved in ER stress, and ALS may be involved in the same way (11). HMSN-P could serve as a disease model in which the causative gene mutation is clear and may contribute to the elucidation of the pathomechanisms of many neurodegenerative diseases.

Under these circumstances, it is important to clarify the natural history of HMSN-P in order to better maintain the patient's quality of life, predict the prognosis of each case, and consider new treatments that will become available in the future. It is difficult to describe the whole disease course because of its length, therefore, there are few reports focusing on clinical status at advanced stages in which swallowing/respiratory abnormalities affect the clinical course.

We reviewed the detailed clinical course from more than 130 cases from 28 families of HMSN-P patients

in the medical records at our hospital during a 30-year period, and tried to clarify the characteristics of the clinical course of HMSN-P, particularly the long-term disease progression.

2. Materials and Methods

In National Hospital Organization Okinawa National Hospital (Okinawa hospital), among more than 130 patients examined as HMSN-P since 1980, the clinical course of 97 patients whom we could confirm detailed medical records retrospectively were evaluated (a typical family tree is presented on Figure 1). Evaluation items were as follows: age at first visit, symptom onset age (regardless of subjective or objective) for painful muscle spasm, upper and lower limb muscular strength, sense, standing, walking, swallowing, respiration, age at death, the CK value at the first visit, and the type of TFG mutation. For the analysis of the advanced stage, we confirmed the onset/start age of dysphagia, respiratory failure, tube feeding and tracheotomy, age of death, and situation at the time of death (presence of tube feeding/tracheostomy, cause of death). We summarized the age at which each symptom was first recognized (Figure 2). The ratio of the number of the patients with each symptom at each age (every 5 years) to the total number of patients was calculated (Figure 3). The onset age of each symptom in each case that was confirmed for respiratory failure, tracheostomy, dysphagia, tube feeding and death was further examined especially in the advanced stage after age 50 (Figure 4). The age at first visit and the CK values measured at that visit were examined (Figure 5).

This study was discussed and approved by the ethics committee at Okinawa Hospital (# 29-8).

3. Results

An example of a family tree of HMSN-P (Figure 1) shows more than half of the brothers and sisters were afflicted and the penetration rate is high. Similar penetration rates are found in other families in this study. The progression details of 55 men and 42 females were analyzed. TFG mutation was confirmed in 79 cases (81.4%), all of which were p.Pro 285 Leu. Genetic testing was not possible in all cases because 5 patients died before the test, 9 patients moved to different hospitals, 2 could not be examined due to sample defect, and 2 patients dropped out before the exam. The average of age at the initial visit was 49.1 years, and the median was 48.5 years (17-74 years). The median of each symptom was 38.0 years (13-59 years) for painful muscle spasm, 47.0 years (25-60 years) for muscle weakness in upper limbs, 48.0 years (31-60 years) for muscle weakness in lower limbs, 50.0 years (40-68 years) for sensory disturbance, 53.0 years (43-69 years) for inability to stand, 58.0 years (44-74

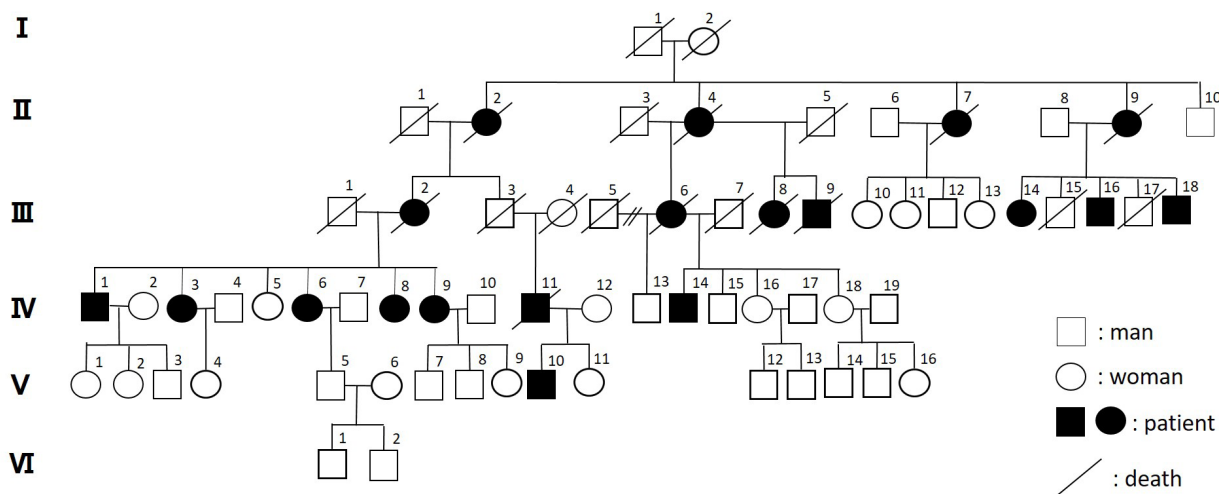


Figure 1. A family Tree of HMSN-P. Autosomal dominant inheritance is shown.

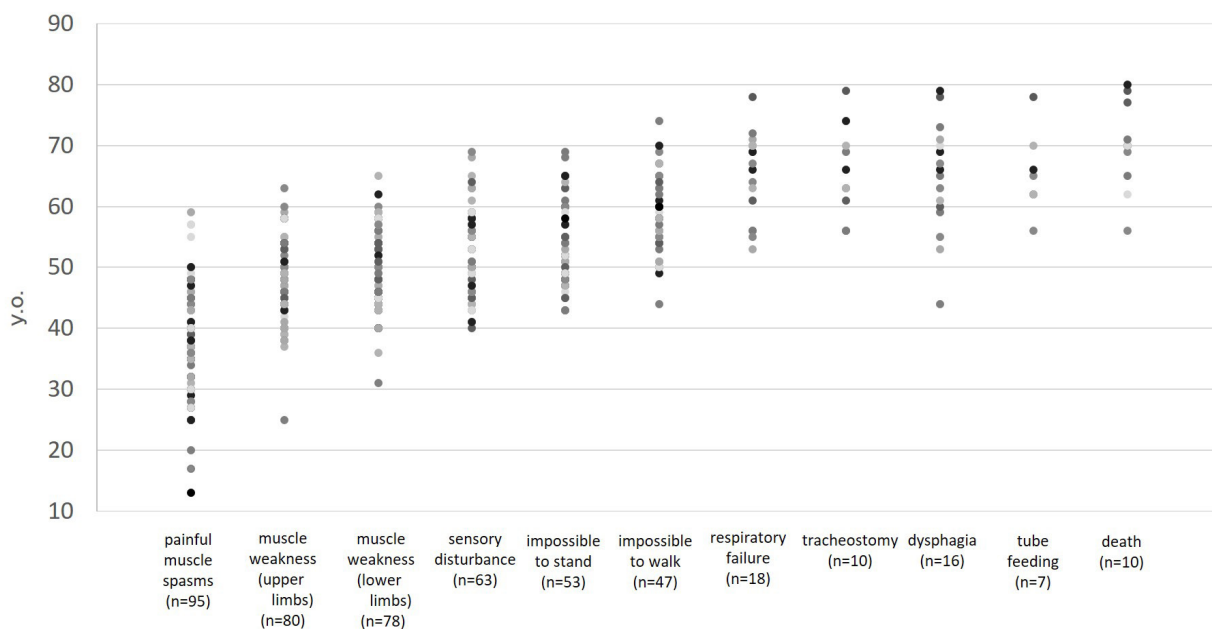


Figure 2. Natural history of HMSN-P. There is a specific order in the appearance of symptoms. There are individual differences in the period of disease onset between 20 and 30 years.

years) for inability to walk, 66.5 years (53-78 years) for respiratory failure, 64.5 years (56-79 years) for tracheostomy, 65.5 years (44-79 years) for dysphagia, 65.0 years (56-78 years) for tube feeding, and 70.0 years (56-80 years) for death (Figure 2 and Figure 3). There was a specific order to the appearance of symptoms (Figure 2). There are individual differences in the period of symptoms appearing between 20 and 30 years.

We further analyzed the disease progression at later stages as shown in Figure 4. There were 21 advanced stage patients who had impaired swallowing and respiration (Figure 4). Among them, 10 patients underwent tube feeding and tracheostomy; 3 had tracheostomy only, 0 had tube feeding only and 7 had both. Five patients had both tracheostomy and tube

feeding at the same time or within one year. However, 3 patients, who had have been admitted for a long time in Okinawa hospital due to respiratory disturbance and had tracheotomy and respiratory management done soon after the occurrence of the problems, could extend the period with possible oral intake from 2 to 6 years after the tracheostomy. One patient died without tube feeding. Another patient, followed at a different clinic, was still orally ingestible even 7 years after tracheotomy. The death age was confirmed in 17 patients, including those who died at other hospitals. In 10 patients, the cause of death was aspiration/pneumonia or respiratory failure due to sudden deterioration of unexpected respiratory condition. Seven patients died due to other causes: acute myocardial infarction (n = 2), cancer (n = 2), cerebral infarction (n = 1), postoperative septicemia (n = 1), and

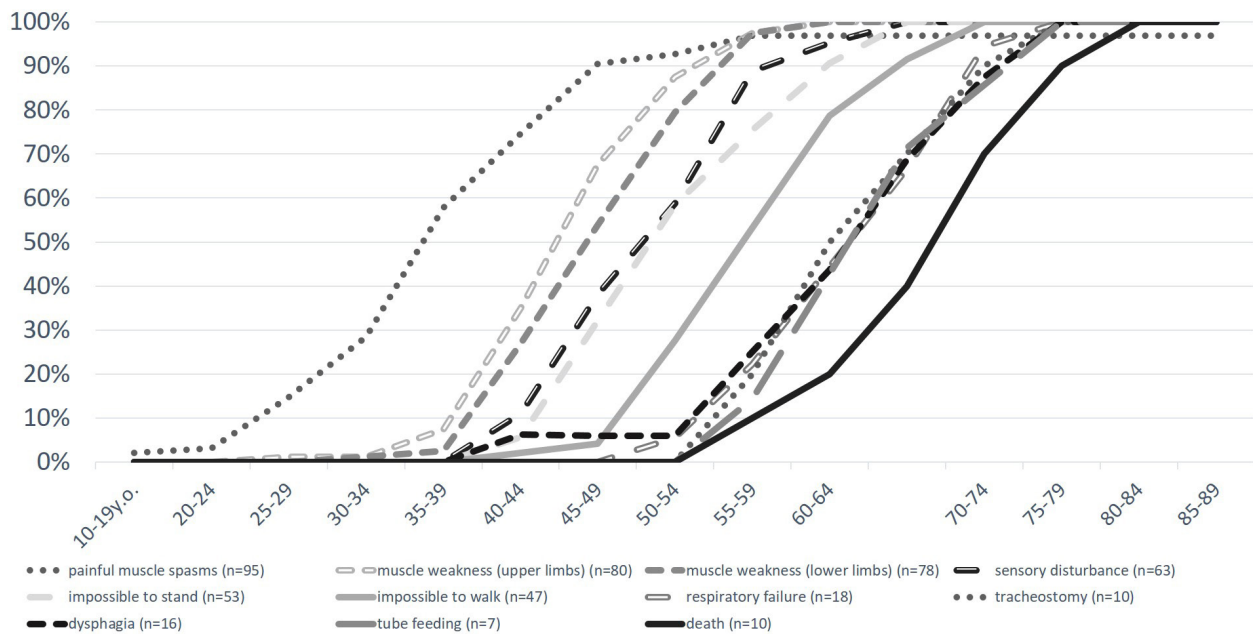


Figure 3. Natural history of HMSN-P. Observed symptom frequency in 5 bins (see Materials and Methods for calculation). Dysphagia and breathing disorders begin to increase after the patients' 50s.

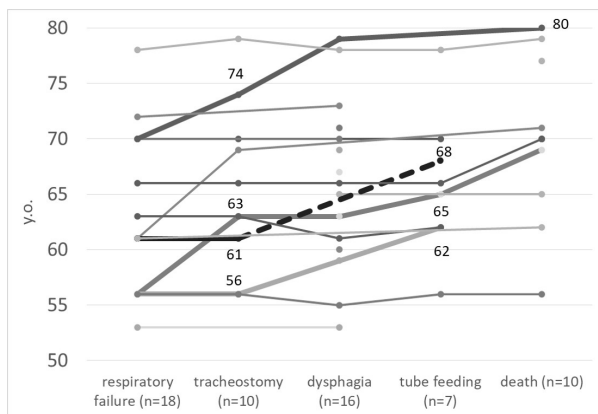


Figure 4. Natural history (advanced stage). Natural history of several cases with detailed course information at advanced stages.

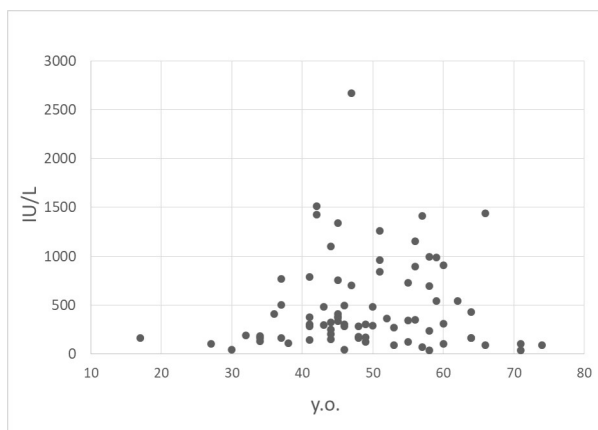


Figure 5 CK value (first visit). The CK value tends to be high in the 40s and 50s, and decrease from the late 50s when walking becomes impossible.

unknown cause ($n = 1$).

Painful muscle spasms that appears early in the disease tended to decrease at later stages. Three out of 97 cases did not show painful muscle spasm during the entire course. CK also tended to decrease after the age of 60 (Figure 5).

4. Discussion

Disease progression, in terms of the order of the appearance of each symptom, is usually variable within a neurodegenerative disease entity, including Alzheimer disease, ALS, and Parkinson's disease. However, the current study confirmed that the clinical course of HMSN-P is extremely uniform with slow progression, *i.e.*, the order of symptom appearance is almost identical in every patient for long after the onset (Figure 2 and Figure 3), although the onset age varied 20-30 years. This fact might be attributed to the proposed pathophysiological mechanisms that HMSN-P is caused by single gene abnormality. As a disease model for neurodegenerative disorders of protein metabolism failure based on a single gene abnormality, HMSN-P provides a suitable example with some hope to plan treatment strategies.

Recently many interesting observations are accumulating about the role of TFG protein, which belongs to the coat protein complex II transportation system from the endoplasmic reticulum (ER) to the ER-Golgi intermediate compartment (ERGIC), and plays a very important role in maintaining the efficacy of the vesicles (12), in various areas of basic cellular biology

(13), insulin metabolism (14), and in a discussion of future cancer therapy (15). It is very important with this background to shed lights on the detailed clinical facts and the natural history in patients with HMSN-P.

In 2016, p.Gly269Val was reported as a second genetic mutation of HMSN-P (8), which is identical to the mutation found in autosomal dominant Charcot-Marie-Tooth disease Type 2 (CMT2) families (9). Although careful consideration and further examination will be needed to determine whether the phenotype differs between two different mutations within a gene, the clinical manifestation in their reports might be different from our experience on HMSN-P.

The factors causing individual differences in disease onset could not be elucidated in the current study. It has been reported that HMSN-P patients have many complications of diabetes and dyslipidemia (1), and the treatment of such complications may change the clinical course. Since the effects of those factors on the survival rate were not analyzed in this survey, differences in prognosis due to the presence or absence of those complications are subjects for the future analysis.

Another feature of the current study is the detailed clinical descriptions of the advanced stage of HMSN-P. The life-threatening risks for the patients with advanced stage HMSN-P may be comparable to those for the patients with ALS. However, because HMSN-P progresses more slowly than ALS, the period for which careful attention to risk management is needed can be much longer than that for ALS. It is necessary to carefully observe symptom progressions of HMSN-P patients from the age of 50, when fatalities begin to increase due to impaired swallowing and respiration (Figure 3).

Compared to the circumstances for the patients 30 years ago when the HMSN-P study was initiated, many medical situations have dramatically changed, including managements of nutrition and respiratory failure, owing to development of medical technology and equipment. The clinical course of HMSN-P may be further improved by providing advanced medical treatment with higher quality and developing new treatments in the future. Today, if a patient visits the hospitals, the swallowing/respiratory state can be regularly evaluated, and tracheotomy and tube feeding can be performed at an appropriate time if needed. It is noteworthy that there exist HMSN-P patients who can survive beyond the age of 70 if optimal care is provided with optimal timing. This fact also suggests that providing detailed and precise information about natural history is crucial for optimal treatment for patients with HMSN-P.

When the current study was began, we expected that swallowing/respiration problems progress in this order; breathing earlier and swallowing later. However, there was no clear difference of the start time of disability between these two. This is one of the limitations of the current study. One possible explanation for this

is that as symptoms progressed and activity of daily life declined, many patients had difficulty visiting the hospital, so they were changed to home care, or entered nursing home facilities. It could then be difficult to have a precise evaluation at such nursing homes.

At motor function declines in the advanced stages, some patients have fewer chances to walk, and they do not report particular problems of respiratory systems while resting. Some patients experienced "sudden" respiratory episodes (e.g., sputum blocks, aspiration), following a very slight physical condition change like catching cold or mild dehydration. After such events, some patients deteriorated to a condition in which they needed to receive advanced respiratory care including tracheostomy. It is noteworthy that in advanced stages, the condition (especially respiratory function) easily deteriorates. Therefore, regardless of the presence or absence of subjective symptoms, regular respiratory function checks are highly recommended starting when patients are in their 50s. For swallowing, it is necessary to establish a better evaluation routine utilizing, for example, videofluorography or videoendoscopy for swallowing.

Clinical reports focusing on disease progression based on many patients with HMSN-P have not yet been published. The current survey provides detailed information that can be widely provided to patients and families who traditionally get information only from their relatives privately.

5. Conclusion

We surveyed medical records in detail from 97 patients with HMSN-P. Disease progression, in terms of the order of the appearance of each symptom, is extremely uniform with slow progression, *i.e.*, the order of symptom appearance is almost identical in every patient for long after the onset, although the onset age varied 20-30 years. At the later stages, the disease progression and prognosis varied among patients, and its reason is unknown yet. As a disease model for neurodegenerative disorders caused by protein metabolism failure at the ERGIC zone based on a single gene abnormality, HMSN-P may provide a suitable example to develop treatment strategies.

Acknowledgements

This work was supported by a Health Labour and Welfare Sciences Research Grant (H29-005). This study was supported in part by grants from the Ministry of Education, Culture, Sports, Science and Technology of Japan (15H05293). This research was also supported by the Research program for conquering intractable disease from Japan Agency for Medical Research and development (AMED)(201442014A, 201442071A).

We thank to the many neurologists, doctors and

other medical staffs who helped those patients in many aspects at our hospital or other facilities.

References

1. Takashima H, Nakagawa M, Nakahara K, Suehara M, Matsuzaki T, Higuchi I, Higa H, Arimura K, Iwamasa T, Izumo S, Osame M. A new type of hereditary motor and sensory neuropathy linked to chromosome 3. *Ann Neurol*. 1997; 41:771-780.
2. Suehara M. Shinkei network series. Hereditary motor and sensory neuropathy with proximal dominant involvement. *Iryo*. 2001; 55:101-103. (In Japanese)
3. Ishiura H, Sako W, Yoshida M, *et al*. The TRK-fused gene is mutated in hereditary motor and sensory neuropathy with proximal dominant involvement. *Am J Hum Genet*. 2012; 91:320-329.
4. Maeda K, Sugiura M, Kato H, Sanada M, Kawai H, Yasuda H. Hereditary motor and sensory neuropathy (proximal dominant form, HMSN-P) among Brazilians of Japanese ancestry. *Clin Neurol Neurosurg*. 2007; 109:830-832.
5. Lee SS, Lee HJ, Park JM, Hong YB, Park KD, Yoo JH, Koo H, Jung SC, Park HS, Lee JH, Lee MG, Hyun YS, Nakhro K, Chung KW, Choi BO. Proximal dominant hereditary motor and sensory neuropathy with proximal dominance association with mutation in the TRK-fused gene. *JAMA Neurol*. 2013; 70:607-615.
6. Alavi A, Shamshiri H, Nafissi S, Khani M, Klotzle B, Fan JB, Steemers F, Elahi E. HMSN-P caused by p.Pro285Leu mutation in TFG is not confined to patients with Far East ancestry. *Neurobiol Aging*. 2015; 36:1606.e1-7.
7. Kawarai T, Morita M, Morigaki R, Fujita K, Nodera H, Izumi Y, Goto S, Nakano I, Kaji R. Pathomechanisms of motor neuron death by mutant TFG. *Rinsho Shinkeigaku*. 2013; 23:1199. (In Japanese)
8. Khani M, Shamshiri H, Alavi A, Nafissi S, Elahi E. Identification of novel TFG mutation in HMSN-P pedigree: Emphasis on variable clinical presentations. *J Neurol Sci*. 2016; 369:318-323.
9. Tsai PC, Huang YH, Guo YC, Wu HT, Lin KP, Tsai YS, Liao YC, Liu YT, Liu TT, Kao LS, Yet SF, Fann MJ, Soong BW, Lee YC. A novel TFG mutation causes Charcot-Marie-Tooth disease type 2 and impairs TFG function. *Neurology*. 2014; 83:903-912.
10. Murakami N, Imamura K, Izumi Y, Egawa N, Tsukita K, Enami T, Yamamoto T, Kawarai T, Kaji R, Inoue H. Proteasome impairment in neural cells derived from HMSN-P patient iPSCs. *Mol Brain*. 2017; 10:7.
11. Robberecht W, Philips T. The changing scene of amyotrophic lateral sclerosis. *Nat Rev Neurosci*. 2013; 14:248-264.
12. Hanna MG 4th, Block S, Frankel EB, Hou F, Johnson A, Yuan L, Knight G, Moresco JJ, Yates JR 3rd, Ashton R, Schekman R, Tong Y, Audhya A. TFG facilitates outer coat disassembly on COPII transport carriers to promote tethering and fusion with ER-Golgi intermediate compartments. *Proc Natl Acad Sci U S A*. 2017; 114:E7707-E7716.
13. Kanadome T, Shibata H, Kuwata K, Takahara T, Maki M. The calcium-binding protein ALG-2 promotes endoplasmic reticulum exit site localization and polymerization of Trk-fused gene (TFG) protein. *FEBS J*. 2017; 284:56-76.
14. Yamamotoya T, Nakatsu Y, Kushiya A, Matsunaga Y, Ueda K, Inoue Y, Inoue MK, Sakoda H, Fujishiro M, Ono H, Kiyonari H, Ishihara H, Asano T. Trk-fused gene (*TFG*) regulates pancreatic β cell mass and insulin secretory activity. *Scientific Reports*. 2017; 7:13026.
15. Hsu KT, Yu XM, Audhya AW, Jaume JC, Lloyd RV, Miyamoto S, Prolla TA, Chen H. Novel approaches in anaplastic thyroid cancer therapy. *Oncologist*. 2014; 19:1148-1155.

(Received December 18, 2017; Revised January 8, 2018; Accepted January 20, 2018)

Comparison of the extraction and determination of serum exosome and miRNA in serum and the detection of miR-27a-3p in serum exosome of ALS patients

Qian Xu^{1,2}, Yuying Zhao³, Xiaoyan Zhou², Jing Luan², Yazhou Cui², Jinxiang Han^{1,2,*}

¹ School of Medicine and Life Sciences, University of Jinan-Shandong Academy of Medical Sciences, Ji'nan, Shandong, China;

² Shandong Medical Biotechnological Center, Shandong Academy of Medical Sciences, Key Laboratory for Rare Disease Research of Shandong Province, Ji'nan, Shandong, China;

³ Laboratory of Neuromuscular Disorders and Department of Neurology, Qilu Hospital, Ji'nan, Shandong, China.

Summary

Amyotrophic Lateral Sclerosis (ALS) is a muscle-bone degenerative disease, which lacks a specific index for diagnosis. In our previous studies, we found that exosomes mediated the interaction mechanism between muscle and bone at the cellular level, and myoblast exosomes can transfer miR-27a-3p to promote osteoblast mineralization. Therefore, we suppose that the expression of miR-27a-3p in the serum exosomes of ALS patients also changes. In this study, we used healthy human serum as a sample to find out the conditions and methods for extraction and detection. Then through comparison of the expression of miR-27a-3p in the serum exosomes of 10 ALS patients and healthy subjects, we found that in the ALS patients miR-27a-3p was down-regulated, and may be involved in the development of ALS, and therefore has potential as a reference for the diagnosis of ALS in the clinic.

Keywords: Amyotrophic Lateral Sclerosis (ALS), exosome, miR-27a-3p, serum, stem loop

1. Introduction

Amyotrophic Lateral Sclerosis (ALS) is a progressive and fatal motor neuron degenerative disease, in which the main manifestation is progressive muscle weakness and atrophy, and gradually develops into systemic muscle atrophy and paralysis, with death finally due to respiratory failure. The cause is not yet clear, the early symptoms are not obvious, and lack of specific biological indicators makes clinical diagnosis difficult with a high misdiagnosis rate (1). Once diagnosed, the average survival time of patients are three to five years. The disease develops rapidly, and there is a significant difference between patients, with no definite diagnosis and cure method.

Exosomes are double lipid vesicles with a diameter

about 40-100 nm, which are secreted by a variety of cells. Exosomes are widespread in the peripheral body fluid, can carry and enrich various biologically active molecules, such as proteins, nucleic acids and so on, and have high stability, agility and specificity (2). Exosomes can reflect the physiological and pathological changes of the source cells, including proteins and nucleic acids, which have a potential biomarker function, and make exosomes have potential to be a new biomarker for disease diagnosis (3). MicroRNA (miRNA) is a class of endogenous non-encoding small RNA, with a length of 18-22 nt. MiRNAs are enriched in exosomes, and the exosome membrane structure can protect miRNA from degradation by RNA enzymes, this has made exosome miRNA become a hotspot in recent years (4,5).

In this experiment, we used the serum of healthy subjects, and compared and analyzed different extraction methods for serum exosomes and exosome miRNAs. Detection of miRNA expression was by polyadenylate poly A tail and stem loop methods, in order to find the most suitable method for extraction and detection of serum exosomes and exosome miRNAs. Then we compared the expression level of miR-27a-3p in serum

*Address correspondence to:

Dr. Jinxiang Han, School of Medicine and Life Sciences, University of Jinan-Shandong Academy of Medical Sciences; Shandong Medical Biotechnological Center, Shandong Academy of Medical Sciences, Key Laboratory for Rare Disease Research of Shandong Province, Ji'nan, 250062, China. E-mail: jxhan9888@aliyun.com

exosomes of ALS patients and healthy subjects, which laid a foundation for further research on the role of exosomes in the early diagnosis of ALS (Figure 1).

2. Materials and Methods

2.1. Materials

Serum from 20 healthy persons and 10 ALS patients were provided by Qilu Hospital and Ji'nan infectious diseases hospital, and stored at -80°C . Exoquick reagent and Anti CD63 were purchased from System Biosciences (Mountain View, CA, USA). ExoEasy Maxi Kit and miRNeasy Mini Kit were purchased from Qiagen (Valencia, CA, USA). TRIzol reagent was purchased from Invitrogen (Carlsbad, CA, USA). MiDETECT A Track™ miRNA qRT-PCR Starter Kit was purchased from RiboBio (Guangzhou, China). Reverse transcriptase kit was from Toyobo (Osaka, Japan).

2.2. Extraction and identification of serum exosome

The serum exosome was extracted by Exoquick reagent (System Biosciences, Mountain View, CA, USA) according to the manufacturer's protocol with minor modifications. The specific steps were as follows: the serum was centrifuged at $3,000 \times g$ for 30 min (4°C), to obtain the supernatant. We used a 1 mL syringe and repeatedly sucked 5 times. Exoquick reagent was added in a proportion of 4:1, and mix thoroughly by pipetting. It was stored at 4°C for 30 min, centrifuged at $13,000 \times g$ for 2 min, discarded the supernatant; centrifuged again and discarded the supernatant, then 100 μL phosphate-buffered saline (PBS) was added for resuspension, the exosome resuspension named exo-A was obtained.

The serum exosome was extracted by exoEasy Maxi Kit (Qiagen, Valencia, CA, USA) according to the manufacturer's protocol with minor modifications. Briefly, serum filtration was used to remove diameters greater than 0.8 μm particles, an equal volume of buffer XBP was added mixed well immediately, and transferred into the exoEasy spin column and centrifuged 1 min at $500 \times g$, the flow-through was discarded; 10 ml Buffer XWP was added and centrifuged 5 min at $5,000 \times g$, the flow-through was discarded; the spin column was transferred to a new collection tube, 100 μL Buffer XE was added and centrifuged 5 min at $5,000 \times g$, the flow-through was collected as exosome resuspension B, named exo-B.

Western-blot for detection of exosome specific marker proteins: Exosome protein content was measured using the BCA protein assay kit (Beyotime Institute of Biotechnology, Shanghai, China). Equal amounts (20 μg) of exosome resuspension were taken respectively, subjected to sodium dodecyl sulfate

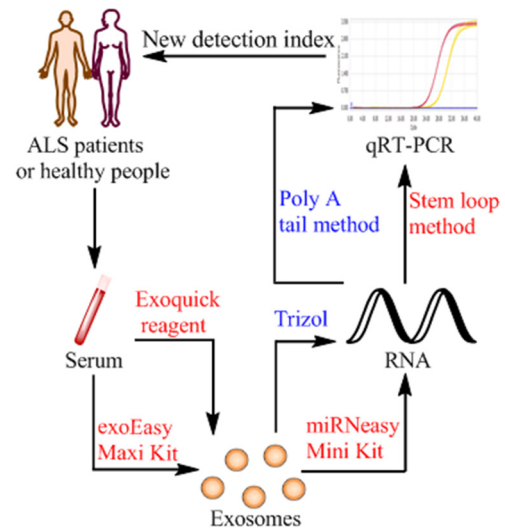


Figure 1. Extraction and identification methods of exosome miRNA in the study of ALS patients. A diagram showing the conditions and methods for extraction and detection and their applications. Exosome were isolated from ALS patients and healthy subject's serum by Exoquick reagent or exoEasy Maxi Kit, then using Qiagen miRNeasy Mini Kit to isolate RNA from serum exosomes, finally using stem loop method to detect the expression of miR-27a-3p in two groups of RNA samples. The results of the different expressions can be used for the clinical diagnosis of ALS patients.

polyacrylamide gel electrophoresis and transferred to a polyvinylidene fluoride (PVDF) membrane. After blocking, membrane was washed with TBST and then incubated overnight using antibodies against CD63 (1:1,000, System Biosciences, Mountain View, CA, USA). The blots signals were developed using ECL Plus (Millipore, Billerica, MA, USA) and visualized with Fusion SOLO S (Vilber, Collégien, France).

2.3. Isolation of total RNA from serum exosomes

Combined with the extraction of serum exosomes, we used two different methods to isolate total RNA from serum exosomes.

Using the traditional TRIzol reagent method to isolate total RNA from serum exosomes: The extracted exosome was mixed with a proper volume of TRIzol reagent (Invitrogen, Carlsbad, CA, USA), stored at room temperature for 5 min; chloroform was added according to a proportion of 1:5 in order to separated the lysate, transfer the upper aqueous phase to a new collection tube, and add isopropyl alcohol to precipitate the RNA, finally the RNA precipitation was cleaned using 75% ethanol, and then RNA could be precipitated after centrifugation.

Using Qiagen miRNeasy Mini Kit (Qiagen, Valencia, CA, USA) to isolate total RNA from serum exosomes: the extracted exosomes were washed and centrifuged using Buffer XBP and XWP, and mixed with a proper volume of QIAzol lysate, stored at room temperature for 5 min; and chloroform was

Table 1. Sequences of primers used in this study

Gene	Primers
miR-27a-3p	RT: GTCGTATCCAGTGCAGGGTCCGAGGTATTTCGACTGGATACGACGCGGAA Forward: CGGCGGTTTCACAGTGGCTAAG Reverse: CCAGTGCAGGGTCCGAGGTAT
miR-16	RT: GTCGTATCCAGTGCAGGGTCCGAGGTATTTCGACTGGATACGACCGCCAAT Forward: CGCGCTAGCAGCACGTAAT Reverse: GTGCAGGGTCCGAGGT

added according to the proper proportion to separate the lysate, the upper aqueous phase was transferred to a new collection tube, after addition of 2 volumes of 100% ethanol, the mixture was transferred into an RNeasy MinElute spin column in a 2 ml collection tube, after centrifugation, RNA was combined on the column membrane, and then washed with Buffer RWT and RPE, DNase/RNase-Free water was added and centrifuged 1 min at $12,000 \times g$, the flow-through collected was the exosome total RNA.

The concentration and purity of RNA samples were detected by Thermo micro spectrophotometer NanoDrop2000, and values were recorded.

2.4. Quantitative real-time PCR (qRT-PCR)

The expression level of miR-27a-3p in serum exosomes was detected by fluorescence quantitative polyadenylate poly A tail and stem loop methods, with miR-16 as endogenous exosome control. We compared the difference in expression of miR-27a-3p between ALS patients and healthy subjects.

Polyadenylate poly A tail method: mature miRNA sequences were provided (<http://www.mirbase.org>), the primers were designed by RiboBio company, and included reverse transcription, forward and reverse primers. The qRT-PCR was performed with miDETECT A Track™ miRNA qRT-PCR Starter Kit (RiboBio, Guangzhou, China), specific steps and the reaction system was conducted according to the manufacturer's protocol.

Stem loop method: Based on the miRNA mature sequences and the stem loop frame, we designed specific RT primers with a stem loop structure and forward-reverse primers, the sequence of the primers for miR-27a-3p and miR-16 are listed in the Table 1. RNA samples were premodified at 65°C for 5 min, and a reverse transcriptase kit (Toyobo, Osaka, Japan) was used for the RT reactions. After cDNA and diluted 20 times, the qRT-PCR reaction was performed according to the following reaction system: Realtime PCR Master Mix 5 µL, forward primer (10 µmol/L) 1 µL, reverse primer (10 µmol/L) 1 µL, and 3 µL cDNA dilution solution. The conditions of qRT-PCR reaction were: 95°C 10 min; 95°C 2 s, 60°C 20 s, 70°C 10 s, 45 cycles. After the end of the cycle, the melting curve was analyzed immediately.



Figure 2. Identification of surface marker proteins of exosomes. Using Exoquick and exoEasy Maxi Kit extract exosomes from serum, respectively. CD63 level was monitored by Western blot.

2.5. Statistical analysis

All data were analyzed statistically by SPSS software (version 19.0). The measurement data are expressed as mean \pm standard deviation (S.D.), the mean values between groups were compared by one-way analysis of variance (ANOVA), and $p < 0.05$ was considered statistically significant.

3. Results

3.1. Identification of exosome

Western-blot was used to detect the specific marker proteins (6) of serum exosomes extracted by the two methods, and CD63 is one of the most commonly used for identification of exosome protein molecules. The results showed that CD63 proteins were all expressed in two groups (Figure 2).

3.2. Comparison of the concentration and purity of RNA were extracted by 4 different methods

In order to facilitate the description, the RNA samples obtained by Exoquick-Trizol method were named group A, those obtained by Exoquick- miRNeasy Mini Kit were named group B, the exoEasy Maxi Kit – Trizol method used to obtain the RNA samples were named group C, and the exoRNeasy Serum/Plasma Midi Kit method for the RNA samples were named group D.

The A group was extremely unstable, the concentration range is wide and distributed from 3.6-120.4 ng/µL, the mean value of OD260/280 was 1.42 ± 0.02 and quality was bad. The concentration and purity of group B were improved compared with group A, and the mean value of OD260/280 was 1.54 ± 0.051 . The concentration of group C tended to be stable, but the purity of the group changed a little. Group D used

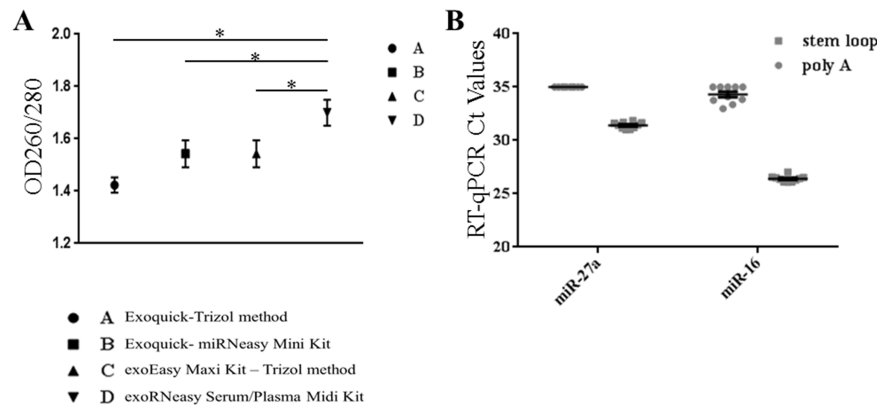


Figure 3. Comparing the different extraction and identification methods. The exosome RNA were extracted by 4 different methods and identified by poly A tail or stem loop method, respectively. (A) The purity of Exosome RNA were extracted by 4 different methods, and group D was extracted by exoRNeasy Serum/Plasma Midi Kit compared with the other groups, the difference was statistically significant ($p < 0.05$); (B) The Ct values of miR-27a-3p and miR-16 were detected by poly A tail or stem loop method.

a Qiagen kit to extracted exosomes from the serum, we continued to use the kit to isolate RNA, the concentration was about 10 ng/ μ L and the purity was obviously improved, the mean value of OD260/280 was 1.70 ± 0.05 , it basically met the requirements of the experiment, and compared with the other groups, the difference was statistically significant ($p < 0.05$) (Figure 3).

3.3. Comparison of the difference in expression of miRNA by qRT-PCR

The exoRNeasy Serum/Plasma Midi Kit isolated RNA from the serum exosomes, expression level of miR-27a-3p was detected by fluorescence quantitative polyadenylate poly A tail and stem loop methods respectively, the internal control selected miR-16 which is a serum exosome and was relatively stable.

Comparing the specificity of PCR products detected by the two methods, dissolution curves were all a single peak, which proved that the designed primers had effectiveness and specificity.

When the poly A tail method was used to detect miR-27a-3p and miR-16, the Ct values of the partially complex hole is greater than 35, the test results were negative, and the Ct values were unstable, and did not have reproducibility. The qRT-PCR again after changing the concentration of cDNA samples, the relative results are the same as before. The results of the stem loop method showed that the Ct values of miR-27a-3p ranged from 31.31 to 31.71, the Ct values of miR-16 were from 25.5-26.1, which are less than 35 (Figure 3). It was proved that the stem loop method is more sensitive than the polyadenylate poly A tail method, the repeatability of the compound holes is good and the stability is strong.

3.4. Comparing the difference in expression of miR-27a-3p between ALS patients and healthy subjects

We used the exoRNeasy Serum/Plasma Midi Kit

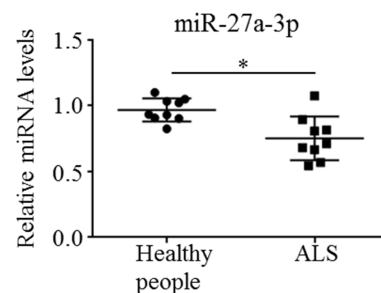


Figure 4. Comparing the difference in expression of miR-27a-3p between ALS patients and healthy subjects. Using stem loop method to detected the miR-27a-3p in 10 ALS patients and healthy subject's serum exosomes, respectively. Compared with the control group, the expression of miR-27a-3p in the ALS group was down-regulated, and the difference was statistically significant ($p < 0.05$).

to extract RNA from 10 ALS patients and healthy subject's serum exosomes, respectively. The difference in expression of miR-27a-3p in the two groups of RNA samples was detected by the fluorescence quantitative stem loop method. The Ct values of all the samples were less than 35, the dissolution curves were all a single peak, which proved that the amplification of data was effective and the specificity was good. Compared with the control group, the expression of miR-27a-3p in the ALS group was down-regulated, and the difference was statistically significant ($p < 0.05$) (Figure 4).

4. Discussion

Exosomes are a vesicular structure secreted by a variety of cells, and has become a hotspot issue in the field of biomedical research. It has the characteristics of easy to collect and noninvasive or minimally invasive. Noninvasive detection can be realized through the identification of tumor exosomes, or detection of individual biological characteristics used for individualized diagnosis and treatment (7,8). It has

been found that exosomes can reflect the phenotype of the source of tumor cells through their molecular characteristics, and the tumor specific antigen or miRNA carried by them can be used as tumor diagnostic markers. Thompson *et al.* studies have shown that the exosome source of the central nervous system is related to neurodegenerative diseases, and the exosomes in cerebrospinal fluid and serum is an early diagnostic marker for some neurodegenerative diseases by carrying proteins and nucleic acids (9). According to blood tests, researchers from Irish University found that miRNA imbalance appeared in the exosomes of breast cancer, so breast cancer cells can be monitored through miRNA changes in the exosome, and it has proved that exosome miRNA has potential as a marker for breast cancer diagnosis (10). All these suggested that miRNA has the potential to be used as a tumor marker for early diagnosis, evaluation of curative effect, and metastasis or recurrence of the tumor.

The extraction of exosomes by overspeed centrifugation or sucrose gradient centrifugation are the most common methods (11). However, the operation is time-consuming, has a low recovery rate, has an important influence on exosomes, and it is not suitable for extracting sample volumes from a small initial volume. However, Exoquick reagent and Qiagen exoEasy Maxi Kit have obtained exosomes by compound polymerization precipitation or membrane affinity centrifugation columns. The operation is simple and fast, and it is suitable for extraction of serum exosomes (12,13).

In isolation of serum derived exosome RNA, two different principles including traditional TRIzol and miRNeasy Mini Kits were used in this study. The isolation of RNA by TRIzol is a method of splitting decomposition of phenol lysate, as chloroform makes a two-phase separation with a final alcohol precipitation. MiRNeasy Mini Kit was adopted for the phenol type lysate combined with an affinity filtration column, use of a membrane for particle adsorption, and the purified RNA was obtained by different buffer multiple purification.

The current methods of qRT-PCR mainly include a TaqMan probe method and fluorescent dye method. The TaqMan probe method specificity is strong, but the cost is high. Therefore, in this experiment, the qRT-PCR was carried out by combining the poly A tail method or the stem loop method with the fluorescent dye. The polyA tail method was added to miRNA under the action of poly A polymerase, the template chain was obtained by reverse transcription through specific primers, and the fluorescence quantitative PCR was detected at last. Stem loop method used primers with a folded structure like stem loop, directly complementary miRNA to get reverse transcriptional template chains (14,15). Experiments have shown that the stem loop method has high sensitivity, specificity and less sample demand

for miRNA. It can effectively detect the expression of miRNA in the samples, and laid a foundation for the next step to effectively detect the expression of miRNA in ALS patients.

As a fatal neurodegenerative disease, ALS seriously influences and endangers the quality of daily life of middle-aged and elderly people. The specific pathogenesis is complex. Now, more detailed studies are being carried out in order to find out the related mechanisms of skeletal degenerative diseases, so as to develop new preventive strategies and therapies. Our previous study found that myoblast exosomes can stimulate mineralization of osteoblasts through miR-27a-3p regulation of the Wnt signaling pathway, which proves that exosomes can regulate the interaction between myoblasts and osteoblasts through miR-27a-3p, and there may be a positive feedback mechanism.

So in this experiment, we compared the expression of miR-27a-3p in patients with ALS and healthy human serum exosomes, found compared with the healthy group, miR-27a-3p expression in ALS patients was down-regulated, and suggested that exosome miR-27a-3p may act as a detection index of ALS, but the specific mechanism is unclear and needs further study.

Acknowledgements

This study was supported by National Natural Science Foundation of China (81772300, 81371909) and The Innovation Project of Shandong Academy of Medical Sciences.

References

1. Worms PM. The epidemiology of motor neuron diseases: a review of recent studies. *J Neurol Sci.* 2001; 191:3-9.
2. Tkach M, Théry C. Communication by Extracellular Vesicles: Where We Are and Where We Need to Go. *Cell.* 2016; 164:1226-1232.
3. Bang C, Thum T. Exosomes: new players in cell-cell communication. *Int J Biochem Cell Biol.* 2012; 44:2060-2064.
4. Koga Y, Yasunaga M, Moriya Y, Akasu T, Fujita S, Yamamoto S, Matsumura Y. Exosome can prevent RNase from degrading microRNA in feces. *J Gastrointest Oncol.* 2011; 2:215-222.
5. Valadi H, Ekström K, Bossios A, Sjöstrand M, Lee JJ, Lötvall JO. Exosome-mediated transfer of mRNAs and microRNAs is a novel mechanism of genetic exchange between cells. *Nat Cell Biol.* 2007; 9:654-659.
6. Khatun Z, Bhat A, Sharma S, Sharma A. Elucidating diversity of exosomes: biophysical and molecular characterization methods. *Nanomedicine.* 2016; 11:2359-2377.
7. Tan KH, Tan SS, Sze SK, Lee WK, Ng MJ, Lim SK. Plasma biomarker discovery in preeclampsia using a novel differential isolation technology for circulating extracellular vesicles. *Am J Obstet Gynecol.* 2014; 211:380.
8. Liu WH, Ren LN, Wang X, Wang T, Zhang N, Gao Y, Luo

- H, Navarro-Alvarez N, Tang LJ. Combination of exosomes and circulating microRNAs may serve as a promising tumor marker complementary to alpha-fetoprotein for early-stage hepatocellular carcinoma diagnosis in rats. *J Cancer Res Clin Oncol.* 2015; 141:1767-1778.
9. Thompson AG, Gray E, Heman-Ackah SM, Mäger I, Talbot K, Andaloussi SE, Wood MJ, Turner MR. Extracellular vesicles in neurodegenerative disease - pathogenesis to biomarkers. *Nat Rev Neurol.* 2016; 12:346-357.
 10. Joyce DP, Kerin MJ, Dwyer RM. Exosome-encapsulated microRNAs as circulating biomarkers for breast cancer. *Int J Cancer.* 2016; 139:1443-1448.
 11. Théry C, Amigorena S, Raposo G, Clayton A. Isolation and Characterization of exosomes from cell culture supernatants and biological fluids. *Curr Protoc Cell Biol.* 2006; Unit 3.22.
 12. Cui Y, Luan J, Li H, Zhou X, Han J. Exosomes derived from mineralizing osteoblasts promote ST2 cell osteogenic differentiation by alteration of microRNA expression. *FEBS Lett.* 2016; 590:185-192.
 13. Enderle D, Spiel A, Coticchia CM, Berghoff E, Mueller R, Schlumpberger M, Sprenger-Haussels M, Shaffer JM, Lader E, Skog J, Noerholm M. Characterization of RNA from Exosomes and Other Extracellular Vesicles Isolated by a Novel Spin Column-Based Method. *PLoS One.* 2015; 10:e0136133.
 14. Wu RM, Wood M, Thrush A, Walton EF, Varkonyi-Gasic E. Real-time PCR quantification of plant miRNA using universal probeLibrary technology. *Biochemica.* 2007; 202:12-15.
 15. Wu Y, Xing X, You T, Liang R, Liu J. RT-qPCR with chimeric dU stem-loop primer is efficient for the detection of bacterial small RNAs. *Appl Microbiol Biotechnol.* 2017; 101:4561-4568.

(Received December 28, 2017; Revised February 23, 2018; Accepted February 25, 2018)

Complex heterozygous *WNT1* mutation in severe recessive osteogenesis imperfecta of a Chinese patient

Yanqin Lu^{1,2,§}, Yunzhang Dai^{1,2,§}, Yanzhou Wang³, Naixiang Zhai^{1,2}, Jian Zhang^{1,2}, Junlong Liu⁴, Xiaoli Yin^{1,2}, Tianyou Li³, Xiuzhi Ren^{4,**}, Jinxiang Han^{1,2,**}

¹Key Laboratory for Biotech-Drugs Ministry of Health, Key Laboratory for Rare & Uncommon Diseases of Shandong Province, Shandong Medicinal Biotechnology Centre, Shandong Academy of Medical Sciences, Ji'nan, China;

²School of Medicine and Life Sciences, University of Jinan-Shandong Academy of Medical Sciences, Ji'nan, China;

³Department of Paediatric Surgery, Shandong Provincial Hospital, Ji'nan, China;

⁴Department of Orthopaedic Surgery, The People's Hospital of Wuqing District, Tianjin, China.

Summary

Osteogenesis imperfecta (OI) is a heritable connective tissue disorder with a predominately autosomal-dominant inheritance pattern. Recessive forms of OI are rare and involve many different causative genes. *WNT1* mutations were found to cause either autosomal-recessive OI or dominantly inherited early-onset osteoporosis. Here we describe a 32-year-old boy with severe osteopenia and deformity of the extremities. The relative long thumb and ring finger are obvious. We identified a novel combination of complex heterozygous *WNT1* mutation of c.397 A>T (p.Ala133Thr) and c.506dupG (p.Cys170Leufs*) in the proband, both parents and young brother were shown to be heterozygous asymptomatic carriers of the mutation. This is the eleventh family and the thirteenth patient we have ever found in China. Mutation of c.397 A>T (p.Ala133Thr) was found for the third time following our previous findings in two individual families with four patients in total, and may be a hotspot mutation in Chinese *WNT1*-related OI patients. *In silico* programs supported the damaging effects for both mutations. The three-D structure demonstrated the severely destroyed stability of WNT1. Serum levels of WNT1, LRP5, and β -catenin were decreased, while higher levels of GSK-3 β were detected. The molecular mechanisms of the complex heterozygous mutations need further study.

Keywords: Osteogenesis imperfecta, *WNT1* mutation, Wnt signaling pathway, *in silico* prediction, three-dimensional structure

1. Introduction

Osteogenesis imperfecta (OI) is a group of genetic connective tissue diseases characterized by the occurrence of frequent fractures and reduced bone mass. Blue or grey sclera and dentinogenesis imperfecta are also common (1). The primary inheritance pattern of OI

is autosomal dominant and most causative mutations are in *COL1A1* and *COL1A2*, which encode collagen type I α chains (2,3). Recessively inherited forms of OI are rare and are caused by mutations in many different genes (4,5).

WNT1 was identified as a pathogenic gene for autosomal-recessive OI (6-9), or early-onset osteoporosis (7,8,10). The molecular pathogenesis of *WNT1*-induced OI differs from that of other recessive OI types. *In vitro* study showed that the *WNT1* mutant interferes with the LRP5-mediated β -catenin signaling pathway, although the exact mechanism is currently unclear (7). Meanwhile, decreased mTORC1-dependent osteoblast function due to loss of WNT1 signaling in osteocytes is part of the reason for WNT1-related OI and osteoporosis according to mouse studies (11). In addition, OI patients with *WNT1* mutations do

[§]These authors contributed equally to this work.

*Address correspondence to:

Dr. Jinxiang Han, Shandong Medicinal Biotechnology Centre, Shandong Academy of Medical Sciences, 18877 Jingshi Road, Ji'nan 250062, China.
E-mail: samshjx@sina.com

Dr. Xiuzhi Ren, Department of Orthopaedic Surgery, The People's Hospital of Wuqing District, 100 Yogyang West Rd, Tianjin 301700, China.
E-mail: xiuzhiren@hotmail.com

not gain a substantial therapeutic effect using oral and intravenous bisphosphonate therapy, which is effective in OI patients with type I collagen mutations and anti-sclerostin antibody is a potential option for OI patient's treatment (11). Thus far, no more than 30 *WNT1* mutations are identified and listed in the OI mutation database (6,7,9,12-18). In this study, we present the genetic and functional changes of a patient with compound heterozygous mutation of *WNT1* gene in a 32-year-old Chinese boy with severe autosomal-recessive OI.

2. Materials and Methods

2.1. Clinical phenotype and mutation detection of OI genes

This study was performed in accordance with The Code of Ethics of the World Medical Association (Declaration of Helsinki) for experiments involving humans. The study was approved by the Ethical Committee of Shandong Medicinal Biotechnology Central and informed consent was obtained from the patient.

Peripheral blood was drawn from the patient and his parents, and genomic DNA was extracted using the E.Z.N.A.[®] Blood DNA Kit (Omega Bio-Tek, Norcross, GA, USA). Initially, we sequenced only *COL1A1* and *COL1A2* genes (19), but later we sequenced all reported causative genes of recessive OI with the exception of *MBTPS2* and *PLS3*. A total of four PCR reactions were conducted to cover the entire genetic coding region and intron-exon boundaries of *WNT1*. PCR products were subjected to Sanger sequencing (Beijing Genomics Institute, Qingdao, China), and genetic variations were analyzed by Mutation Surveyor 4.0 software (SoftGenetics LLC, State College, PA, USA).

2.2. Molecular and 3-D structural predication of the *WNT1* mutation

Predication of the mutational effect on protein function was performed using Polyphen (20), Align-GVGD (21), SIFT (22), and Mutation Taster (23) software. Alignment of 19 different human Wnt family members and *WNT1* from different animal species was conducted by the Clustal X2 program (24). The *WNT1* mutation was located on the N-terminal domain (PDB ID 4F0A) of the WNT1 protein by the PyMOL (Schrodinger LLC, Portland, OR, USA) program.

2.3. Serum ELISA assay of Wnt signaling pathway molecules

Serum ELISA assays for WNT1, LPR5, and β -catenin were performed according to the manufacturer's instructions (Beinglay Biotech Co. Ltd., Wuhan, China). Three age-matched healthy serums were included in the

assay as controls for the patient (control 1) and patient's father (controls 2 and 3). Absorbance values were measured at 450 nm on a Synergy HT multiplate reader (Bio-tek, Winooski, VT, USA).

3. Results

3.1. Clinical description of the proband

The patient was born with normal height and weight at delivery. He was around 1 meter tall and weighed 26kg. He was born to non-consanguineous parents with no obvious phenotypic abnormalities. His sclerae were normal in color, vision, and intellectual function was normal. Teeth were sparse and progressive hearing loss was obvious after 28 years old. Pectus cranatum and scoliosis was obvious. Patient has a long face, with abnormal facial features including tip head, narrowing forehead, widening distance between the eyes and eyelashes and hypogynous ears. His head leans backward slightly. A relatively long thumb and ring finger was obvious (Figure 1A) His first left humerus fracture was documented over 1 year after birth. He then sustained recurrent bilateral femur fractures ($n = 7-8$), and angled malformation was obvious in upper and lower extremities. Lower extremities are in a frog position (Figure 1B). Most of his fractures occurred before 10 years old and no fracture has occurred after 13 years old, and this may partly due to long-term bed life. Cortical bone was extremely thin according to parents description, but X imaging was unavailable.

3.2. Molecular and 3-D structural analysis

The compound heterozygous mutation of c.397C>T (p.Ala133Thr) and c.506dupG (p.Cys170Leufs*) in the N-terminal α -helical domain (NTD) of *WNT1* were identified in the patient and was present in both parents, sibling has a heterozygous mutation (Figure 1C). SIFT and Mutation Taster programs predicted these two mutations to have a damaging effect, and class values of C55 and C65 were predicted by Align-GVGD in c.397C>T and c.506dupG, respectively. The Polyphen program predicted both mutations to have a probably damaging effect. Both alignments of different types of human Wnt family members (Figure 1D) and WNT1 among different species (Figure 1E) show high degrees of conservation.

Figure 2D shows the 3D structural model of WNT1. No obvious difference was observed between the wild-type and mutant with respect to p.Ala133Thr change (Figure 2A). Change of p.Cys170Leufs* induced the loss of C-terminal domain, which is responsible for Wnt binding and signaling transduction. Compared with the wild-type residues, a large amount of β -sheet structure was displaced by a loop region, with a loose and truncated structure (Figure 2B).

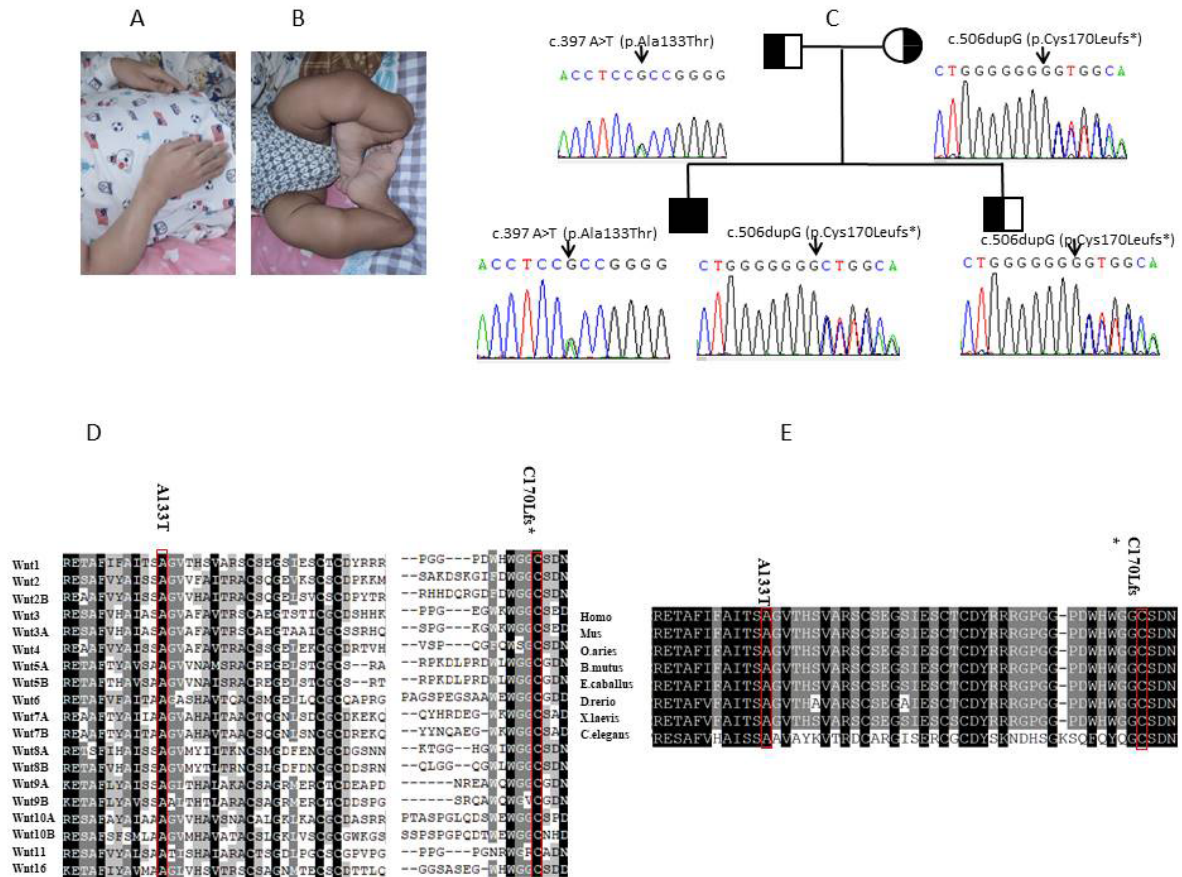


Figure 1. Clinical phenotype and Sanger sequencing results. (A) Abnormal finger, (B) Deformity in lower extremities, (C) Pedigree map and identified mutations of patient and their family members, (D-E) Highly conserved mutation in WNT family members and different species by alignment.

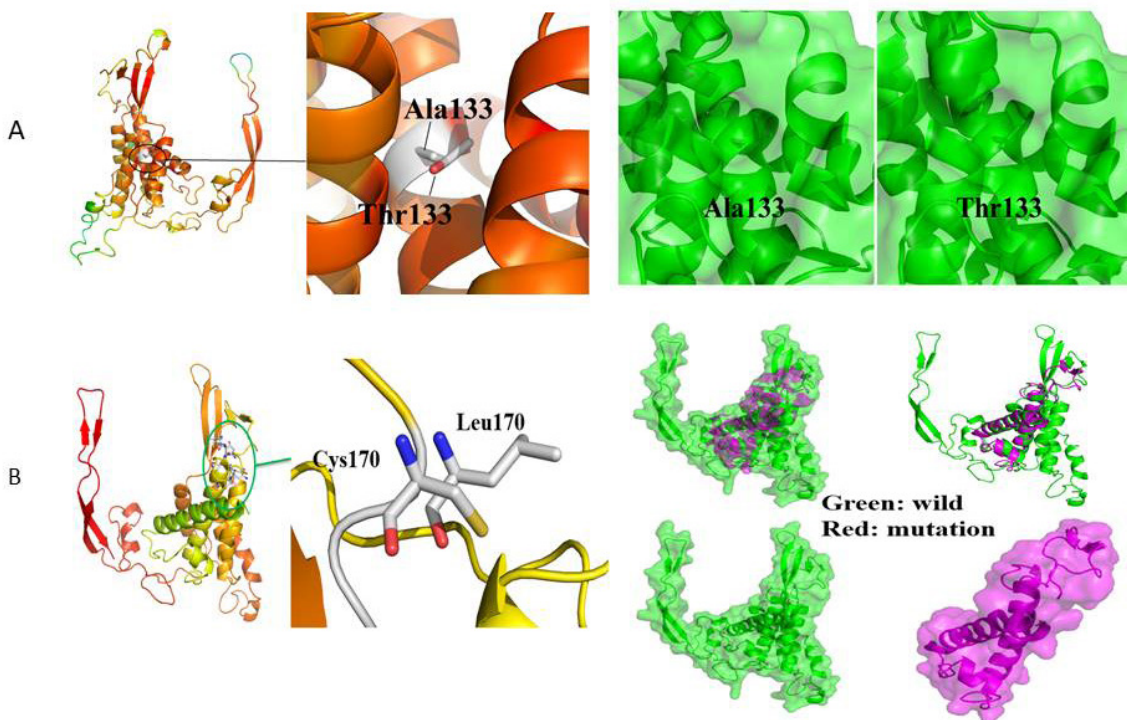


Figure 2. Location and 3-D structure of WNT1 variants. (A) p.Ala133Thr, (B) p.Cys170Leufs*.

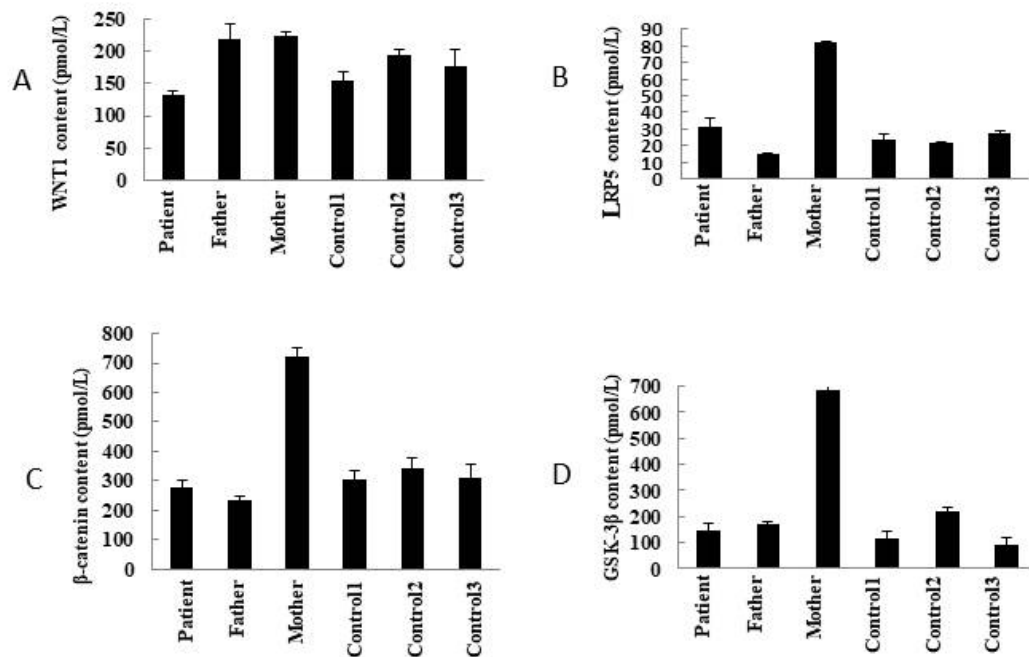


Figure 3. ELISA assay for serum quantification. (A) WNT1, (B) LRP5, (C) β-catenin, (D) GSK-3β.

3.3. Wnt signaling pathway molecules

Serum ELISA assays showed a significant difference in the WNT signaling pathway molecule. The expression of WNT1, β-catenin, GSK-3β were decreased and the level of LRP5 increased (Figure 3).

4. Discussion

We report one Chinese OI patient with an autosomal-dominant *WNT1* mutation following our previously identified 11 mutations (9 novel) from 10 individual Chinese families, which was the largest group of patients with recessive OI ever reported (revision data). The patient in our present paper has complex heterozygous of c.397C>T (p.Ala133Thr) and c.506dupG (p.Cys170Leufs*). Abnormalities in facial and finger characteristics extended the phenotype spectrum of OI patients with *WNT1* mutations. Serum ELISA analysis revealed decreased WNT1 and impaired canonical Wnt/β-catenin pathway.

For heterozygous c.397C>T (p.Ala133Thr) mutation, it was the third time that we found and the fifth patient from three individual families. It was identified to be combined with heterozygous c.667C>T (p. Ser226Leu) and c.774C>A (p.Tyr258*) in two individual families, respectively. This mutation may be a hotspot mutation (with 27.3%) in Chinese type XV OI patient. For c.506dupG (p.Cys170Leufs*), it was recorded in the list of Osteogenesis Imperfecta Variant Database (<http://www.le.ac.uk/ge/collagen>) (12,13) four times, including two homozygous mutations (both type III) and two heterozygous mutations in correlated

c.506G>A (17), and c.259C>T (p.Gln87*). For the patient carrying c.506dupG and c.259C>T mutations, multiple fractures, delayed development, recurrent infections, ptosis, and high arched palate were seen (9). However, no ptosis and multiple fractures were observed in our patient, though these are common phenotypes in related type XV OI according to the data from our previous 10 *WNT1* OI families. *WNT1* knockout mouse model and spontaneous *WNT1* mutations have demonstrated that it is necessary for the formation of the cerebellum and midbrain (25,26), and severe bone fragility (11).

Three D analysis predicted that the p.Ala133Thr change would nearly have no effect on protein structure. Same results were obtained from expression of WNT1 by Western blot (unpublished data). The change of cysteine to leucine at position of 170 leads to formation of a loop region instead of the original β-sheet, and hence, the stability of WNT1 is severely destroyed as predicted. Premature termination codon mutations mediate mRNA degradation through nonsense-mediated RNA decay (27). Wnt has an N-terminal α-helical domain (NTD) and C-terminal cysteine-rich domain (CTD). The NTD contains seven α-helices with five disulfide bonds formed by conserved cysteine residues, while the CTD has two β-sheets stabilized by disulfide bonds. Both the thumb loop from the NTD and index finger from the CTD grasp the frizzled cysteine-rich domain (Fz-CRD), which is responsible for Wnt binding and signaling transduction. Wnts are post-translationally acylated by the presence of palmitate and/or palmitoleic acid at particular conserved serine residues and further lipidation at the cysteine residue

of the mature secreted protein. The truncated protein caused by p.Cys170Leufs* leads to the loss of the lipidation site and CTD domain. Functional Wnt signaling pathway impaired and this is in line with our unpublished data and other group's finding (8).

Variable clinical phenotypes are notable in OI patients with *WNT1* mutations. One of the most striking phenotypes, compared with type I collagen gene related OI is that no deformities or fracture were noted at birth according to our unpublished Wnt1 OI population. Severe vertebral compressions was also obvious according to a report (28) and our unpublished data. Neurological problems can either be present or absent (29). Other characteristics such as ptosis, recurrent chest infections, hypotonia, and developmental delay have all been documented in these previous OI populations (9,14). The present study shows the obvious abnormality in facial characteristics and fingers in OI patient with identified *WNT1* mutations.

Acknowledgements

We thank the patient and his family members who participated in our study. The study was supported by the grant from Shandong government (No. 2016GSF201222, 2016ZDJS07A10 and 2015ZRC03171)

References

- Sillence DO, Senn A, Danks DM. Genetic heterogeneity in osteogenesis imperfecta. *J Med Genet.* 1979; 16:101-116.
- Forlino A, Marini JC. Osteogenesis imperfecta. *Lancet.* 2016; 387:1657-1671.
- Trejo P, Rauch F. Osteogenesis imperfecta in children and adolescents-new developments in diagnosis and treatment. *Osteoporos Int.* 2016; 27:3427-3437.
- Bardai G, Moffatt P, Glorieux FH, Rauch F. DNA sequence analysis in 598 individuals with a clinical diagnosis of osteogenesis imperfecta: Diagnostic yield and mutation spectrum. *Osteoporos Int.* 2016; 27:3607-3613.
- Lu Y, Ren X, Wang Y, Han J. Molecular mechanisms of osteogenesis imperfecta. *Prog.Biochem.Biophys.* 2015; 42:511-518
- Fahiminiya S, Majewski J, Mort J, Moffatt P, Glorieux FH, Rauch F. Mutations in WNT1 are a cause of osteogenesis imperfecta. *J Med Genet.* 2013; 50:345-348.
- Keupp K, Beleggia F, Kayserili H, *et al.* Mutations in WNT1 cause different forms of bone fragility. *Am J Hum Genet.* 2013; 92:565-574.
- Laine CM, Joeng KS, Campeau PM, *et al.* WNT1 mutations in early-onset osteoporosis and osteogenesis imperfecta. *N Engl J Med.* 2013; 368:1809-1816.
- Pyott SM, Tran TT, Leistriz DF, Pepin MG, Mendelsohn NJ, Temme RT, Fernandez BA, Elsayed SM, Elsobky E, Verma I, Nair S, Turner EH, Smith JD, Jarvik GP, Byers PH. WNT1 mutations in families affected by moderately severe and progressive recessive osteogenesis imperfecta. *Am J Hum Genet.* 2013; 92:590-597.
- Mäkitie RE, Niinimäki T, Nieminen MT, Schalin-Jäntti C, Niinimäki J, Mäkitie O. Impaired WNT signaling and the spine-Heterozygous WNT1 mutation causes severe age-related spinal pathology. *Bone.* 2017; 101:3-9.
- Joeng KS, Lee YC, Lim J, Chen Y, Jiang MM, Munivez E, Ambrose C, Lee BH. Osteocyte-specific WNT1 regulates osteoblast function during bone homeostasis. *J Clin Invest.* 2017; 127:2678-2688.
- Dalgleish R. The human type I collagen mutation database. *Nucleic Acids Res.* 1997; 25:181-187.
- Dalgleish R. The Human Collagen Mutation Database 1998. *Nucleic Acids Res.* 1998; 26:253-255.
- Faqeih E, Shaheen R, Alkuraya FS. WNT1 mutation with recessive osteogenesis imperfecta and profound neurological phenotype. *J Med Genet.* 2013; 50:491-492.
- Stephen J, Girisha KM, Dalal A, Shukla A, Shah H, Srivastava P, Kornak U, Phadke SR. Mutations in patients with osteogenesis imperfecta from consanguineous Indian families. *Eur J Med Genet.* 2015; 58:21-27.
- Aldinger KA, Mendelsohn NJ, Chung BH, Zhang W, Cohn DH, Fernandez B, Alkuraya FS, Dobyns WB, Curry CJ. Variable brain phenotype primarily affects the brainstem and cerebellum in patients with osteogenesis imperfecta caused by recessive WNT1 mutations. *J Med Genet.* 2016; 53:427-430.
- Liu Y, Song L, Ma D, Lv F, Xu X, Wang J, Xia W, Jiang Y, Wang O, Song Y, Xing X, Asan, Li M. Genotype-phenotype analysis of a rare type of osteogenesis imperfecta in four Chinese families with WNT1 mutations. *Clin Chim Acta.* 2016; 461:172-180.
- Caparros-Martin JA, Aglan MS, Temtamy S, *et al.* Molecular spectrum and differential diagnosis in patients referred with sporadic or autosomal recessive osteogenesis imperfecta. *Mol Genet Genomic Med.* 2016; 5:28-39.
- Lu Y, Ren X, Wang Y, Li T, Li F, Wang S, Xu C, Wu G, Li H, Li G, Zhao F, Wang Z, Mo X, Han J. Mutational and structural characteristics of four novel heterozygous C-propeptide mutations in the proalpha1(I) collagen gene in Chinese osteogenesis imperfecta patients. *Clin Endocrinol (Oxf).* 2014; 80:524-531.
- Sunyaev S, Ramensky V, Koch I, Lathe W, 3rd, Kondrashov AS, Bork P. Prediction of deleterious human alleles. *Hum Mol Genet.* 2001; 10:591-597.
- Tavtigian SV, Deffenbaugh AM, Yin L, Judkins T, Scholl T, Samollow PB, de Silva D, Zharkikh A, Thomas A. Comprehensive statistical study of 452 BRCA1 missense substitutions with classification of eight recurrent substitutions as neutral. *J Med Genet.* 2006; 43:295-305.
- Ng PC, Henikoff S. Predicting deleterious amino acid substitutions. *Genome Res.* 2001; 11:863-874.
- Schwarz JM, Rodelsperger C, Schuelke M, Seelow D. MutationTaster evaluates disease-causing potential of sequence alterations. *Nat Methods.* 2010; 7:575-576.
- Larkin MA, Blackshields G, Brown NP, Chenna R, McGettigan PA, McWilliam H, Valentin F, Wallace IM, Wilm A, Lopez R, Thompson JD, Gibson TJ, Higgins DG. Clustal W and Clustal X version 2.0. *Bioinformatics.* 2007; 23:2947-2948.
- Clevers H, Nusse R. Wnt/ β -catenin signaling and disease. *Cell.* 2012;149:1192-1205.
- Inestrosa NC, Toledo EM. The role of Wnt signaling

- in neuronal dysfunction in Alzheimer's Disease. *Mol Neurodegener.* 2008; 3:9.
27. Lejeune F. Nonsense-mediated mRNA decay at the crossroads of many cellular pathways. *BMB Rep.* 2017; 50:175-185.
28. Palomo T, Al-Jallad H, Moffatt P, Glorieux FH, Lentle B, Roschger P, Klaushofer K, Rauch F. Skeletal characteristics associated with homozygous and heterozygous WNT1 mutations. *Bone.* 2014; 67:63-70.
29. Won JY, Jang WY, Lee HR, Park SY, Kim WY, Park JH, Kim Y, Cho TJ. Novel missense loss-of-function mutations of WNT1 in an autosomal recessive Osteogenesis imperfecta patient. *Eur J Med Genet.* 2017; 60:411-415.
30. Janda CY, Waghray D, Levin AM, Thomas C, Garcia KC. Structural basis of Wnt recognition by Frizzled. *Science.* 2012; 337:59-64.

(Received February 1, 2018; Revised February 25, 2018; Accepted February 26, 2018)

Carotid strain measurement in patients with pseudoxanthoma elasticum – Hint for a different pathomechanism?

Sebastian Gorgonius Passon^{1,§,*}, Viviane Küllmar^{1,§}, Anna Katharina Blatzheim¹, Kristin Solveig Pausewang¹, Max Jonathan Stumpf¹, Doris Hendig², Martin Gliem³, Simon Pingel¹, Robert Schueler¹, Dirk Skowasch¹, Najib Schahab¹, Georg Nickenig¹, Christian Alexander Schaefer¹

¹Department of Internal Medicine II- Cardiology, Pulmonology and Angiology, University Hospital Bonn, Bonn, Germany;

²Institute for Laboratory and Transfusion Medicine, Heart and Diabetes Center North Rhine-Westphalia, University Hospital of the Ruhr University of Bochum, Bad Oeynhausen, Germany;

³Department of Ophthalmology, University of Bonn, Bonn, Germany.

Summary

Pseudoxanthoma Elasticum (PXE), caused by autosomal-recessive mutations in the ATP-binding cassette transporter (ABCC6) gene, is known for high prevalence of atherosclerosis. A novel method investigating elastic properties of arteries in atherosclerotic patients is vascular strain analysis. We compared 44 PXE patients with peripheral artery disease (PXE+PAD group) with 50 control patients, each 25 without (control group) and with PAD (PAD group). All participants underwent an angiological examination including ankle-brachial index (ABI) and were examined with speckle-tracking based vascular strain analysis of common carotid arteries, measuring radial displacement (r.Dis), radial velocity (r.Vel), radial strain (r.Str), circumferential strain (c.Str), radial strainrate (r.SR) and circumferential strainrate (c.SR). We found significant lower ABI in patients with PXE compared to all other groups (each $p < 0.01$). The vascular strain analysis resulted in significantly decreased values in the PAD group compared to PXE with PAD (each $p \leq 0.01$) and controls without PAD (each $p \leq 0.05$), whereas no significant difference could be found between PXE+PAD and controls without PAD. We found significant negative correlations between low strain values and a higher prevalence of PAD in non-PXE patients (r.Str $r = -0.34$; c.Str $r = -0.35$; r.SR: $r = -0.51$; c.SR: $r = -0.53$). In conclusion, PXE patients had similar values for arterial stiffness compared to controls without PAD in vascular strain analysis. In this group, arterial stiffness parameters were significantly higher compared to non-PXE PAD patients. It is worth to discuss whether PAD-like manifestations in PXE are a different kind of disease and might need another strategy in diagnostics and therapy.

Keywords: Pseudoxanthoma Elasticum (PXE), carotid strain, vascular stiffness, ATP-binding cassette transporter (ABCC6), peripheral artery disease (PAD)

1. Introduction

Pseudoxanthoma Elasticum (PXE) is a rare, autosomal

recessive disorder with a prevalence of 1:25,000 to 1:100,000 caused by loss of function mutations in the ATP-binding cassette transporter (ABCC6) gene (1–4). It is also known as Grönblad-Strandberg syndrome and represents a systemic mineralization disorder due to a defect in the ABCC6 on the basolateral cell surface, which influences the peripheral concentration of pyrophosphate (PPi) in healthy persons (5,6). As PPi is a strong inhibitor of calcification processes and PXE patients had lower levels of PPi, this is a potential reason for the observed manifestations including

Released online in J-STAGE as advance publication February 26, 2018.

[§]These authors contributed equally to this work.

*Address correspondence to:

Sebastian Passon, Department of Internal Medicine II - Cardiology, Pulmonology and Angiology, University of Bonn, Sigmund-Freud Str. 25, 53127 Bonn, Germany.
E-mail: s.passon@uni-bonn.de

calcification and fragmentation of elastic fibres and soft connective tissues (6–9). Histologic studies revealed a thickening and calcification of Bruch's membrane, mineralisation and fragmentation in the mid-dermal layer elastic fibres and several vascular changes in different organs (*i.e.* heart, muscles, lung, kidney *etc.*) (2,4,10,11). Neither the signal pathways from loss of function mutation of ABCC6 to structural changes in soft tissues are known, nor is the underlying pathomechanism of functional alterations in the vessel wall or other organ systems completely understood (7,12).

Characteristic clinical symptoms of PXE include typical skin signs including yellowish papules and inelastic skinfolds especially on the lateral neck, the axillae and the popliteal fossae (1,2). Other characteristic signs are ophthalmologic alterations like angoid streaks or retinal pigment epithelium atrophy and cardiovascular manifestations such as a high prevalence of peripheral artery disease (PAD), intermittent claudication or chronic vascular occlusions which are mostly localized in the lower limb specially the femoral arteries (13–15). Atherosclerosis and PAD are associated with changes in vascular elasticity as observed in non-PXE patients (16). These changes may lead to hypertension and a decreased vascular compliance, which is documented as an independent risk factor for cardiovascular events (17–19). There are only few existing studies with PXE patients in which arterial stiffness is investigated with conventional methods like carotid-femoral pulse wave velocity or distensibility coefficient analysis (20,21). Results vary a lot between different authors and cohorts. The findings are contradictory as they spread between a more elastic artery, no changes or stiffer arteries at different sites of the arterial tree (1,9).

Speckle-tracking based vascular strain analysis is a novel method to examine arterial elasticity used since 2010 and has been demonstrated as a feasible and reliable method (22,23). The technique is easy to apply, provides information on the mechanical properties of arteries and is proven to be as a superior method for detecting patients with cardiovascular risks and subclinical atherosclerosis (24–26).

Purpose of our study was to examine the elastic properties of carotid arteries in PXE patients with the technique of vascular strain imaging to generate more information about mechanical changes caused by the mineralisation disorder.

2. Materials and Methods

2.1. Patients

For this retrospective register data analysis, we enrolled 94 subjects. 44 patients had a clinical or a combined clinical and genetical evidence of PXE. The clinical

evidence consists of characteristic skin lesions and typical eye and retina changes, whereas the combined evidence implies a genetical evidence of a biallelic loss of function mutation in the ABCC6 gene, assessed in the Institute for Laboratory and Transfusion Medicine at the Heart and Diabetes Centre Bad Oeyenhausen and at least one clinical sign as described above (14).

PAD was defined by ultrasonographic findings (*i.e.* calcified or inhomogeneous vessel wall deformations and plaques) or an ankle-brachial index (ABI) lower than 0.9 or higher than 1.3.

All 44 PXE patients had a proven PAD, including 11 patients with a chronic vascular occlusion (CVO), and were classified as "PXE+PAD". Patients with PXE without a proven PAD were excluded due to a very small number of patients. 25 non PXE patients were confirmed to have PAD and were rated as "PAD". The last group named "control" comprised 25 patients without neither signs of PAD nor of PXE. For baseline characteristics see Table 1.

2.2. Angiological examination

Angiological examinations took place in the Department for Internal Medicine II at the University Hospital Bonn. Common cardiovascular risk factors such as age, sex, smoking, diabetes, hypertonia, fat metabolism disorder and an existing coronary artery disease were recorded from our register data.

The investigated functional parameters were the ankle-brachial index (ABI) (Vasoquant VQ 4000: ELCAT, Wolfratshausen, Germany), the pulse-wave index (PWI) and the central pulse wave velocity (cPWV) (PWI and cPWV: Angio Experience Pro 8: Sonoteknik Karl Glantschnig GmbH, Kärnten, Austria). The PWI is a novel marker which might allow an early detection of subclinical atherosclerosis and is calculated as follows (27):

$$PWI = \frac{\text{higher amplitude of upper limb pulse wave}}{\text{amplitude of corresponding lower limb pulse wave}} \times \text{peak time}$$

Values greater than 180 were considered as pathological (28).

All patients underwent ultrasonographic examination performed by experienced physicians. (iE 33 xMatrix Echocardiography System equipped with a L11-3 Line Array Scanner, Philips Healthcare, PC Best, Netherlands) Bilateral images and maximum velocities of the common carotid artery (CCA), internal and external carotid artery, and vertebral artery were acquired. Lower limb arteries were also examined. Additionally, during ultrasound examination an ECG-triggered sequence of both CCA from all enrolled patients was captured over five cardiac cycles during a short breath hold for the following vascular strain analysis.

Table 1. Baseline characteristics

Items	PXE+PAD (n = 44)	Control (n = 25)	PAD (n = 25)	ANOVA p-value	PXE+PAD vs. Control	PXE+PAD vs. PAD	PAD vs. Control
Age (years)	54.25 ± 8.93	49.32 ± 9.76	53.60 ± 6.07	0.064			
BMI	28.19 ± 6.16	24.10 ± 3.52	23.28 ± 4.46	0.014	0.03	0.24	0.96
Sex (male) [%]	19 [43.2]	11 [44.0]	12 [48.0]	0.925			
Smoking [%]	20 [45.5]	6 [24.0]	12 [48.0]	0.381			
Diabetes [%]	1 [2.3]	0 [0.0]	2 [8.0]	0.252			
Hypertension [%]	19 [43.2]	8 [32.0]	14 [56.0]	0.231			
Dyslipidämia [%]	18 [40.9]	4 [16.0]	9 [36.0]	0.121			
Coronary heart disease [%]	5 [11.4]	0 [0.0]	5 [20.0]	0.101			

PXE = patients with pseudoxanthoma elasticum; PAD = peripheral artery disease; BMI = body mass index.

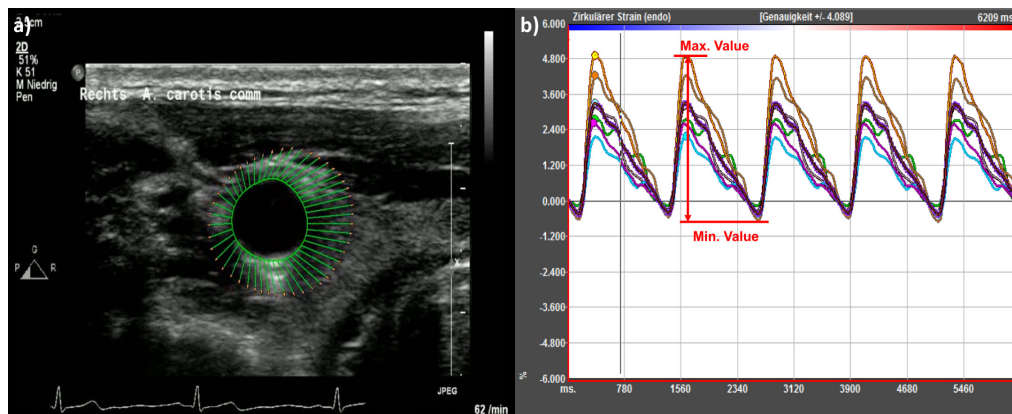


Figure 1. Carotid strain analysis. a) Region of interest (ROI) marked by green line with vectors of vessel movement. b) Graphic display of 6 parts of circumferential strain by software.

2.3. Vascular strain analysis

As we described previously, vascular strain analysis was performed at an offline work station equipped with Image Arena™ Version 4.6 Build 4.6.2.12 (TomTec Imaging Systems, Unterschleissheim, Germany) (29). After choosing the sequence with the least motion artefacts, a "region of interest" (ROI) was placed by marking indicator points in the intima-media complex so that the software was able to calculate the circumferential contour of the vessel (30,31) (Figure 1a). Adequate speckle-tracking based analysis was verified by the operator and adjusted if necessary (22). The vessel wall was divided automatically into six parts and local parameters were assessed. For further analysis, the six values were averaged (Figure 1b). For characterisation of the arterial motion and deformation six parameters were recorded: radial displacement (r.Dis) (mm) describes the motion of the entire vessel wall, whereas the radial strain (r.Str) (%) represents the radial expansion during the cardiac cycle. Circumferential strain (c.Str) (%) describes the circumferential stretching and constriction of the artery. For these parameters the maximum and minimum values were recorded by the software and the amplitudes were calculated (26,31). Radial velocity (r.Vel) (cm/s), radial strain rate (r.SR) (1/s) and circumferential strain rate (c.SR) (1/s) correspond as temporal derivation to the dynamic motion of the

Table 2. Reliability analysis with interclass correlation coefficient (ICC)

Items	Interrater ICC (95% CI)	Intrater ICC (95% CI)
r.Str (%)	0.895 (0.755-0.952)	0.891 (0.745-0.955)
c.Str (%)	0.958 (0.897-0.983)	0.940 (0.855-0.976)
r.SR (%)	0.883 (0.729-0.952)	0.823 (0.606-0.926)
c.SR (%)	0.980 (0.950-0.992)	0.964 (0.912-0.986)

r.Str = radial strain; c.Str = circumferential strain; r.SR = radial strain rate; c.SR = circumferential strain rate.

vessel wall. For these parameters, the maximum value was recorded.

To consider stabilizing effects of current statin therapy on radial strain in PAD patients we compared existing statin therapy between PXE+PAD group and PAD group but found no significant difference (40/43 (93%) vs. 23/25 (92%); $p = 0.876$) (29).

A reliability analysis for vascular strain measurement was performed by calculating the interclass correlation coefficient (ICC) for 20 random patients by two experienced observers. The results are displayed in Table 2 and for all investigated strain values (r.Str, c.Str, r.SR and c.SR) we found good agreement for inter- and intra-reader reliability.

2.4. Statistical analysis

Statistical Analysis was performed with SPSS 23®

Table 3. Angiological examination with arterial stiffness analysis

Items	PXE+PAD (n = 44)	Control (n = 25)	PAD (n = 25)	ANOVA p-value	PXE+PAD vs. Control	PXE+PAD vs. PAD	PAD vs. Control
ABI	0.83 ± 0.19	1.09 ± 0.07	1.04 ± 0.12	0.001	0.001	0.001	0.373
PWI	259.20 ± 124.05	115.47 ± 33.83	181.80 ± 180.77	0.002	0.001	0.349	0.397
cPWV (m/s)	5.10 ± 1.04	5.65 ± 1.14	6.27 ± 2.07	0.058			
r.Vel (cm/s)	0.07 ± 0.08	0.11 ± 0.04	0.07 ± 0.04	0.048	0.06	0.982	0.003
r.Dis (mm)	0.15 ± 0.05	0.15 ± 0.05	0.11 ± 0.06	0.008	0.997	0.014	0.041
r.Str (%)	5.30 ± 1.72	4.73 ± 1.56	3.62 ± 1.68	0.001	0.396	0.001	0.069
c.Str (%)	4.05 ± 1.44	4.09 ± 1.47	2.90 ± 1.73	0.007	0.991	0.014	0.026
r.SR (1/s)	0.39 ± 0.11	0.36 ± 0.10	0.25 ± 0.10	0.001	0.685	0.001	0.001
c.SR (1/s)	0.28 ± 0.10	0.30 ± 0.11	0.18 ± 0.10	0.001	0.799	0.001	0.001

ABI = ankle brachial index; PWI = pulse wave index; cPWV = central pulse wave velocity; r.Vel = radial velocity; r.Dis = radial displacement; r.Str = radial strain; c.Str = circumferential strain; r.SR = radial strain rate; c.SR = circumferential strain rate.

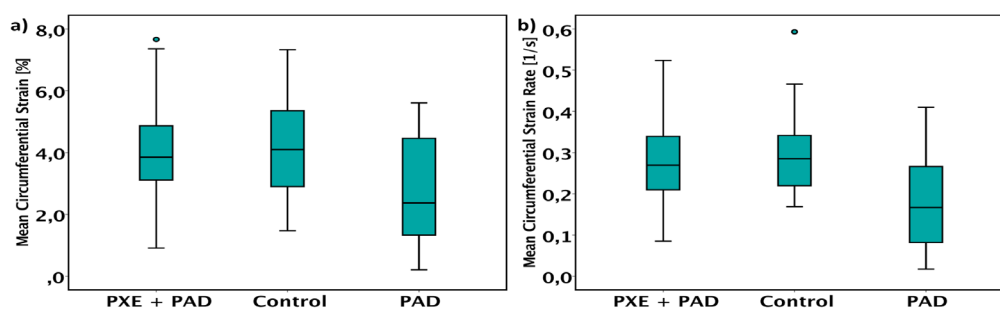


Figure 2. Analysis of circumferential strain and circumferential strain rate. a) Comparison of circumferential strain [%] between all groups. (PXE+PAD: 4.05 ± 1.44 vs. Control: 4.09 ± 1.47 vs. PAD: 2.90 ± 1.73; $p = 0.007$). **b)** Comparison of circumferential strain rate [1/s] between all groups. (PXE+PAD: 0.28 ± 0.10 vs. Control: 0.30 ± 0.11 vs. PAD: 0.18 ± 0.10; $p = 0.004$).

(SPSS Inc. Chicago, IL, USA) and all values were presented as mean ± standard deviation. A significant p -value was assumed as a two-sided $p < 0.05$. To investigate distributions of non-parametric variables Chi² test was applied, whereas parametric variables were explored with ANOVA test in case of comparison of more than two groups. As post-hoc analysis we made use of Tahame-T2 test for inhomogeneous variances and a Scheffé procedure for homogenous variances. In case of comparison of two groups a Gaussian distribution was verified. For this purpose, a t -test was used, while in non-Gaussian distributions a Mann-Whitney- U -test was applied. Correlation analysis was performed with Pearson's test for parametric variables and Spearman-Rho test for non-parametric variables.

3. Results

Patients' baseline characteristics are displayed in Table 1. We found no differences in age and cardiovascular risk profiles.

3.1. Angiological parameters

Analysing functional angiological parameters we found significant differences in ABI ($p < 0.01$) and post-hoc analysis revealed lower ABI in the PXE+PAD group compared to all other groups (each $p < 0.01$). Likewise,

the ANOVA test for PWI resulted in a significant overall difference ($p < 0.01$) and in pairwise analysis the PXE+PAD group had significant higher values compared to control group (259.20 ± 124.05 vs. 115.47 ± 33.83; $p < 0.01$). (Table 3)

3.2. Vascular stiffness analysis

Exploration of vascular stiffness parameters presented a trend for cPWV to be higher in the PAD group ($p = 0.06$). Results of vascular strain analysis are also displayed in Table 3. For all six parameters the ANOVA test produced significant p -values for overall differences (r.Dis: $p < 0.01$; r.Str: $p < 0.01$; c.Str: $p < 0.01$; r.Vel: $p = 0.048$; r.SR: $p < 0.01$; c.SR: $p < 0.01$). For each mentioned strain value, except radial velocity and radial strain in comparison of PAD to control, we found significant lower values in the PAD group compared with PXE+PAD (r.Dis: $p = 0.01$; r.Str: $p < 0.01$; c.Str: $p = 0.01$; r.SR: $p < 0.01$; c.SR: $p < 0.01$) and controls (r.Dis: $p = 0.04$; r.Str: $p = 0.07$; c.Str: $p = 0.03$; r.SR: $p < 0.01$; c.SR: $p < 0.01$) in post-hoc analysis, whereas no significant difference could be found between PXE+PAD and controls without PAD (r.Dis: $p = 0.99$; r.Str: $p = 0.40$; c.Str: $p = 0.99$; r.SR: $p = 0.69$; c.SR: $p = 0.80$) (Figure 2).

Across all groups we found weak but significant negative correlations for cPWV and r.SR ($r = -0.362$; $p <$

Table 4. Subgroup analysis

Items	PXE+PAD (n = 33)	PXE+CVO (n = 11)	p-value
Age	53.84 ± 9.39	55.73 ± 8.14	0.577
ABI	0.90 ± 0.15	0.66 ± 0.20	0.000
PWI	237.70 ± 119.14	353.80 ± 108.54	0.047
cPWV (m/s)	5.27 ± 1.15	4.67 ± 0.58	0.243
r.Vel (cm/s)	0.06 ± 0.09	0.09 ± 0.07	0.226
r.Dis (mm)	0.14 ± 0.05	.15 ± 0.06	0.563
r.Str (%)	5.24 ± 1.54	5.51 ± 2.28	0.668
c.Str (%)	4.01 ± 1.35	4.20 ± 1.77	0.712
r.SR (1/s)	0.38 ± 0.10	0.41 ± 0.14	0.474
c.SR (1/s)	0.27 ± 0.09	0.30 ± 0.12	0.325

ABI = ankle brachial index; PWI = pulse wave index; cPWV = central pulse wave velocity; r.Vel = radial velocity; r.Dis = radial displacement; r.Str = radial strain; c.Str = circumferential strain; r.SR = radial strain rate; c.SR = circumferential strain rate.

0.01) and cPWV and c.SR ($r = -0.329$; $p = 0.02$). Within the non-PXE group (controls; PAD) we observed highly significant correlations for the existence of PAD and r.Str ($r = -0.34$; $p = 0.02$), PAD and c.Str ($r = -0.345$; $p = 0.01$), PAD and r.SR ($r = -0.51$; $p < 0.01$) and PAD and c.SR ($r = -0.53$; $p < 0.01$).

3.3. Subgroup analysis

For a subgroup analysis, the PXE+PAD group is divided into a group with PAD and another group with chronic vascular occlusions (CVO). ABI was lower in the PXE+CVO group compared to the PXE+PAD subgroup (0.66 ± 0.20 vs. 0.90 ± 0.15 ; $p < 0.01$) and PWI was higher in the PXE+CVO group (353.80 ± 168.54 vs. 237.70 ± 119.14 ; $p = 0.047$). Parameters for vascular stiffness did not differ between these groups (Table 4).

4. Discussion

The present study demonstrated similar carotid strain values of PXE patients with PAD and control patients without PAD. Contrary to our expectation PXE patients with PAD presented higher carotid strain values compared to "normal" PAD patients, even if they suffered from severe PAD with a high amount of chronic vascular occlusions, as we already have demonstrated (15). Additionally, subgroup analysis revealed no differences between PXE patients with PAD and PXE patients with CVO, even their strain values are consistent with the results of healthy controls.

In 2003 Germain *et al.* described a more elastic radial artery, as well as less carotid wall stress in PXE patients assessed with conventional methods of vascular stiffness measurement (21). As demonstrated by Kornet *et al.*, PXE patients show a stable compliance coefficient of carotid arteries with increasing age in comparison to controls with decreasing coefficients over time. (9). Leftheriotis *et al.* published in 2011 that patients with lower ABI were older and had a higher carotid femoral PWV, but they were not able to prove

that PWV could serve as predictor of ABI (20). To our knowledge, the latest study regarding the vascular stiffness of PXE patients, was performed by Campens *et al.* in 2013 and showed that PXE had a higher PWV compared to controls. They concluded, that PXE patients' aorta was stiffer (1).

Studies with non PXE-patients described an association of arterial stiffness with PAD in connected with higher values for PWV (16). In addition, Podgórski *et al.* already performed vascular strain analysis to examine arterial calcification (26). Bjällmark *et al.* and Park *et al.* also revealed the association between the novel parameters and subclinical atherosclerosis in which they saw vascular strain imaging as a superior method (22,32).

Another disease with a high prevalence of PAD is obstructive sleep apnoea. It is associated with low vascular stiffness values assessed by speckle tracking strain analysis (33,34). Following these studies, we expected low strain values in PXE patients as well. In contrast to our expectation PXE patients had inconspicuous values similar to controls without PAD.

The first histomorphological study of three PXE patients was performed in 1978 where Mendelson *et al.* described fragmented and elastic laminae in the muscle arteries followed by vascular calcification (35). In the last decade studies from Nolte *et al.* and Miki *et al.* also discussed degenerated, fragmented and calcified elastic fibres (10,36). An autopsy study of two PXE patients was published in 2003 by Gheduzzi *et al.* In their studied cases they found similar damages in arteries and veins including fragmentation and mineralization of elastic fibres. Additionally they observed changes in collagen fibrils (37). To our knowledge, the latest histomorphological study of the vascular system was accomplished in 2004 by Kornet *et al.* Besides the well-known fragmented elastic fibres and calcifications processes, which were found especially in the media of the arterial wall, they found increased quantity of proteoglycans in the media which may lead to a diminished arterial stiffness (9).

PAD in non PXE patients is predominantly characterized as a process affecting the intima of the vessel wall with endothelial dysfunction, lipid deposition, local inflammation, affection the smooth muscles and remodelling of the extracellular matrix resulting in an atherosclerotic plaque (38). Whereas histomorphological changes regarding PAD in PXE patients are mainly described in the media of the vessel wall and the surrounding elastic laminae (9,35).

Having in mind the described histomorphological changes, a possible explanation for the clinical results of vascular strain analysis could be a combined pathomechanism. On the one hand, the calcification and mineralization of the arterial wall as observed in non-PXE PAD patients, increase the arterial stiffness. On the other hand, the combined effect of damaged arterial wall

architecture – caused by fragmentation and degeneration of elastic fibres – and changed vessel wall composition with more proteoglycans leads to decreased arterial stiffness. As final result of the antagonizing processes, it is understandable that vascular stiffness measured by vascular strain analysis did not change within PXE patients with progressive PAD. In contrast, it seems to be stable and similar to people without PAD. It is worth to be discussed if PAD-like manifestations in PXE, with its separate pathomechanism, are a fundamentally different disease than PAD caused by "normal" atherosclerosis. Following this consideration, we should think about other diagnostic strategies for detection of CVO.

Limitations of the present study imply a lack of information due to the design as register study, such as baseline characteristics and measurement results, but for all patients age, ABI and vascular strain data was completely recorded. Another limitation is the small number of patients. In further studies, we would like to confirm our results with more patients and controls to validate the unexpected inconspicuous strain values of PXE patients with PAD and investigate the change of vascular strain in patients with PXE over time.

5. Conclusion

Assessed by vascular strain analysis of common carotid arteries PXE patients had unremarkable values for arterial stiffness compared to controls without PAD. Their arterial stiffness parameters were significantly better than in non-PXE PAD patients, even if they had a more servant PAD. In addition, we found a negative correlation in non-PXE patients between low strain values and a higher prevalence of PAD. We have to consider a combined pathway of vascular alteration as well as PXE as a fundamentally different disease which needs other therapy strategies in those patients.

Acknowledgement

We would like to thank Sonotechnik Austria for providing the Angio Experience Pro 8.

References

- Campens L, Vanakker OM, Trachet B, Segers P, Leroy BP, De Zaeijtj J, Voet D, De Paepe A, De Backer T, De Backer J. Characterization of cardiovascular involvement in pseudoxanthoma elasticum families. *Arterioscler Thromb Vasc Biol.* 2013; 33:2646-2652.
- Marconi B, Bobyr I, Campanati A, Molinelli E, Consales V, Brisigotti V, Scarpelli M, Racchini S, Offidani A. Pseudoxanthoma elasticum and skin: Clinical manifestations, histopathology, pathomechanism, perspectives of treatment. *Intractable rare Dis Res.* 2015; 4:113-122.
- Koblos G, Andrikovics H, Prohaszka Z, Tordai A, Varadi A, Aranyi T. The R1141X loss-of-function mutation of the ABCC6 gene is a strong genetic risk factor for coronary artery disease. *Genet Test Mol Biomarkers.* 2010; 14:75-78.
- Gliem M, Fimmers R, Müller PL, Brinkmann CK, Finger RP, Hendig D, Holz FG, Charbel Issa P. Choroidal Changes Associated With Bruch Membrane Pathology in Pseudoxanthoma Elasticum. *Am J Ophthalmol.* 2014; 158:198-207.e3.
- Li Q, Jiang Q, Uitto J. Ectopic mineralization disorders of the extracellular matrix of connective tissue: Molecular genetics and pathomechanisms of aberrant calcification. *Matrix Biol.* 2014; 33:23-28.
- Jansen RS, Duijst S, Mahakena S, Sommer D, Szeri F, Váradi A, Plomp A, Bergen AA, Oude Elferink RP, Borst P, van de Wetering K. ABCC6-mediated ATP secretion by the liver is the main source of the mineralization inhibitor inorganic pyrophosphate in the systemic circulation – Brief report. *Arterioscler Thromb Vasc Biol.* 2014; 34:1985-1989.
- Lefthériotis G, Omarjee L, Le Saux O, Henrion D, Abraham P, Prunier F, Willoteaux S, Martin L. The vascular phenotype in Pseudoxanthoma elasticum and related disorders: contribution of a genetic disease to the understanding of vascular calcification. *Front Genet.* 2013; 4:4.
- Jansen RS, Küçükosmanoglu A, de Haas M, Saptho S, Otero JA, Hegman IE, Bergen AA, Gorgels TG, Borst P, van de Wetering K. ABCC6 prevents ectopic mineralization seen in pseudoxanthoma elasticum by inducing cellular nucleotide release. *Proc Natl Acad Sci U S A.* 2013; 110:20206-20211.
- Kornet L, Bergen AAB, Hoeks APG, Cleutjens JP, Oostra RJ, Daemen MJ, van Soest S, Reneman RS. In patients with pseudoxanthoma elasticum a thicker and more elastic carotid artery is associated with elastin fragmentation and proteoglycans accumulation. *Ultrasound Med Biol.* 2004; 30:1041-1048.
- Miki K, Yuri T, Takeda N, Takehana K, Iwasaka T, Tsubura A. An autopsy case of pseudoxanthoma elasticum: Histochemical characteristics. *Med Mol Morphol.* 2007; 40:172-177. 5
- Pingel S, Passon SG, Pausewang KS, Blatzheim AK, Pizarro C, Tuleta I, Gliem M, Charbel Issa P, Schahab N, Nickenig G, Skowasch D, Schaefer CA. Pseudoxanthoma elasticum – Also a lung disease? the respiratory affection of patients with pseudoxanthoma elasticum. *PLoS One.* 2016;11: e0162337.
- Hosen MJ, Coucke PJ, Le Saux O, De Paepe A, Vanakker OM. Perturbation of specific pro-mineralizing signalling pathways in human and murine pseudoxanthoma elasticum. *Orphanet J Rare Dis.* 2014; 9: 66.
- Finger RP, Issa PC, Ladewig M, Götting C, Holz FG, Scholl HP. Fundus autofluorescence in Pseudoxanthoma elasticum. *Retin (Philadelphia, Pa).* 2009; 29:1496-1505.
- Uitto J, Jiang Q, Váradi A, Bercovitch LG, Terry SF. Pseudoxanthoma elasticum: Diagnostic features, classification, and treatment options. *Expert Opin orphan drugs.* 2014; 2:567-577.
- Pingel S, Pausewang KS, Passon SG, Blatzheim AK, Gliem M, Charbel Issa P, Hendig D, Horlbeck F, Tuleta I, Nickenig G, Schahab N, Skowasch D, Schaefer CA. Increased vascular occlusion in patients with pseudoxanthoma elasticum. *Vasa.* 2017; 46:47-52.
- van Popele NM, Grobbee DE, Bots ML, Asmar R, Topouchian J, Reneman RS, Hoeks AP, van der Kuip DA,

- Hofman A, Witteman JC. Association between arterial stiffness and atherosclerosis: the Rotterdam Study. *Stroke*. 2001; 32:454-460.
17. Liao D, Arnett DK, Tyroler HA, Riley WA, Chambless LE, Szklo M, Heiss G. Arterial stiffness and the development of hypertension: The ARIC study. *Hypertension*. 1999; 34:201-206.
 18. Yang EY, Dokainish H, Virani SS, Misra A, Pritchett AM, Lakkis N, Brunner G, Bobek J, McCulloch ML, Hartley CJ, Ballantyne CM, Nagueh SF, Nambi V. Segmental Analysis of Carotid Arterial Strain Using Speckle-Tracking. *J Am Soc Echocardiogr*. 2011; 24:1276-1284. e5.
 19. Laurent S. Arterial stiffness: Intermediate or surrogate endpoint for cardiovascular events? *Eur Heart J*. 2005; 26:1152-1154.
 20. Lefthériotis G, Abraham P, Le Corre Y, Le Saux O, Henrion D, Ducluzeau PH, Prunier F, Martin L. Relationship between ankle brachial index and arterial remodeling in pseudoxanthoma elasticum. *J Vasc Surg*. 2011; 54:1390-1394.
 21. Germain DP, Boutouyrie P, Laloux B, Laurent S. Arterial remodeling and stiffness in patients with pseudoxanthoma elasticum. *Arterioscler Thromb Vasc Biol*. 2003; 23:836-841.
 22. Bjällmark A, Lind B, Peolsson M, Shahgaldi K, Brodin LK, Nowak J. Ultrasonographic strain imaging is superior to conventional non-invasive measures of vascular stiffness in the detection of age-dependent differences in the mechanical properties of the common carotid artery. *Eur J Echocardiogr*. 2010; 11:630-636.
 23. Yang WI, Ha JW. Non-invasive assessment of vascular alteration using ultrasound. *Clin Hypertens*. 2015; 21:25.
 24. Catalano M, Lamberti-Castronuovo A, Catalano A, Filocamo D, Zimbalatti C. Two-dimensional speckle-tracking strain imaging in the assessment of mechanical properties of carotid arteries: Feasibility and comparison with conventional markers of subclinical atherosclerosis. *Eur J Echocardiogr*. 2011; 12:528-535.
 25. Zou C, Jiao Y, Li X, Zheng C, Chen M, Hu C. Role of ultrasonography in the evaluation of correlation between strain and elasticity of common carotid artery in patients with diabetic nephropathy. *Int J Clin Exp Med*. 2015; 8:17765-17772.
 26. Podgórski M, Grzelak P, Szymczyk K, Szymczyk E, Drozd J, Stefańczyk L. Peripheral vascular stiffness, assessed with two-dimensional speckle tracking versus the degree of coronary artery calcification, evaluated by tomographic coronary artery calcification index. *Arch Med Sci*. 2015; 11:122-129.
 27. Tuleta I, Pingel S, Biener L, Pizarro C, Hammerstingl C, Öztürk C, Schahab N, Grohé C, Nickenig G, Schaefer C, Skowasch D. Atherosclerotic Vessel Changes in Sarcoidosis. *Adv Exp Med Biol*. 2015; 910:23-30.
 28. Pizarro C, Schaefer C, Kimeu I, Pingel S, Horlbeck F, Tuleta I, Nickenig G, Skowasch D. Underdiagnosis of obstructive sleep apnoea in peripheral arterial disease. *Respiration*. 2015; 89:214-220.
 29. Schaefer CA, Blatzheim AK, Passon SG, Pausewang KS, Schahab N, Nickenig G, Skowasch D, Schueler R, Hammerstingl C, Pingel S. Modulation of carotid strain by statin therapy in atherosclerosis patients. *Vasa*. 2017; 79:1-8.
 30. Yang JW, Cho KI, Kim JH, Kim SY, Kim CS, You GI, Lee JY, Choi SY, Lee SW, Kim HS, Heo JH, Cha TJ, Lee JW. Wall shear stress in hypertensive patients is associated with carotid vascular deformation assessed by speckle tracking strain imaging. *Clin Hypertens*. 2014; 20:10.
 31. Charwat-Resl S, Niessner A, Mueller M, Bartko PE, Giurgea GA, Zehetmayer S, Willfort-Ehringer A, Koppensteiner R, Schlager O. Speckle-tracking-based evaluation of vascular strain at different sites of the arterial tree in healthy adults. *Ultraschall Med*. 2016; 37:503-508.
 32. Park HE, Cho GY, Kim HK, Kim YJ, Sohn DW. Validation of circumferential carotid artery strain as a screening tool for subclinical atherosclerosis. *J Atheroscler Thromb*. 2012; 19:349-356.
 33. Schaefer CA, Adam L, Weisser-Thomas J, Pingel S, Vogel G, Klarman-Schulz U, Nickenig G, Pizarro C, Skowasch D. High prevalence of peripheral arterial disease in patients with obstructive sleep apnoea. *Clin Res Cardiol*. 2015; 104:719-726.
 34. Tuleta I, Skowasch D, Krycki J, Pizarro C, Hammerstingl C, Weber M, Schahab N, Nickenig G, Schaefer C, Pingel S. Obstructive Sleep Apnea Is Related to Increased Arterial Stiffness in Ultrasound Speckle-Tracking Analysis. *Adv Exp Med Biol*. 2016; 910:9-14.
 35. Mendelsohn G, Bulkley BH, Hutchins GM. Cardiovascular manifestations of Pseudoxanthoma elasticum. *Arch Pathol Lab Med*. 1978; 102:298-302.
 36. Nolte KB. Sudden cardiac death owing to pseudoxanthoma elasticum: A case report. *Hum Pathol*. 2000; 31:1002-1004.
 37. Gheduzzi D, Sammarco R, Quaglino D, Bercovitch L, Terry S, Taylor W, Ronchetti IP. Extracutaneous ultrastructural alterations in pseudoxanthoma elasticum. *Ultrastruct Pathol*. 2003; 27:375-384.
 38. Badimon L, Vilahur G. Thrombosis formation on atherosclerotic lesions and plaque rupture. *J Intern Med*. 2014; 276:618-632.

(Received January 7, 2018; Revised February 18, 2018; Accepted February 19, 2018)

Alzheimer's disease pathology in Nasu-Hakola disease brains

Jun-ichi Satoh^{1,*}, Yoshihiro Kino¹, Motoaki Yanaizu¹, Yuko Saito²

¹Department of Bioinformatics and Molecular Neuropathology, Meiji Pharmaceutical University, Tokyo, Japan;

²Department of Laboratory Medicine, National Center Hospital, NCNP, Tokyo, Japan.

Summary

Nasu-Hakola disease (NHD) is a rare autosomal recessive disorder, characterized by progressive presenile dementia and formation of multifocal bone cysts, caused by genetic mutations of either triggering receptor expressed on myeloid cells 2 (*TREM2*) or TYRO protein tyrosine kinase binding protein (*TYROBP*), alternatively named DNAX-activation protein 12 (*DAP12*), both of which are expressed on microglia in the brain and form the receptor-adaptor complex that chiefly recognizes anionic lipids. *TREM2* transmits the signals involved in microglial survival, proliferation, chemotaxis, and phagocytosis. A recent study indicated that a loss of *TREM2* function causes greater amounts of amyloid- β ($A\beta$) deposition in the hippocampus of a mouse model of Alzheimer's disease (AD) owing to a dysfunctional response of microglia to amyloid plaques, suggesting that *TREM2* facilitates $A\beta$ clearance by microglia. *TREM2/DAP12*-mediated microglial response limits diffusion and toxicity of amyloid plaques by forming a protective barrier. However, the levels of $A\beta$ deposition in postmortem brains of NHD, where the biological function of the *TREM2/DAP12* signaling pathway is completely lost, remain to be investigated. By immunohistochemistry, we studied the expression of $A\beta$ and phosphorylated tau (p-tau) in the frontal cortex and the hippocampus of five NHD cases. Although we identified several small $A\beta$ -immunoreactive spheroids, amyloid plaques were almost undetectable in NHD brains. We found a small number of p-tau-immunoreactive neurofibrillary tangle (NFT)-bearing neurons in NHD brains. Because AD pathology is less evident in NHD than the full-brown AD, it does not play an active role in the development of NHD.

Keywords: Alzheimer's disease, amyloid- β , Nasu-Hakola disease, phosphorylated tau

1. Introduction

Nasu-Hakola disease (NHD), also designated polycystic lipomembranous osteodysplasia with sclerosing leukoencephalopathy (PLOS; OMIM 221770), is a rare autosomal recessive disorder, characterized by progressive presenile dementia and formation of multifocal bone cysts, caused by genetic mutations of either triggering receptor expressed on myeloid cells 2 (*TREM2*) or TYRO protein tyrosine kinase binding protein (*TYROBP*), alternatively named DNAX-

activation protein 12 (*DAP12*), both of which are expressed on microglia in the brain (1). Clinically, the patients with NHD show recurrent bone fractures during the third decade of life, and a frontal lobe syndrome during the fourth decade of life, and progressive dementia and death until the fifth decade of life (2). Pathologically, the brains of NHD patients exhibit extensive demyelination designated leukoencephalopathy, astrogliosis, accumulation of axonal spheroids, and remarkable activation of microglia predominantly in the white matter of frontal and temporal lobes and the basal ganglia (3). *TREM2*, expressed exclusively on microglia in the brain, serves as a receptor for anionic lipids, lipoproteins and apolipoproteins (4,5). *TREM2* forms a complex with *DAP12*, a signaling adaptor having an immunoreceptor tyrosine-based activation motif (ITAM) capable of recruiting the protein tyrosine kinase Syk that transduces a variety of downstream signals (6). *TREM2* transmits microglial signals involved in survival,

Released online in J-STAGE as advance publication February 26, 2018.

*Address correspondence to:

Dr. Jun-ichi Satoh, Department of Bioinformatics and Molecular Neuropathology, Meiji Pharmaceutical University, 2-522-1 Noshio, Kiyose, Tokyo, Japan.
E-mail: satoj@my-pharm.ac.jp

proliferation, chemotaxis, and phagocytosis (7).

Alzheimer's disease (AD) is characterized by the hallmark pathology comprised of widespread amyloid- β ($A\beta$) deposition, formation of neurofibrillary tangles (NFTs) composed of abnormally phosphorylated tau (p-tau), extensive neurodegeneration, and profound activation of microglia in the brain (8). Recent studies identified rare genetic variants of *TREM2*, such as R47H and R62H, closely associated with an increased risk for development of AD (9).

A recent study showed that *TREM2* deficiency generates greater amounts of $A\beta$ deposition in the hippocampus of 5XFAD mice, a mouse model of AD, due to a dysfunctional response of microglia to amyloid plaques, suggesting that *TREM2* facilitates $A\beta$ clearance by microglia (4). *TREM2* interacts with fibrillar $A\beta$ decorated with anionic and zwitterionic lipids (4). $A\beta$ -lipoprotein complexes are efficiently taken up by microglia, depending on *TREM2* (5). *TREM2* deficiency induces apoptosis of microglia and reduces recruitment of microglia around $A\beta$ plaques in the brains of mouse models of AD (4). Furthermore, microglial processes enriched in *TREM2* tightly surround early amyloid fibrils and plaques, and promote their compaction and insulation (10). In *TREM2*- or *DAP12*-deficient mouse models of AD, microglia showed a markedly reduced ability to envelope amyloid deposits, leading to an increase in less compact and more diffuse plaques associated with greater neuritic damage (10). These observations suggest that *TREM2*/*DAP12*-mediated microglial response limits diffusion and toxicity of amyloid plaques by forming a protective barrier (10,11). However, at present, the levels of $A\beta$ deposition in postmortem NHD brains, where the biological function of *TREM2*/*DAP12* signaling pathway is completely lost, remain unknown. A previous study reported a 48-year-old man of NHD with numerous senile plaques and neurofibrillary tangles throughout the cerebral cortex (12), suggesting that an impaired *TREM2*/*DAP12* signaling function facilitates $A\beta$ accumulation in the human brain. In the present study by immunohistochemistry, we investigate the expression of $A\beta$ and p-tau in NHD brains to clarify whether the Alzheimer's disease pathology is augmented in NHD.

2. Materials and Methods

2.1. Human brain tissues

The brain autopsies were performed at the National Center Hospital, National Center of Neurology and Psychiatry (NCNP), Japan and affiliated hospitals of Research Resource Network (RRN), Japan. The comprehensive examination by an established neuropathologist (YS) validated the pathological diagnosis. In all cases, written informed consent was

obtained. The Ethics Committee of the NCNP for the Human Brain Research and the Human Research Ethics Committee of the Meiji Pharmaceutical University (MPU) approved the present study.

For immunohistochemical studies, serial sections of the frontal cortex and the hippocampus were prepared from five AD patients, composed of a 68-year-old woman (AD1), a 68-year-old woman (AD3), a 56-year-old man (AD4), a 59-year-old man (AD5), and an 80-year-old man (AD8) and five NHD patients, composed of a 42-year-old man (NHD1), a 48-year-old woman (NHD2), a 44-year-old man (NHD3), a 32-year-old woman (NHD4), and a 38-year-old man (NHD5). The homozygous mutation of a single base deletion of 141G (c.141delG) in exon 3 of *DAP12* was identified in NHD1, NHD2, and NHD5, while the genetic analysis was not performed in NHD3 or NHD4. All AD cases were satisfied with the Consortium to Establish a Registry for Alzheimer's Disease (CERAD) criteria for diagnosis of definite AD (13). They were categorized into the stage C of amyloid deposition and the stage VI of neurofibrillary degeneration, following the Braak's staging (14).

2.2. Immunohistochemistry

After deparaffination, tissue sections were heated in 10 mM citrate sodium buffer, pH 6.0 by autoclave at 110°C for 15 min in a temperature-controlled pressure chamber (Biocare Medical, Pacheco, CA, USA). Then, they were treated at room temperature (RT) for 5 min with formic acid before labeling with anti- $A\beta$ antibody. They were incubated with phosphate-buffered saline (PBS) containing 10% normal goat serum at RT for 15 min to block non-specific staining, followed by incubation in a moist chamber at 4°C overnight with mouse monoclonal anti- $A\beta$ peptide antibody at a concentration of 1 $\mu\text{g}/\text{mL}$ (12B2; Immunobiological Laboratories, Gunma, Japan) that reacts with $A\beta$ 40, $A\beta$ 42, and $A\beta$ 43 or mouse monoclonal anti-phosphorylated tau (Ser202, Thr205) antibody at 0.025 $\mu\text{g}/\text{mL}$ (AT8; ThermoFisher Scientific, Waltham, MA, USA). After washing with PBS, tissue sections were incubated at RT for 30 min with alkaline phosphatase (AP)-conjugated secondary antibody (Nichirei, Tokyo, Japan), followed by exposure to Warp Red chromogen (Biocare Medical). For double immunolabeling, following heat treatment, tissue sections were treated with 3% hydrogen peroxide-containing water to block the endogenous peroxidase activity, and immunolabeled at 4°C overnight with rabbit polyclonal anti-Iba1 antibody at 0.5 $\mu\text{g}/\text{mL}$ (Wako Pure Chemical, Tokyo, Japan) for a marker specific for microglia. They were incubated at RT for 30 min with horseradish peroxidase (HRP)-conjugated secondary antibody (Nichirei), followed by exposure to diaminobenzidine tetrahydrochloride (DAB) substrate (Vector, Burlingame, CA, USA). The

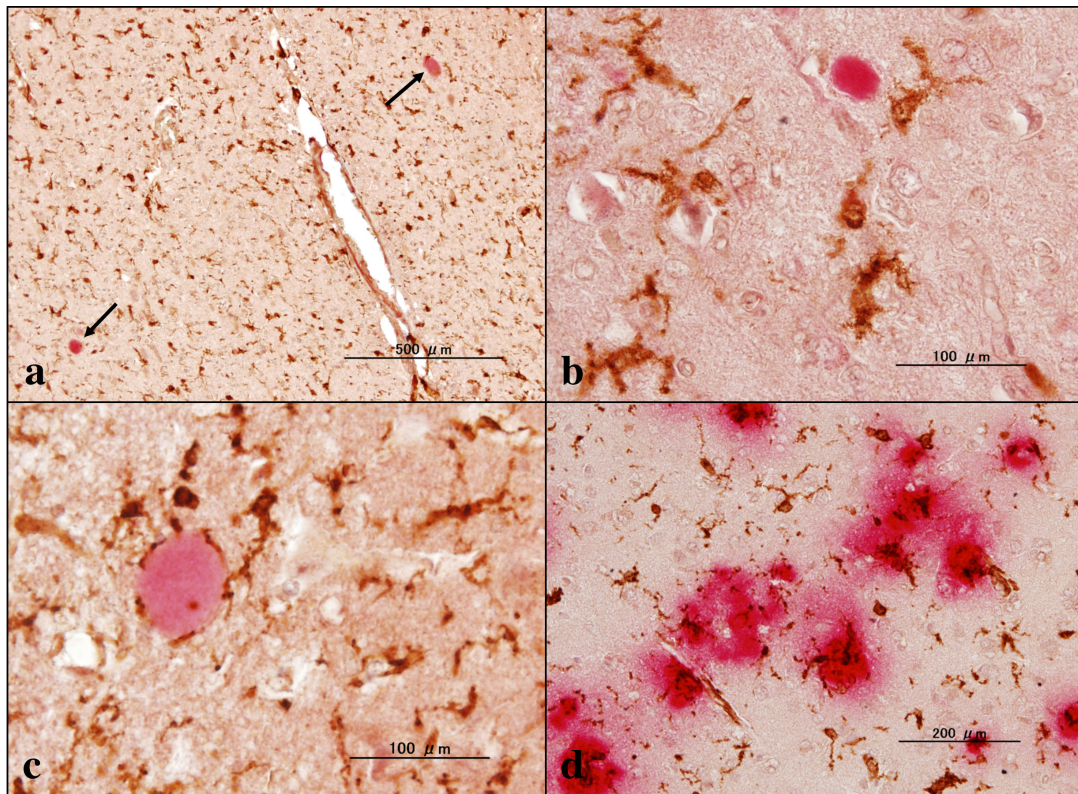


Figure 1. A β immunoreactivity in NHD and AD brains. (a) the hippocampus white matter of NHD (NHD4), A β (red) and Iba1 (brown), spheroids (arrows), (b) the frontal lobe white matter of NHD (NHD5), A β (red) and Iba1 (brown), spheroid, (c) the hippocampus white matter of NHD (NHD2), A β (red) and Iba1 (brown), spheroid, and (d) the frontal cortex of AD (AD8), A β (red) and Iba1 (brown), amyloid plaques.

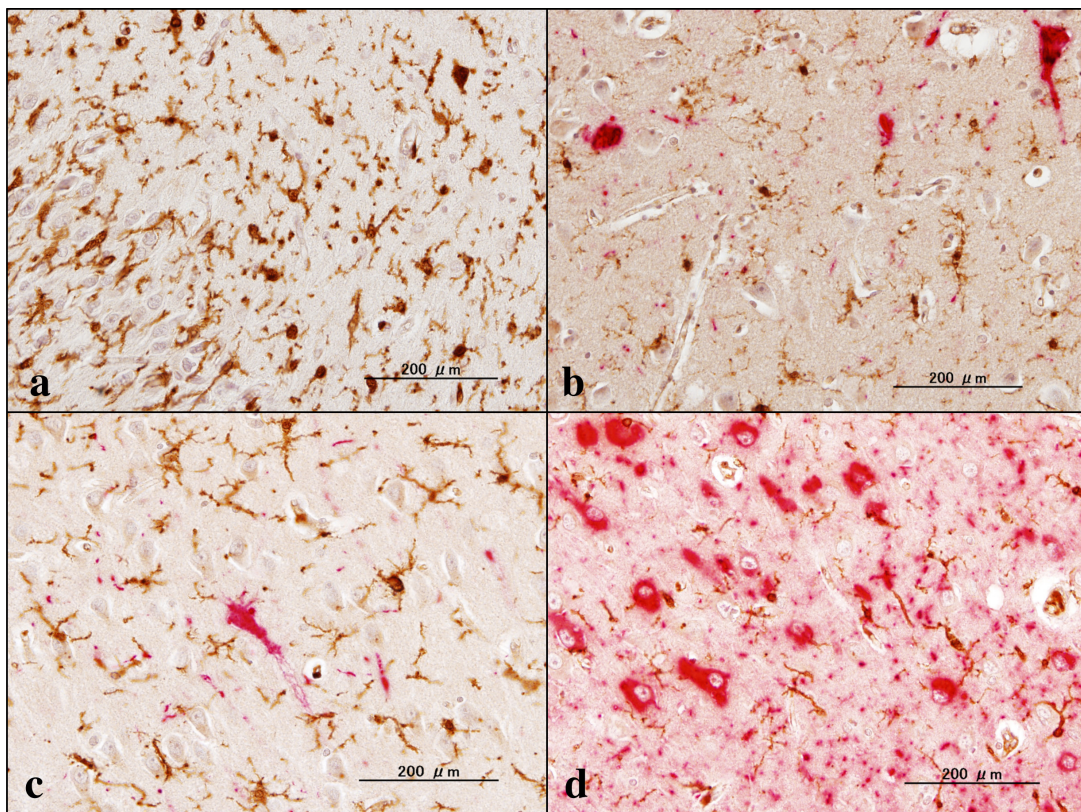


Figure 2. P-tau immunoreactivity in NHD and AD brains. (a) the hippocampus of NHD (NHD5), p-tau (red) and Iba1 (brown), no NFT, (b) the hippocampus of NHD (NHD1), p-tau (red) and Iba1 (brown), several NFTs, (c) the hippocampus of NHD (NHD2), p-tau (red) and Iba1 (brown), one NFT, and (d) the hippocampus of AD (AD5), p-tau (red) and Iba1 (brown), numerous NFTs.

tissue sections were processed for a counterstain with hematoxylin. Negative controls underwent all the steps except for exposure to the primary antibody.

3. Results and Discussion

In mouse models of AD, the loss of function of TREM2 increases A β plaque burden possibly through decreased phagocytic clearance of A β by microglia (4). Loss of TREM2 function reduces the ability of microglia to engulf A β (15). AD patients with the TREM2 variant of R47H showed fewer microglia surrounding plaques, increased numbers of filamentous non-compacted plaques, and more p-tau-positive neurites around plaques (10). In all NHD cases, we found several small A β -immunoreactive deposits, and some of them might represent axonal spheroids located chiefly in the white matter of the frontal cortex and the hippocampus (Figure 1a-c). They were spherical in shape with smooth margins devoid of the core. Iba1+ microglia occasionally contacted these spheroids (Figure 1c). In support of these observations, a previous study showed the persistent accumulation of A β 42 in axonal spheroids in a rat model of traumatic injury (16). In contrast, amyloid plaques, compact or diffuse, and amyloid angiopathy were almost undetectable in any cases. A β -immunoreactive spheroids consisted of 4-22 spots/20 fields in the frontal cortex and 2-16 spots/20 fields in the hippocampus of NHD brains under microscopic examination at a magnification of 200 \times . In contrast, the deposition of A β was much extensive in AD brains (Figure 1d). The omission of the primary antibody did not show any positive reactions. In NHD brains except for NHD5, we identified a small cluster of NFT-bearing neurons labeled by anti-p-tau antibody located predominantly in the hippocampus (Figure 2a-c). NFT-bearing neurons consisted of 0-11 neurons/20 fields in the frontal cortex and 0-34 neurons/20 fields in the hippocampus of NHD brains under microscopic examination at a magnification of 200 \times . We found a trend for the age-dependent increase in p-tau-immunoreactive NFT-bearing neurons. In contrast, numerous p-tau-immunoreactive neuronal deposits, composed of NFTs and dystrophic neurites, were observed in AD brains (Figure 2d). These results indicated that the loss of function of TREM2/DAP12 signaling pathway does not accelerate AD pathology in NHD brains.

The discrepancy between TREM2-deficient AD mice showing greater amounts of A β deposition in the hippocampus (4) and NHD patients not exhibiting the acceleration of A β deposition in the frontal cortex and the hippocampus is attributable to a difference in species, ages, and genetic backgrounds. Plaque accumulation is exacerbated at later ages in a TREM2 knockout AD mouse model (17). In AD patients, A β plaques appear a decade or two before clinical

symptoms of AD (18). In the present study, NHD patients are 32- to 48-year-old. Therefore, they could be affected by the early AD pathology according to their ages. Importantly, by using florbetapir-amyloid-positron emission tomography (PET), a recent study demonstrated extensive A β deposition in the grey matter of the inferior frontal and occipital lobes of a 39-year-old Italian NHD woman with a homozygous Q33X mutation in TREM2, suggesting the existence of overlapping pathogenic mechanisms between NHD and AD (19). In the present study, three cases of NHD showed the homozygous mutation of c.141delG in exon 3 of DAP12. A recent study showed that deficiency of DAP12 does not modify the number and size of A β plaque deposition in the prefrontal cortex and the hippocampus of APP/PSEN1 mice, although DAP12 deficiency reduces plaque compaction, microglial clustering, and phagocytosis (20). Furthermore, phosphorylation of tau is attenuated in female APP/PSEN1 mice with loss of DAP12. In contrast, silencing of brain TREM2 exacerbates tau pathology in P301S tau transgenic mice, associated with neuroinflammation-induced overactivation of tau kinases, such as cyclin dependent kinase 5 (CDK5) and glycogen synthase kinase 3 beta (GSK3B) (21). Thus, the absence of either DAP12 or TREM2 produces apparently opposing effects on progression of AD pathology in mouse models of AD.

In summary, we identified no obvious A β plaques and a small number of p-tau-immunoreactive NFT-bearing neurons in NHD brains. Because AD pathology is less evident in NHD than the full-brown AD, it does not play an active role in the development of NHD.

Acknowledgements

The authors thank Drs. Kenji Jinnai, Nobutaka Arai, Kiyotaka Nakamagoe, Nobutaka Motohashi, and Saburo Yagishita for providing us brain samples. This work was supported by grants from the Research on Intractable Diseases, entitled "Clinicopathological and genetic studies of Nasu-Hakola disease" (H21-Nanchi-Ippan-201; H22-Nanchi-Ippan-136), the Ministry of Health, Labour and Welfare of Japan, and grants from the JSPS KAKENHI (C25430054 and 16K07043) and the Dementia Drug Resource Development Center (DRC) project (S1511016), the Ministry of Education, Culture, Sports, Science and Technology (MEXT), Japan.

References

1. Klünemann HH, Ridha BH, Magy L, Wherrett JR, Hemelsoet DM, Keen RW, De Bleecker JL, Rossor MN, Marienhagen J, Klein HE, Peltonen L, Paloneva J. The genetic causes of basal ganglia calcification, dementia, and bone cysts: DAP12 and TREM2. *Neurology*. 2005;

- 64:1502-1507.
2. Bianchin MM, Capella HM, Chaves DL, Steindel M, Grisard EC, Ganey GG, da Silva Júnior JP, Neto Evaldo S, Poffo MA, Walz R, Carlotti Júnior CG, Sakamoto AC. Nasu-Hakola disease (polycystic lipomembranous osteodysplasia with sclerosing leukoencephalopathy - PLOSL): A dementia associated with bone cystic lesions. From clinical to genetic and molecular aspects. *Cell Mol Neurobiol.* 2004; 24:1-24.
 3. Satoh J, Tabunoki H, Ishida T, Yagishita S, Jinnai K, Futamura N, Kobayashi M, Toyoshima I, Yoshioka T, Enomoto K, Arai N, Arima K. Immunohistochemical characterization of microglia in Nasu-Hakola disease brains. *Neuropathology.* 2011; 31:363-375.
 4. Wang Y, Cella M, Mallinson K, Ulrich JD, Young KL, Robinette ML, Gilfillan S, Krishnan GM, Sudhakar S, Zinselmeyer BH, Holtzman DM, Cirrito JR, Colonna M. TREM2 lipid sensing sustains the microglial response in an Alzheimer's disease model. *Cell.* 2015; 160:1061-1071.
 5. Yeh FL, Wang Y, Tom I, Gonzalez LC, Sheng M. TREM2 binds to apolipoproteins, including APOE and CLU/APOJ, and thereby facilitates uptake of amyloid-beta by microglia. *Neuron.* 2016; 91:328-340.
 6. Xing J, Titus AR, Humphrey MB. The TREM2-DAP12 signaling pathway in Nasu-Hakola disease: A molecular genetics perspective. *Res Rep Biochem.* 2015; 5:89-100.
 7. Jay TR, von Saucken VE, Landreth GE. TREM2 in neurodegenerative diseases. *Mol Neurodegener.* 2017; 12:56.
 8. Serrano-Pozo A, Frosch MP, Masliah E, Hyman BT. Neuropathological alterations in Alzheimer disease. *Cold Spring Harb Perspect Med.* 2011; 1:a006189.
 9. Guerreiro R, Wojtas A, Bras J, *et al.* TREM2 variants in Alzheimer's disease. *N Engl J Med.* 2013; 368:117-127.
 10. Yuan P, Condello C, Keene CD, Wang Y, Bird TD, Paul SM, Luo W, Colonna M, Baddeley D, Grutzendler J. TREM2 haploinsufficiency in mice and humans impairs the microglia barrier function leading to decreased amyloid compaction and severe axonal dystrophy. *Neuron.* 2016; 90:724-739.
 11. Wang Y, Ulland TK, Ulrich JD, *et al.* TREM2-mediated early microglial response limits diffusion and toxicity of amyloid plaques. *J Exp Med.* 2016; 213:667-675.
 12. Bird TD, Koerker RM, Leaird BJ, Vlcek BW, Thorning DR. Lipomembranous polycystic osteodysplasia (brain, bone, and fat disease): A genetic cause of presenile dementia. *Neurology.* 1983; 33:81-86.
 13. Mirra SS, Heyman A, McKeel D, Sumi SM, Crain BJ, Brownlee LM, Vogel FS, Hughes JP, van Belle G, Berg L. The Consortium to Establish a Registry for Alzheimer's Disease (CERAD). Part II. Standardization of the neuropathologic assessment of Alzheimer's disease. *Neurology.* 1991; 41:479-486.
 14. Braak H, Alafuzoff I, Arzberger T, Kretschmar H, Del Tredici K. Staging of Alzheimer disease-associated neurofibrillary pathology using paraffin sections and immunocytochemistry. *Acta Neuropathol.* 2006; 112:389-404.
 15. Kleinberger G, Yamanishi Y, Suárez-Calvet M, *et al.* TREM2 mutations implicated in neurodegeneration impair cell surface transport and phagocytosis. *Sci Transl Med.* 2014; 6:243ra86.
 16. Iwata A, Chen XH, McIntosh TK, Browne KD, Smith DH. Long-term accumulation of amyloid- β in axons following brain trauma without persistent upregulation of amyloid precursor protein genes. *J Neuropathol Exp Neurol.* 2002; 61:1056-1068.
 17. Jay TR, Hirsch AM, Broihier ML, Miller CM, Neilson LE, Ransohoff RM, Lamb BT, Landreth GE. Disease progression-dependent effects of TREM2 deficiency in a mouse model of Alzheimer's disease. *J Neurosci.* 2017; 37:637-647.
 18. Jack CR Jr, Knopman DS, Jagust WJ, Petersen RC, Weiner MW, Aisen PS, Shaw LM, Vemuri P, Wiste HJ, Weigand SD, Lesnick TG, Pankratz VS, Donohue MC, Trojanowski JQ. Tracking pathophysiological processes in Alzheimer's disease: An updated hypothetical model of dynamic biomarkers. *Lancet Neurol.* 2013; 12:207-216.
 19. Ghezzi L, Carandini T, Arighi A, *et al.* Evidence of CNS β -amyloid deposition in Nasu-Hakola disease due to the TREM2 Q33X mutation. *Neurology.* 2017; 89:2503-2505.
 20. Haure-Mirande JV, Audrain M, Fanutza T, Kim SH, Klein WL, Glabe C, Readhead B, Dudley JT, Blitzer RD, Wang M, Zhang B, Schadt EE, Gandy S, Ehrlich ME. Deficiency of TYROBP, an adapter protein for TREM2 and CR3 receptors, is neuroprotective in a mouse model of early Alzheimer's pathology. *Acta Neuropathol.* 2017; 134:769-788.
 21. Jiang T, Tan L, Zhu XC, Zhou JS, Cao L, Tan MS, Wang HF, Chen Q, Zhang YD, Yu JT. Silencing of TREM2 exacerbates tau pathology, neurodegenerative changes, and spatial learning deficits in P301S tau transgenic mice. *Neurobiol Aging.* 2015; 36:3176-3186.

(Received December 24, 2017; Revised January 23, 2018; Accepted January 25, 2018)

Osteogenesis imperfecta type III/Ehlers-Danlos overlap syndrome in a Chinese man

Yanqin Lu^{1,2}, Yanzhou Wang³, Frank Rauch⁴, Hu Li^{1,2,§}, Yao Zhang^{1,2}, Naixiang Zhai^{1,2}, Jian Zhang^{1,2}, Xiuzhi Ren^{5,*}, Jinxiang Han^{1,2,*}

¹Key Laboratory for Rare & Uncommon Diseases of Shandong Province, Shandong Medicinal Biotechnology Centre, Shandong Academy of Medical Sciences, Ji'nan, China;

²School of Medicine and Life Sciences, University of Ji'nan-Shandong Academy of Medical Sciences, Ji'nan, China;

³Department of Paediatric Surgery, Shandong Provincial Hospital, Ji'nan, China;

⁴Shriners Hospital for Children and McGill University, Montreal, Quebec, Canada;

⁵Department of Orthopaedic Surgery, The People's Hospital of Wuqing District, Tianjin, China.

Summary

Osteogenesis imperfecta (OI) and Ehlers-Danlos syndrome (EDS) are rare genetic disorders that are typically inherited in an autosomal dominant manner. Few cases of OI/EDS overlap syndrome have been documented. Described here is a 30-year-old Chinese male with OI type III and EDS. Sequencing of genomic DNA revealed a heterozygous *COL1A1* mutation (c.671G>A, p.Gly224Asp) that affected the N-anchor domain of the alpha 1 chain of collagen type I. Ultrastructural analysis of a skin biopsy specimen revealed thin collagen fibers with irregular alignment of collagen fibers. These findings have expanded the genotypic spectrum of the OI/EDS overlap syndrome.

Keywords: Ehlers-Danlos syndrome, osteogenesis imperfecta, transmission electron microscopy, collagen type I

1. Introduction

Osteogenesis imperfecta is an inherited connective tissue disorder that is mainly characterized by increased bone fragility, short stature, and blue or grey sclera. The condition may also be associated with hearing loss, dentinogenesis imperfecta, and scoliosis (1,2). OI has a wide-ranging clinical spectrum, with type I being the mildest form, types III and IV being more severe forms, and type II usually being lethal (1,3). Mutations in the *COL1A1* and *COL1A2* genes encoding pro- $\alpha 1$ and pro- $\alpha 2$ (I) chains of type I procollagen are present in the large majority of patients with a typical OI phenotype (4,5). Missense mutations are the most common, and especially

glycine substitutions in the helical regions of the pro- $\alpha 1$ (I) and pro- $\alpha 2$ (I) chains.

Mutations in *COL1A1* and *COL1A2* can also lead to Ehlers-Danlos syndrome types VIIA and VIIB when they affect exon 6 of either gene (6,7). Mutations in this region can impede the cleavage of N-proteinase and the normal interhelical cross-linking of collagen fibers (8,9). Individuals affected by such mutations usually suffer from bilateral hip dislocation and severe joint hypermobility (4,7).

A few patients with OI/EDS overlap syndrome have been described as having the clinical symptoms of both OI and EDS with different levels of joint laxity, skin hyperextensibility, atrophic scars, and easy bruising (10-21). OI/EDS phenotypes can be caused by mutations affecting the amino-terminal portion of the collagen type I triple helix with some apparent genotype-phenotype correlation. Patients with mutations that affect the most N-terminal portion of the triple helix, such as exon 7 skipping and p.Gly13Asp substitution, present with relatively mild OI and more severe EDS, whereas individuals harboring mutations in exon 11 (such as p.Gly88Glu in *COL1A1*) have more severe OI and a milder EDS phenotype (8). Described here is a Chinese

[§]Present address, Institute of Medicinal Biotechnology, Chinese Academy of Medical Sciences and Peking Union Medical College, Beijing, China.

*Address correspondence to:

Dr. Jinxiang Han, Shandong Academy of Medical Sciences, 18877 Jingshi Road, 250062 Ji'nan, China.
E-mail: samshjx@sina.com

Dr. Xiuzhi Ren, The People's Hospital of Wuqing District, 100 West Yongyang Road, Tianjin 301700, China.
E-mail: xiuzhiren@hotmail.com

man with OI/EDS overlap syndrome with a heterozygous mutation affecting the N-terminal portion of the pro α 1(I) triple helical domain.

2. Subjects and Methods

2.1. Patient

On examination at the age of 30 years, the patient weighed 28 kg, was 120 cm in height, and had a head circumference of 60 cm. His first femoral fracture had occurred no more than 20 days after birth. He could not walk until he was 7 years old and he had experienced more than 60 fractures during his life. Most of these were bilateral femoral fractures; fractures to the upper limbs and tibiae were less frequent.

The patient's facial features included an oval-shaped face, protuberant eyes and jaw, grayish-blue sclerae, and tooth loss. Severe kyphoscoliosis was present, and both radial heads were dislocated (Figure 1A, 1B, *Supplementary material*, <http://www.irdrjournal.com/action/getSupplementalData.php?ID=17>). Mild skin hyperextensibility and dislocation of the interphalangeal joints were also evident (Figure 1C, 1D, *Supplementary material*, <http://www.irdrjournal.com/action/getSupplementalData.php?ID=17>). The patient suffered from easy bruising. He had a scar on the lower portion of his deformed chest and typical symptoms of marked ligamentous laxity and generalized joint hypermobility. He had a prominent, asymmetric thorax and respiratory distress, which limited his ability to walk. His hearing and vision were normal.

The patient had a Beighton score of 6, but he could not put his hands flat on the floor or bend either elbow backwards due to radial head dislocation and bone deformities. The tourniquet test was positive. X-ray radiography indicated that long bones of the lower limbs were deformed (Figure 1E) and that the heads of both radii were dislocated (Figure 1F).

2.2. Methods

This study was conducted in accordance with the Code of Ethics of the World Medical Association (Declaration of Helsinki) for experiments involving humans. This study was approved by the Ethical Committee of the Shandong Medicinal Biotechnology Center, and informed consent was obtained from the patient. Blood was collected from the patient, his mother, and three of his four sisters after their informed consent was obtained. The patient's medical history and radiographs were obtained from hospital records.

Genomic DNA was extracted using the E.Z.N.A.[®] Blood DNA Kit according to the manufacturer's instructions (Omega Bio-Tek, Norcross, GA, USA). A total of 65 PCR reactions were performed to cover the entire coding regions, intron-exon boundaries, and flanking intronic sequences of *COL1A1* and *COL1A2* (22). PCR products were subjected to direct DNA sequencing (Beijing Genomics Institute, Qingdao, China). Genetic variations were analyzed with the software Mutation Surveyor 4.0 (SoftGenetics LLC, State College, PA, USA) using the human osteogenesis imperfecta variant database. The following software was used to assess the potential effect of a mutation on functional changes: Polyphen; Align GVGD, SIFT Human Coding SNPs, and RESCUE-ESE.

A skin biopsy sample was obtained from the proband, fixed in 2.5% glutaraldehyde, post-fixed in 1% OsO₄, and stained with 2% uranyl acetate. After dehydration, the specimen was embedded in Spurr's plastic resin. Thin sections (60 nm) were cut and placed on formvar-coated grids and then counterstained with 7% methanolic uranyl acetate and lead citrate. The stained grids were viewed with a transmission electron microscope (JEOL-1200ES, Japan Spectroscopic, Tokyo, Japan) and images were photographed. The diameter of collagen fibers was determined using the software Image-Pro Plus 6.0.

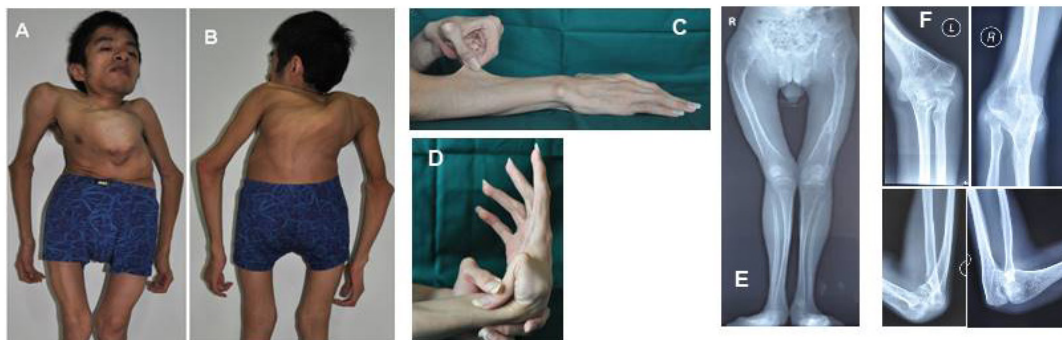


Figure 1. Clinical and radiographic features of the patient. (A), The patient presented with an oval face, protuberant eyes, a short thorax, distinctive thoracic asymmetry, and dislocation of both radial heads; (B), Severe kyphoscoliosis; (C), Skin hyperextensibility; (D), Dislocation of the interphalangeal joints; (E), The femoral neck was thick and short, both femoral shafts were irregular, and tibial and fibular shafts on both sides were slender with expanded ends; (F), Bone structures were thin on both sides of the elbow, with some expansion at the epiphysis. The olecranon process was small, and subluxation of the elbow was also present.

3. Results and Discussion

Sequencing revealed a heterozygous c.671G>A (p.Gly224Asp) in exon 9 of COL1A1 in the patient but not in his family members (Figures 2A and 2B). Polyphen, Align GVGD, and SIFT analyses predicted that this substitution would have a damaging effect.

Transmission electron microscopy revealed irregularly arranged thin collagen fibers (Figure 2C). Quantification of the diameter of the collagen fibers revealed that they were significantly thinner in the patient compared to those in the healthy controls (Figure 2D).

Previously reported COL1A1 mutations associated with OI/EDS overlap syndrome mostly result from glycine substitutions in the aminoterminal portion of the triple helical domain (Table 1), but three Y-position substitutions of arginine by cysteine, alanine by valine, and one C-propeptide mutation have also been reported

(4,15,17,20).

The current study reported on a Chinese man with OI/EDS overlap syndrome who presented with the typical features of severe OI. He also has marked ligamentous laxity, joint hypermobility, and skin hyperextension. These features were more severe than what is usually seen in OI and are compatible with a diagnosis of EDS.

The current authors previously identified a heterozygous p.Gly224Asp mutation in COL1A1 and submitted it to the OI mutation database (13,14). This mutation is located in the anchor domain of type I collagen. Besides this mutation, a c.3733G>A (pval1245Met) variation in the COL1A2 gene was also noted, though this was later excluded by the Exome Aggregation Consortium (ExAC) browser. A mutation of p.Gly224Asp in COL1A1 was noted by Liu *et al.*, who regarded a patient with this mutation as having OI type I (23). The anchor domain consists of the first 85

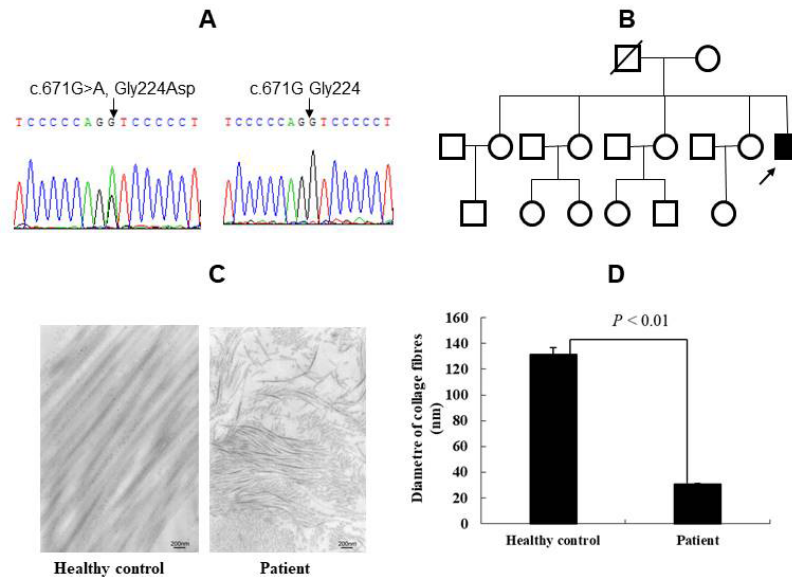


Figure 2. COL1A1 gene mutation and the structure and diameter of collagen fibers. (A), There is a heterogeneous G>A mutation (p.Gly224Asp) of COL1A1 in the patient but not in healthy family members; (B), Pedigree map of the patient; (C), Irregular fibers in the patient; (D) Collagen fibers with significantly smaller diameters in the patient.

Table 1. Overview of COL1A1 mutations causing OI/EDS overlap syndrome

Exon	DNA change	aa substitution	Position	Ref.
7	c.563G>A	p.Gly188Asp	Gly	Malfait <i>et al.</i> , 2013 (18)
7	c.572G>A	p.Gly191Asp	Gly	Cabral <i>et al.</i> , 2005 (8)
07 i	c.588+4A>T	-	-	Cabral <i>et al.</i> , 2005 (8)
8	c.590G>A	p.Gly197Asp	Gly	Marini <i>et al.</i> , 2007 (4)
8	c.607G>T	p.Gly203Cys	Gly	Malfait <i>et al.</i> , 2013 (18)
8	c.609G>A	p.Gly203Val	Gly	Cabral <i>et al.</i> , 2005 (8)
8	c.617G>A	p.Gly206Asp	Gly	Belgium:Ghent (13,14)
8	c.634G>C	p.Gly212Arg	Gly	Cabral <i>et al.</i> , 2005 (8)
9	c.643G>A	p.Gly215Ser	Gly	Vandersteen <i>et al.</i> , 2014 (21)
11	c.761G>A	p.Gly254Glu	Gly	Cabral <i>et al.</i> , 2005 (8)
11	c.796G>A	p.Gly266Glu	Gly	Cabral <i>et al.</i> , 2005 (8)
44	c.3106C>T	p.Arg1036Cys	Y	Lund <i>et al.</i> , 2008 (15)
44	c.3196C>T	p.Arg1066Cys	Y	Cabral <i>et al.</i> , 2007 (16)
37,44	c.2522delC+ c.3196C>T	p.Pro841Leufs*266+ p.Arg1066Cys	Y	Ackermann <i>et al.</i> , 2017 (19)
48	c.3521C>T	p.Ala1174Val	Y	Shi <i>et al.</i> , 2015 (20)
49	c.3790A>G	p.Met1264Val	Met	Symoens <i>et al.</i> , 2004 (17)

residues of the helical region (residues 179 to 263 of the alpha 1 chain of procollagen type I) and is essential for the correct folding and stability of the N-terminal end of the triple helix. Therefore, mutations in this domain usually lead to the unfolding of the helix and an abnormal conformation of the N-propeptide cleavage site. Hence, N-propeptide processing by procollagen I N-proteinase is delayed, leading to defective collagen crosslinking and thus the EDS phenotype (9). Direct evidence for a defective collagen structure was found in a skin biopsy specimen that also had collagen fibers with a thin diameter. These changes may contribute to the clinical observation of very thin and velvety skin.

The glycine to aspartate change that was found in the current patient introduces a charged amino acid that presumably leads to severe disruption of the triple helix. This may explain why the current patient had more severe bone fragility than a previously reported individual with a glycine-to-cysteine substitution at codon 224, which was associated with an OI type I phenotype (24). A glycine to aspartic acid change in exon 6 to 11 has been noted in phenotypes of both OI and OI/EDS overlap syndrome. Severe and moderate phenotypes are more prevalent than a mild phenotype in patients with OI (13,14).

In conclusion, this report describes a man with OI/EDS overlap syndrome caused by a novel heterozygous p.Gly224Asp mutation in *COL1A1*. These findings have expanded the genotypic spectrum of the OI/EDS overlap syndrome.

Web Resources

Align GVGD: http://gvgd.iarc.fr/agvgd_input.php
 Osteogenesis Imperfecta Variant database: <http://www.le.ac.uk/genetics/collagen>
 Polyphen: <http://genetics.bwh.harvard.edu/pph>
 RESCUE-ESE: <http://genes.mit.edu/burgelab/rescue-ese/>
 SIFT: http://provean.jcvi.org/genome_submit.php

Acknowledgements

The authors wish to thank the patient and his family members who participated in this study. This study was supported by grants from the Shandong Key Research and Development Plan (2016ZDJS07A10, 2016GSF201222,) and the Shandong Provincial Natural Science Foundation of China (2015ZRC03171).

References

- Sillence DO, Senn A, Danks DM. Genetic heterogeneity in osteogenesis imperfecta. *J Med Genet.* 1979; 16:101-116.
- Byers PH, Cole WJ. Connective tissue and its heritable disorders. Molecular, genetic, and medical aspects (Royce PM, Steinmann B. eds.) 2nd Ed., Wiley-Liss, Inc., New York, USA, 2002; pp. 385-430.
- Rauch F, Glorieux FH. Osteogenesis imperfecta. *Lancet.* 2004; 363:1377-1385.
- Marini JC, Forlino A, Cabral WA, et al. Consortium for osteogenesis imperfecta mutations in the helical domain of type I collagen: Regions rich in lethal mutations align with collagen binding sites for integrins and proteoglycans. *Hum Mutat.* 2007; 28:209-221.
- Bardai G, Moffatt P, Glorieux FH, Rauch F. DNA sequence analysis in 598 individuals with a clinical diagnosis of osteogenesis imperfecta: Diagnostic yield and mutation spectrum. *Osteoporos Int.* 2016; 27:3607-3613.
- Beighton P, De Paepe A, Steinmann B, Tsipouras P, Wenstrup RJ. Ehlers-Danlos syndromes: Revised nosology, Villefranche, 1997. Ehlers-Danlos National Foundation (USA) and Ehlers-Danlos Support Group (UK). *Am J Med Genet.* 1998; 77:31-37.
- Holmes DF, Watson RB, Steinmann B, Kadler KE. Ehlers-Danlos syndrome type VIIIB. Morphology of type I collagen fibrils formed *in vivo* and *in vitro* is determined by the conformation of the retained N-propeptide. *J Biol Chem.* 1993; 268:15758-15765.
- Cabral WA, Makareeva E, Colige A, Letocha AD, Ty JM, Yeowell HN, Pals G, Leikin S, Marini JC. Mutations near amino end of $\alpha 1(I)$ collagen cause combined osteogenesis imperfecta/Ehlers-Danlos syndrome by interference with N-propeptide processing. *J Biol Chem.* 2005; 280:19259-19269.
- Makareeva E, Cabral WA, Marini JC, Leikin S. Molecular mechanism of $\alpha 1(I)$ -osteogenesis imperfecta/Ehlers-Danlos syndrome: Unfolding of an N-anchor domain at the N-terminal end of the type I collagen triple helix. *J Biol Chem.* 2006; 281:6463-6470.
- Raff ML, Craigen WJ, Smith LT, Keene DR, Byers PH. Partial *COL1A2* gene duplication produces features of osteogenesis imperfecta and Ehlers-Danlos syndrome type VII. *Hum Genet.* 2000; 106:19-28.
- Chiodo AA, Hockey A, Cole WG. A base substitution at the splice acceptor site of intron 5 of the *COL1A2* gene activates a cryptic splice site within exon 6 and generates abnormal type I procollagen in a patient with Ehlers-Danlos syndrome type VII. *J Biol Chem.* 1992; 267:6361-6369.
- Nicholls AC, Valler D, Wallis S, Pope FM. Homozygosity for a splice site mutation of the *COL1A2* gene yields a non-functional pro $\alpha 2(I)$ chain and an EDS/OI clinical phenotype. *J Med Genet.* 2001; 38:132-136.
- Dalgleish R. The human type I collagen mutation database. *Nucleic Acids Res.* 1997; 25:181-187.
- Dalgleish R. The Human Collagen Mutation Database 1998. *Nucleic Acids Res.* 1998; 26:253-255.
- Lund A, Joensen F, Christensen E, Duno M, Skovby F, Schwartz M. A novel arginine-to-cysteine substitution in the triple helical region of the $\alpha 1(I)$ collagen chain in a family with an osteogenesis imperfecta/Ehlers-Danlos phenotype. *Clin Genet.* 2008; 73:97-101.
- Cabral WA, Makareeva E, Letocha AD, Scribanu N, Fertala A, Steplewski A, Keene DR, Persikov AV, Leikin S, Marini JC. Y-position cysteine substitution in type I collagen ($\alpha 1(I)$ R888C/p.R1066C) is associated with osteogenesis imperfecta/Ehlers-Danlos syndrome phenotype. *Hum Mutat.* 2007; 28:396-405.
- Symoens S, Nuytinck L, Legius E, Malfait F, Coucke PJ, De Paepe A. Met>Val substitution in a highly conserved

- region of the pro- α 1(I) collagen C-propeptide domain causes alternative splicing and a mild EDS/OI phenotype. *J Med Genet.* 2004; 41:e96.
18. Malfait F, Symoens S, Goemans N, Gyftodimou Y, Holmberg E, Lopez-Gonzalez V, Mortier G, Nampoothiri S, Petersen MB, De Paepe A. Helical mutations in type I collagen that affect the processing of the amino-propeptide result in an Osteogenesis Imperfecta/Ehlers-Danlos Syndrome overlap syndrome. *Orphanet J Rare Dis.* 2013; 8:78.
 19. Ackermann AM, Levine MA. Compound heterozygous mutations in *COL1A1* associated with an atypical form of type I osteogenesis imperfecta. *Am J Med Genet A.* 2017. doi: 10.1002/ajmg.a.38238.
 20. Shi X, Lu Y, Wang Y, Zhang YA, Teng Y, Han W, Han Z, Li T, Chen M, Liu J, Fang F, Dou C, Ren X, Han J. Heterozygous mutation of c.3521C>T in *COL1A1* may cause mild osteogenesis imperfecta/Ehlers-Danlos syndrome in a Chinese family. *Intractable Rare Dis Res.* 2015; 4:49-53.
 21. Vandersteen AM, Lund AM, Ferguson DJ, Sawle P, Pollitt RC, Holder SE, Wakeling E, Moat N, Pope FM. Four patients with Sillence type I osteogenesis imperfecta and mild bone fragility, complicated by left ventricular cardiac valvular disease and cardiac tissue fragility caused by type I collagen mutations. *Am J Med Genet A.* 2014; 164a:386-391.
 22. Lu Y, Ren X, Wang Y, Li T, Li F, Wang S, Xu C, Wu G, Li H, Li G, Zhao F, Wang Z, Mo X, Han J. Mutational and structural characteristics of four novel heterozygous C-propeptide mutations in the pro α 1(I) collagen gene in Chinese osteogenesis imperfecta patients. *Clin Endocrinol (Oxf).* 2014; 80:524-531.
 23. Liu Y, Asan, Ma D, *et al.* Gene mutation spectrum and genotype-phenotype correlation in a cohort of Chinese osteogenesis imperfecta patients revealed by targeted next generation sequencing. *Osteoporos Int.* 2017; 28:2985-2995.
 24. Byers PH, Wallis GA, Willing MC. Osteogenesis imperfecta: Translation of mutation to phenotype. *J Med Genet.* 1991; 28:433-442.
- (Received January 20, 2018; Revised February 20, 2018; Accepted February 21, 2018)

A *de novo* and novel mutation in the *EYAI* gene in a Chinese child with branchio-oto-renal syndrome

Guomin Li¹, Qian Shen¹, Li Sun¹, Haimei Liu¹, Yu An², Hong Xu^{1,*}

¹ Children's Hospital of Fudan University, Shanghai, China;

² Institutes of Biomedical Sciences of Fudan University, Shanghai, China.

Summary

Branchio-oto-renal (BOR) syndrome is a rare autosomal dominant disorder characterized by branchial cleft fistulae or cysts, preauricular pits, ear malformations, hearing loss, and renal anomalies. Mutations in the human homologue of the *Drosophila* eyes absent gene (*EYAI*) are the most common cause of BOR syndrome. PCR and direct sequencing were used to investigate all of the exons and exon-intron boundaries in the *EYAI* gene in a patient with BOR syndrome from China. The patient was a child who displayed clinical features of BOR syndrome. Analysis of mutations in the *EYAI* gene revealed a novel single base-pair deletion resulting in a truncated protein (c.1381delA; p.R461fs467X), and an analysis of mutations in the family revealed that this mutation was a *de novo* mutation. This is the first case of BOR syndrome in mainland China to be diagnosed based on clinical manifestations and mutations in the *EYAI* gene. The novel c.1381delA mutation detected here expands the spectrum of known mutations in the *EYAI* gene.

Keywords: *EYAI* gene, branchio-oto-renal syndrome, novel mutation

1. Introduction

Branchio-oto-renal (BOR) syndrome (MIM#113650) is an autosomal dominant disorder that is associated with branchial fistulae or cysts, preauricular pits, ear malformations, hearing impairment, and renal anomalies (1). The incidence of BOR syndrome is approximately 1:40,000 (2). Mutations in the *EYAI* gene, the human homologue of the *Drosophila* eyes absent gene, have been shown to cause BOR syndrome (3,4). The *EYAI* gene consists of 16 exons spanning 156 kb on chromosome 8q13.3 (5). The *EYAI* gene is a member of the EYA family, which is characterized by a divergent N-terminal activation domain and a conserved C-terminal Eya domain, and the gene functions as a transcriptional co-activator in the Eya-Six regulatory network for early development of different organs, including the ear and kidney (3). Over 202 different mutations in the *EYAI*

gene that cause disease have been found in various populations (<http://www.hgmd.cf.ac.uk/>, last updated December 2017). However, few mutations have been identified in the Chinese population (6). Reported here is a *de novo* mutation of the *EYAI* gene first identified in a Chinese child with BOR syndrome.

2. Subjects and Methods

2.1. Patient

A girl was admitted to a local hospital in 2010 because of her short stature at age 3. Proteinuria (2+) and abnormal renal function (BUN 17.2 mmol/L, creatinine level 140 μmol/L) were noted by the local hospital, and renal ultrasound indicated that the left kidney was 24.4 mm × 18.9 mm in size while the right kidney was 55.4 mm × 23.0 mm in size. In March 2011, the girl was referred to this facility for evaluation because of the continuing deterioration of renal function at age 4.6. She underwent surgery to remove a branchial cleft cyst at age 1.1 and surgery to repair pre-auricular fistulae at age 4.

On admission, a clinical examination revealed scars from surgery to repair fistulae in the preauricular region and surgery to remove a branchial cleft cyst in the neck (Figures 1A and 1B). Her height was between the 25th

Released online in J-STAGE as advance publication February 26, 2018.

*Address correspondence to:

Dr. Hong Xu, Department of Nephrology, Children's Hospital of Fudan University, 399 Wanyuan Road, Minhang District, Shanghai 201102, China.

E-mail: hxu@shmu.edu.cn

and 50th percentile, and her body weight was in the 50th percentile. Laboratory tests revealed proteinuria (2+, total urine protein of 0.44 g/24 h), abnormal hemoglobin (7.7 g/100 mL), and renal insufficiency (filtration rate < 15 mL/min/1.73m², creatinine level of 505.0 mol/L, and BUN of 44.9 mmol/L). Blood gases revealed metabolic acidosis (pH 7.303, BE-7.8 mmol/L). Abdominal magnetic resonance urography (MRU) revealed left kidney hypoplasia. However, her hearing test was normal.

The family's medical history was also investigated. Informed consent was obtained from the parents. Ethical approval to conduct this study was obtained from the Ethics Committee of the Children's Hospital of Fudan University.

2.2. Methods

In 2011, genomic DNA was extracted and purified from



Figure 1. Clinical manifestations of BOR syndrome. (A), scars from surgery to repair fistulae in the preauricular region (B), scars from surgery to remove a branchial cleft cyst in the neck.

peripheral leukocytes in whole-blood samples using a DNA isolation kit (Qiagen, Hilden, Germany). All exons of the *EYA1* gene were amplified using a polymerase chain reaction (PCR). Primers for the *EYA1* gene were designed based on previously published information regarding intron-exon boundaries. The PCR product was purified with a QIA Quick PCR Purification Kit (Qiagen, Hilden, Germany). The purified product was cycle-sequenced with Big-Dye terminators (Applied Biosystems, Foster City, CA, USA), and the cycle sequence product was analyzed with an automated sequencer (ABI Prism 310 Genetic Analyzer). Novel mutations in *EYA1* were investigated in 100 healthy controls using direct sequencing. Mutation nomenclature was based on the *EYA1* cDNA sequence of NM_000503.3 (<http://www.ncbi.nlm.nih.gov>).

3. Results and Discussion

The patient's parents had no consanguinity, and there was no family history of branchial cleft cyst, preauricular fistulae, renal disease, or hearing loss. A novel deletion mutation, c.1381delA, was detected in the *EYA1* gene, and the patient was heterozygous for this change (Figure 2A). This deletion causes a frameshift of amino acids and results in a truncated protein

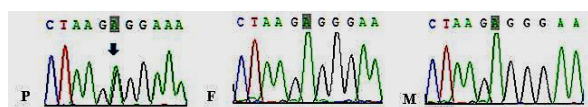


Figure 2. Analysis of mutations in the *EYA1* gene (the arrow indicates the mutation). P: patient; M: mother; F: father.

Table 1. Genotype of 21 patients with BOR syndrome from East Asia

Nation	Patient	EYA1 gene			Year	Ref.
		exon	nucleotide sequence	amino acid sequence		
China*	1	6	c.446C>T	p.Q156X	2012	(7)
	2	17	c.1735del G	p.D579fs	2012	(7)
Korea	3	14	c.1474insC	p.R492Pfs	2005	(16)
	4	7	c.430C>T	p.Q144X	2007	(17)
Japan	5	6	c.321delT	p.A107fs	2009	(18)
	6	-		IVS8-2AG	2009	(19)
	7	10	c.965 A>G	p.E332G	2013	(20)
	8	6	c.418G>A	p.G140S	2014	(10)
	9	7	c.579C>G	p.Y193fs	1999	(21)
	10	9	c.792	R264X	2001	(22)
	11	8	c.625A>G	p.S189G	2003	(23)
Japan	12	14	c.1402_1408delACAACTA	p.T468fs	2004	(24)
	13	6	c.533C>G	p.S178X	2004	(25)
	14	6	c.497T>A	p.Y163X	2006	(26)
	15	12	c.1107T>A	p.Y370X	2006	
	16	10	c.952G>A	p.D318Y	2006	
	17	-		IVS9-2A>G	2006	
	18	-		IVS14-1G>A	2006	
	19	17	c.1667insT	p.D556fs	2007	(27)
	20	5		Del exons 5 to 7	2010	(28)
	21	8	c.634C>T	p.R212X	2015	(29)

*: From Taiwan, -: on intron

(p.R461fs467X). An analysis of mutations in the *EYA1* gene in the family revealed that her parents did not carry the c.1381delA mutation. The mutation was not found in controls.

The patient was diagnosed with BOR syndrome based on clinical features and genetic testing. The patient subsequently received peritoneal dialysis. She was switched to hemodialysis in 2015 due to the loss of peritoneal function, and she received a kidney transplant in 2016. She was assessed at this facility every three to six months. The renal allograft is functioning normally.

BOR syndrome is characterized by a wide spectrum of clinical manifestations that represents a combination of branchial, otic, and renal anomalies (7). Individuals with branchio-otic (BO) syndrome (OMIM#602588) are affected by the same branchial and otic anomalies as in BOR without the associated renal anomalies (8). Due to the wide spectrum of phenotypic findings and the phenotypic variability between and within families, phenotypic criteria for clinical diagnosis of BOR syndrome have been proposed (9). The major criteria include branchial anomalies, deafness, preauricular pits, and renal anomalies, while minor criteria include external, middle, and inner ear anomalies and preauricular tags. A definitive diagnosis is based on meeting ≥ 3 major criteria, meeting 2 major criteria and ≥ 2 minor criteria, or meeting 1 major criterion and having a first-degree relative with BOR syndrome. The patient in this study met 3 major criteria, *i.e.* branchial, preauricular, and renal anomalies. The most common manifestation of BOR is hearing loss, which can be conductive, sensorineural, or mixed (10). Some studies estimate that BO/BOR has a prevalence of 2% amongst profoundly deaf children (2). However, the current patient has no hearing loss.

BOR is genetically heterogeneous, although mutations in *EYA1* are most commonly identified and segregate with the BOR phenotype in about 40% of families (9). Causative variants include point mutations as well as large and small deletions (11-13). *EYA1* encodes a transcriptional regulator, and mice heterozygous for the targeted deletion of this gene have renal abnormalities and a conductive hearing loss similar to the human phenotype (14). *EYA1* homozygous null mice lack ears and kidneys (15).

The current patient has a heterozygous deletion mutation (c.1381delA), which causes a frameshift of amino acids and results in a truncated protein (p.R461fs467X). This mutation is novel, and was not detected in controls. Thus, c.1381delA was deemed to be a disease-causing mutation. Over 202 different mutations in the *EYA1* gene that cause disease have been found in various populations (<http://www.hgmd.cf.ac.uk/>, last updated December 2017), but most have been identified in subjects of European ancestry. More than 21 different mutations in the *EYA1* gene have been identified in patients with BOR/BO syndrome

in South Korea and Japan (Table 1) (10,16-29). In contrast, few mutations have been reported before in patients with BOR syndrome in Taiwan, China (Table 1) (7). All of these mutations were scattered through the *EYA1* coding region; complex mutations involving chromosomal rearrangements have not been found in Asians.

Recent studies have found that mutations in both the *SIX1* and *SIX5* genes are also associated with BOR syndrome (19). *SIX1*, the human homologue of the *Drosophila sine oculis* gene, encodes a DNA-binding protein associated with *EYA1* (19,30). Most mutations identified in *SIX1* are missense mutations, but small deletions have also been reported in patients with BOR syndrome (30). *SIX1* plays a role in *EYA-SIX-PAX* interaction in the development of the ears, kidneys, and other organs (31). Evaluation of *SIX1* and its related target genes may provide clues to the mechanisms involved in causing BOR syndrome (13). The role of *SIX5* in BOR is less clear. Although a few missense mutations in *SIX5* have been reported in patients with BOR syndrome, the role of *SIX5* variants in the pathophysiology of BOR has been questioned (13,19).

In conclusion, this case report has described a Chinese child with BOR syndrome and it has identified a novel frameshift mutation caused by a single base-pair deletion in the *EYA1* gene. The novel c.1381delA mutation is a disease-causing mutation, and this finding expands the spectrum of mutations in the *EYA1* gene.

References

1. Kochhar A, Fischer SM, Kimberling WJ, Smith RJ. Branchio-oto-renal syndrome. *Am J Med Genet A*. 2007; 143A:1671-1678.
2. Fraser FC, Sproule JR, Halal F. Frequency of the branchio-oto-renal (BOR) syndrome in children with profound hearing loss. *Am J Med Genet*. 1980; 7:341-349.
3. Abdelhak S, Kalatzis V, Heilig R, *et al.* A human homologue of the *Drosophila eyes absent* gene underlies branchio-oto-renal (BOR) syndrome and identifies a novel gene family. *Nat Genet*. 1997; 15:157-164.
4. Hwang DY, Dworschak GC, Kohl S, Saisawat P, Vivante A, Hilger AC, Reutter HM, Soliman NA, Bogdanovic R, Kehinde EO, Tasic V, Hildebrandt F. Mutations in 12 known dominant disease-causing genes clarify many congenital anomalies of the kidney and urinary tract. *Kidney Int*. 2014; 85:1429-1433.
5. Kumar S, Kimberling WJ, Kenyon JB, Smith RJ, Marres HA, Cremers CW. Autosomal dominant branchio-oto-renal syndrome—localization of a disease gene to chromosome 8q by linkage in a Dutch family. *Hum Mol Genet*. 1992; 1:491-495.
6. Wang SH, Wu CC, Lu YC, Lin YH, Su YN, Hwu WL, Yu IS, Hsu CJ. Mutation screening of the *EYA1*, *SIX1*, and *SIX5* genes in an East Asian cohort with branchio-oto-renal syndrome. *Laryngoscope*. 2012; 122:1130-1136.
7. Gigante M, d'Altilia M, Montemurno E, Diella S, Bruno F,

- Netti GS, Ranieri E, Stallone G, Infante B, Grandaliano G, Gesualdo L. Branchio-Oto-Renal Syndrome (BOR) associated with focal glomerulosclerosis in a patient with a novel EYA1 splice site mutation. *BMC Nephrol.* 2013; 14:60.
8. Vincent C, Kalatzis V, Abdelhak S, Chaib H, Compain S, Helias J, Vanecloo FM, Petit C. BOR and BO syndromes are allelic defects of EYA1. *Eur J Hum Genet.* 1997; 5:242-246.
 9. Chang EH, Menezes M, Meyer NC, Cucci RA, Vervoort VS, Schwartz CE, Smith RJ. Branchio-oto-renal syndrome: The mutation spectrum in EYA1 and its phenotypic consequences. *Hum Mutat.* 2004; 23:582-589.
 10. Kim HR, Song MH, Kim MA, Kim YR, Lee KY, Sonn JK, Lee J, Choi JY, Kim UK. Identification of a novel nonsynonymous mutation of EYA1 disrupting splice site in a Korean patient with BOR syndrome. *Mol Biol Rep.* 2014; 41:4321-4327.
 11. Amrhein P, Sittel C, Spaich C, Kohlhase J, Boppert R, Kohlhof P, Koitschev A. Middle ear salivary gland choristoma related to branchio-oto-renal syndrome diagnosed by array-CGH. *HNO.* 2014; 62:374-377. (in German)
 12. Brophy PD, Alasti F, Darbro BW, Clarke J, Nishimura C, Cobb B, Smith RJ, Manak JR. Genome-wide copy number variation analysis of a Branchio-oto-renal syndrome cohort identifies a recombination hotspot and implicates new candidate genes. *Hum Genet.* 2013; 132:1339-1350.
 13. Krug P, Moriniere V, Marlin S, Koubi V, Gabriel HD, Colin E, Bonneau D, Salomon R, Antignac C, Heidet L. Mutation screening of the *EYA1*, *SIX1*, and *SIX5* genes in a large cohort of patients harboring branchio-oto-renal syndrome calls into question the pathogenic role of *SIX5* mutations. *Hum Mutat.* 2011; 32:183-190.
 14. Xu PX, Adams J, Peters H, Brown MC, Heaney S, Maas R. Eya1-deficient mice lack ears and kidneys and show abnormal apoptosis of organ primordia. *Nat Genet.* 1999; 23:113-117.
 15. Kwon MJ, Boo SH, Kim HJ, Cho YS, Chung WH, Hong SH. A novel splice site mutation in the *EYA1* gene in a Korean family with branchio-oto (BO) syndrome. *Acta Otolaryngol.* 2009; 129:688-693.
 16. Kim SH, Shin JH, Yeo CK, Chang SH, Park SY, Cho EH, Ki CS, Kim JW. Identification of a novel mutation in the *EYA1* gene in a Korean family with branchio-oto-renal (BOR) syndrome. *Int J Pediatr Otorhinolaryngol.* 2005; 69:1123-1128.
 17. Lee KY, Kim S, Kim UK, Ki CS, Lee SH. Novel EYA1 mutation in a Korean branchio-oto-renal syndrome family. *Int J Pediatr Otorhinolaryngol.* 2007; 71:169-174.
 18. Lee JD, Kim SC, Koh YW, Lee HJ, Choi SY, Kim UK. A novel frameshift mutation in the *EYA1* gene in a Korean family with branchio-oto-renal syndrome. *Ann Clin Lab Sci.* 2009; 39:303-306.
 19. Kwon MJ, Boo SH, Kim HJ, Cho YS, Chung WH, Hong SH. A novel splice site mutation in the *EYA1* gene in a Korean family with branchio-oto (BO) syndrome. *Acta Otolaryngol.* 2009; 129:688-693.
 20. Song MH, Kwon TJ, Kim HR, Jeon JH, Baek JI, Lee WS, Kim UK, Choi JY. Mutational analysis of *EYA1*, *SIX1* and *SIX5* genes and strategies for management of hearing loss in patients with BOR/BO syndrome. *PLoS One.* 2013; 8:e67236.
 21. Usami S, Abe S, Shinkawa H, Deffenbacher K, Kumar S, Kimberling WJ. EYA1 nonsense mutation in a Japanese branchio-oto-renal syndrome family. *J Hum Genet.* 1999; 44:261-265.
 22. Fukuda S, Kuroda T, Chida E, Shimizu R, Usami S, Koda E, Abe S, Namba A, Kitamura K, Inuyama Y. A family affected by branchio-oto syndrome with EYA1 mutations. *Auris Nasus Larynx.* 2001; 28:S7-S11.
 23. Yashima T, Noguchi Y, Ishikawa K, Mizusawa H, Kitamura K. Mutation of the *EYA1* gene in patients with branchio-oto syndrome. *Acta Otolaryngol.* 2003; 123:279-282.
 24. Shimasaki N, Watanabe K, Hara M, Kosaki K. EYA1 mutation in a newborn female presenting with cardiofacial syndrome. *Pediatr Cardiol.* 2004; 25:411-413.
 25. Uno T, Sawada M, Kurotaki T, Shinomiya N. *EYA1* gene nonsense mutation in a Japanese family with branchio-oto-renal syndrome. *Pediatr Int.* 2004; 46:615-617.
 26. Okada M, Fujimaru R, Morimoto N, Satomura K, Kaku Y, Tsuzuki K, Nozu K, Okuyama T, Iijima K. *EYA1* and *SIX1* gene mutations in Japanese patients with branchio-oto-renal (BOR) syndrome and related conditions. *Pediatr Nephrol.* 2006; 21:475-481.
 27. Matsunaga T, Okada M, Usami S, Okuyama T. Phenotypic consequences in a Japanese family having branchio-oto-renal syndrome with a novel frameshift mutation in the gene *EYA1*. *Acta Otolaryngol.* 2007; 127:98-104.
 28. Morisada N, Rendtorff ND, Nozu K, Morishita T, Miyakawa T, Matsumoto T, Hisano S, Iijima K, Tranebjaerg L, Shirahata A, Matsuo M, Kusuvara K. Branchio-oto-renal syndrome caused by partial EYA1 deletion due to LINE-1 insertion. *Pediatr Nephrol.* 2010; 25:1343-1348.
 29. Miyagawa M, Nishio SY, Hattori M, Takumi Y, Usami S. Germinal mosaicism in a family with BO syndrome. *Ann Otol Rhinol Laryngol.* 2015; 124:118S-122S.
 30. Xu PX. The EYA-SO/SIX complex in development and disease. *Pediatr Nephrol.* 2013; 28:843-854.
 31. Brodbeck S, Englert C. Genetic determination of nephrogenesis: The *Pax/Eya/Six* gene network. *Pediatr Nephrol.* 2004; 19:249-255.

(Received November 18, 2017; Revised January 28, 2018; Accepted February 1, 2018)

The ratio of urinary α 1-microglobulin to microalbumin can be used as a diagnostic criterion for tubuloproteinuria

Hongwen Zhang, Fang Wang, Huijie Xiao, Yong Yao*

Department of Pediatric, Peking University First Hospital, Beijing, China.

Summary

Low-molecular-weight proteinuria is one of the characteristic clinical manifestations of renal tubular and interstitial diseases. Low-molecular-weight proteinuria is defined as excessive urinary loss of α 1-microglobulin, β 2-microglobulin, or other low-molecular-weight plasma proteins. The current study examined the ratio of urinary α 1-microglobulin to microalbumin in 24 Chinese pediatric patients with renal tubular and interstitial diseases, including 10 patients with Dent disease, 2 patients with Lowe syndrome, 6 patients with acute tubulointerstitial nephritis (ATIN), 4 patients with acute tubulointerstitial nephritis with uveitis syndrome (TINU), and 2 patients with nephronophthisis (NPHP). Patients with steroid-sensitive nephrotic syndrome, IgA nephropathy, Henoch-Schonlein purpura nephritis, or lupus nephritis served as control groups. In all of the patients with tubular and interstitial disease, urinary α 1-microglobulin increased 10-300-fold above the upper limit of the normal range, the ratio of urinary α 1-microglobulin to microalbumin was greater than 1, and the percentage of low-molecular-weight plasma proteins (LMWP) in urine was greater than 50% according to urine protein electrophoresis. There was close correlation between the ratio of urinary α 1-microglobulin to microalbumin and the percentage of LMWP in urine according to urine protein electrophoresis ($r = 0.797$, $p = 0.000$). We suggested firstly that the ratio of urinary α 1-microglobulin to microalbumin, greater than 1, can be used as a diagnostic criterion for tubuloproteinuria.

Keywords: α 1-microglobulinuria, microalbuminuria, tubuloproteinuria

1. Introduction

Low-molecular-weight proteinuria is one of the characteristic clinical manifestations of renal tubular and interstitial diseases, such as Dent disease, Lowe syndrome, acute tubulointerstitial nephritis (ATIN) without or with uveitis syndrome (TINU), Fanconi syndrome, and nephronophthisis (NPHP) (1,2). Low-molecular-weight proteinuria is usually detected with urine protein electrophoresis (SDS polyacrylamide gel electrophoresis), but this technique is complicated and time-consuming. Elevated levels of urinary β 2-microglobulin and α 1-microglobulin can also serve as markers of low-molecular-weight proteinuria, but there

are no definitive levels of those plasma proteins in urine.

The current study examined the ratio of urinary α 1-microglobulin to microalbumin in several types of renal tubular and interstitial diseases that present in childhood in order to determine whether that ratio could be used as a diagnostic criterion for tubuloproteinuria.

2. Subjects and Methods

2.1. Participants

This study was approved by Peking University First Hospital (No. 2014-826) and followed the guidelines of the 2000 Declaration of Helsinki and the 2008 Declaration of Istanbul. Consent was obtained from all patients and their families.

Data were collected from 24 Chinese pediatric patients with renal tubular and interstitial diseases, including 10 patients with Dent disease, 2 patients with Lowe syndrome, 6 patients with ATIN, 4 patients with

Released online in J-STAGE as advance publication February 26, 2018.

*Address correspondence to:

Dr. Yong Yao, Department of Pediatric, Peking University First Hospital, No.1 Xi An Men Da Jie, Beijing 100034, China.
E-mail: yaoyong3238@126.com

TINU, and 2 patients with NPHP. Patients were seen from January 01, 2014 to December 31, 2016 and were analyzed retrospectively. All patients presented with proteinuria. Patients with steroid-sensitive nephrotic syndrome (NS), IgA nephropathy, Henoch-Schonlein purpura nephritis, or lupus nephritis were also included as control groups. These patients were seen during the same period, and each group consisted of 20 patients. Data were collected upon diagnosis.

The clinical diagnosis of Dent's disease is based on meeting all three of the following criteria: *i*) low-molecular-weight proteinuria (elevated urinary excretion of α 1-microglobulin at least 100-fold greater than the upper limit of the normal range, or greater than 50% low-molecular-weight plasma proteins (LMWP) in urine according to urine protein electrophoresis); *ii*) hypercalciuria (> 0.1 mmol/kg according to 24-hour urine collection or > 0.21 mg/mg calcium to creatinine ratio according to a spot sample); and *iii*) at least one of the following: nephrocalcinosis, kidney stones, hematuria, hypophosphatemia, or renal insufficiency.

The identification of a mutation in either *CLCN5* or *OCRL1* confirms the diagnosis (3,4). The clinical diagnosis of Lowe syndrome is based on meeting three of the following criteria: congenital bilateral cataracts, renal Fanconi syndrome, hypotonia and neonatal areflexia, motor and mental developmental delays, and facial dysmorphisms. The identification of a mutation in *OCRL1* confirms the diagnosis (5,6).

The clinical diagnosis of ATIN without or with uveitis is based on the clinical course and laboratory examinations including urinalysis and a renal function test. A percutaneous renal biopsy reveals diffuse interstitial nephritis with infiltration of neutrophil and eosinophil granulocytes and numerous lymphocytes and plasma cells. No granuloma is found. Typical bilateral anterior uveitis concurrent with or preceding or following the onset of renal dysfunction corroborates the diagnosis of TINU (7,8).

The clinical diagnosis of NPHP is based on multiple organ involvement that includes at least abnormal renal and liver function or cysts, and urinalysis may reveal a renal concentration defect. The identification of a mutation in NPHPs confirms the diagnosis (9,10).

2.2. Clinic and laboratory examinations

Results of all examinations, such as a quantitative test of 24-h urinary protein, were examined. The presence of α 1-microglobulinuria and microalbuminuria was also determined. Results of urine protein electrophoresis were examined.

2.3. Statistical analysis

Statistical analysis was performed with SSPS 12.0 software. Every index was measured three times and

summarized as the mean \pm SD, and the relationship between the ratio of urinary α 1-microglobulin to microalbumin and the percentage of LMWP in urine according to urine protein electrophoresis was analyzed using Pearson's correlation coefficient. An independent-samples test was used to examine the mean ratio of urinary α 1-microglobulin to microalbumin and the mean percentage of LMWP in urine in patients with renal tubular and interstitial disease and the control groups. *P* values less than 0.05 were considered statistically significant.

3. Results and Discussion

All 24 patients presented with proteinuria. Patients with Dent disease or Lowe syndrome had proteinuria in the nephrotic range while patients with ATIN, TINU, or NPHP had proteinuria that did not fall in the nephrotic range. Urinary α 1-microglobulin and microalbumin both increased significantly in all patients. This was especially true for α 1-microglobulin, which increased 10-300-fold above the upper limit of the normal range. In all patients, the percentage of LMWP in urine was greater than 50% according to urine protein electrophoresis, and the ratio of urinary α 1-microglobulin to microalbumin was greater than 1. Urinary α 1-microglobulin and microalbumin and the percentage of LMWP in urine were closely correlated ($r = 0.797$, $p = 0.000$), as shown in Table 1.

In contrast, urinary microalbumin increased substantially but α 1-microglobulin was almost normal in all four control groups. There were almost no LMWP in urine according to urine protein electrophoresis, and the ratio of urinary α 1-microglobulin to microalbumin was near zero. The level of α 1-microglobulin, the ratio of urinary α 1-microglobulin to microalbumin, and the percentage of LMWP in urine according to urine protein electrophoresis were much higher in patients with renal tubular and interstitial diseases than those in the four control groups ($p < 0.01$), while the level of microalbumin was much lower in patients with renal tubular and interstitial diseases than that in the four control groups ($p < 0.01$), as shown in Table 2.

Low-molecular-weight proteinuria is one of the major clinical manifestations of renal tubular and interstitial diseases. Low-molecular-weight proteinuria is defined as excessive urinary loss of α 1-microglobulin, β 2-microglobulin, or other low-molecular-weight plasma proteins. The current study examined the ratio of urinary α 1-microglobulin to microalbumin in several types of renal tubular and interstitial diseases that present in childhood, including Dent disease, Lowe syndrome, acute tubulointerstitial nephritis, and nephronophthisis, in order to find an easy, simple, and quick diagnostic criterion for tubuloproteinuria.

Dent disease is an X-linked recessive renal tubulopathy, and low-molecular-weight proteinuria is its

Table 1. Clinical data on 24 patients with renal tubular and interstitial diseases

Patient	Diagnosis	Age at diagnosis	UPE (mg/kg/24 h)	α 1-MG (mg/L)	MA (mg/L)	α 1-MG/MA	LMWP (%)
No. 1	DS*	9.8 y	64 ± 18	402 ± 113	285 ± 89	1.51 ± 0.12	61.3 ± 9.3
No. 2	DS	5.8 y	58 ± 17	349 ± 125	301 ± 81	1.33 ± 0.14	53.1 ± 7.5
No. 3	DS	5.2 y	55 ± 15	305 ± 108	257 ± 76	1.31 ± 0.11	53.5 ± 8.4
No. 4	DS	4.5 y	51 ± 16	346 ± 101	273 ± 86	1.35 ± 0.12	51.3 ± 8.1
No. 5	DS	5.7 y	53 ± 14	375 ± 134	268 ± 79	1.40 ± 0.10	56.5 ± 7.2
No. 6	DS	5.8 y	53 ± 13	382 ± 120	258 ± 82	1.51 ± 0.16	59.5 ± 7.6
No. 7	DS	3.5 y	62 ± 19	353 ± 131	249 ± 73	1.33 ± 0.15	52.8 ± 9.0
No. 8	DS	1.5 y	50 ± 17	258 ± 102	197 ± 68	1.43 ± 0.13	56.3 ± 6.5
No. 9	DS	5.1 y	56 ± 11	341 ± 116	238 ± 62	1.42 ± 0.12	56.1 ± 7.5
No. 10	DS	5.2 y	57 ± 10	355 ± 124	248 ± 61	1.44 ± 0.13	55.9 ± 6.3
No. 11	LS*	4.6 y	49 ± 12	315 ± 106	216 ± 57	1.46 ± 0.11	54.8 ± 7.2
No. 12	LS	4.9 y	45 ± 11	302 ± 108	237 ± 62	1.27 ± 0.10	53.2 ± 6.6
No. 13	ATIN*	7.5 y	22 ± 5	136 ± 14	102 ± 13	1.33 ± 0.14	54.7 ± 7.6
No. 14	ATIN	8.2 y	17 ± 4	121 ± 12	98 ± 11	1.24 ± 0.11	51.6 ± 7.2
No. 15	ATIN	9.4 y	25 ± 6	135 ± 14	112 ± 16	1.21 ± 0.13	50.3 ± 6.8
No. 16	ATIN	10.8 y	19 ± 5	124 ± 16	89 ± 12	1.40 ± 0.16	54.8 ± 6.5
No. 17	ATIN	12.5 y	23 ± 7	130 ± 15	115 ± 14	1.13 ± 0.14	52.5 ± 6.9
No. 18	ATIN	9.8 y	25 ± 5	138 ± 17	120 ± 13	1.15 ± 0.13	51.3 ± 7.2
No. 19	TINU*	12.4 y	27 ± 8	141 ± 18	124 ± 15	1.17 ± 0.15	52.7 ± 6.8
No. 20	TINU	10.8 y	19 ± 4	118 ± 16	88 ± 12	1.34 ± 0.15	55.7 ± 7.1
No. 21	TINU	11.3 y	12 ± 3	98 ± 10	81 ± 10	1.21 ± 0.11	53.1 ± 6.9
No. 22	TINU	13.6 y	18 ± 5	105 ± 12	94 ± 11	1.12 ± 0.14	52.7 ± 6.6
No. 23	NPHP*	3.8 y	28 ± 5	109 ± 16	87 ± 15	1.25 ± 0.10	53.5 ± 7.1
No. 24	NPHP	9.6 y	23 ± 4	98 ± 11	85 ± 12	1.15 ± 0.12	52.4 ± 7.3

*DS: Dent disease; LS: Lowe syndrome; ATIN: Acute tubulointerstitial nephritis; TINU: Tubulointerstitial nephritis with uveitis; NPHP: Nephronophthisis.

Table 2. Levels of α 1-MG, MA, and α 1-MG/MA and the percentage of LMWP in different groups

Groups	Age (years)	α 1-MG (mg/L)	MA (mg/L)	α 1-MG/MA	LMWP (%)
Renal tubular and interstitial diseases	7.6 ± 3.4	231 ± 78 [▲]	176 ± 43 [▲]	1.31 ± 0.14 [▲]	54.2 ± 7.3 [▲]
Nephrotic syndrome	6.8 ± 3.1	0 ± 0	3015 ± 483	0 ± 0	0 ± 0
IgA nephropathy	7.8 ± 1.7	8 ± 2	1853 ± 665	0 ± 0	3.5 ± 1.6
Henoch-Schonlein Purpura nephritis	7.9 ± 2.3	6 ± 2	1873 ± 587	0 ± 0	3.2 ± 1.5
Lupus nephritis	8.5 ± 1.6	9 ± 3	2981 ± 621	0 ± 0	6.4 ± 3.0

[▲]: $p < 0.01$ compared to other groups.

most constant feature. It mainly affects male children, and female carriers are generally asymptomatic (11,12). The level of proteinuria often reaches the nephrotic range (13,14). This hampers the diagnosis of Dent disease and explains why it is often treated as NS (15-17). The current results indicated that urinary α 1-microglobulin increased markedly (200-300-fold above the upper limit of normal, 0-12 mg/L) in all 10 patients with Dent disease, and the ratio of urinary α 1-microglobulin to microalbumin was greater than 1. This suggests that the ratio of urinary α 1-microglobulin to microalbumin could be used to measure LMWP in urine in patients with Dent disease.

Lowe syndrome is also an X-linked recessive renal tubulopathy that involves the eyes, central nervous system, and kidneys. Renal disease is primarily characterized by renal Fanconi syndrome, including low-molecular-weight proteinuria, proximal renal tubular acidosis, renal phosphate wasting, hypercalciuria, aminoaciduria, and hypokalemia (5,6). The current results indicated that urinary α 1-microglobulin also

increased markedly (about 300-fold above the upper limit of the normal range) in the 2 patients with Lowe syndrome, and the ratio of urinary α 1-microglobulin to microalbumin was greater than 1. This suggests that the ratio of urinary α 1-microglobulin to microalbumin could be used to measure LMWP in urine in patients with Lowe syndrome.

Tubulointerstitial nephritis (TIN) is characterized histologically by inflammation of and damage to tubulointerstitial structures, with relative sparing of glomerular and vascular elements. The clinical manifestations of TIN vary. The severity of renal impairment ranges from asymptomatic urinary abnormalities to mild azotemia, and even to non-oliguric and oliguric acute renal failure (ARF) (18,19). The nonspecific nature of the clinical findings in TIN highlights the need to perform a renal biopsy to make a definitive diagnosis in questionable cases. Systemic manifestations of hypersensitivity, such as a fever, rash, and arthralgia, vary. However, mild to moderate proteinuria (less than 1 g/day, mainly low-molecular-

weight proteinuria) is found in most patients with TIN. When tubulointerstitial nephritis is combined with uveitis, the condition is known as tubulointerstitial nephritis and uveitis (TINU) syndrome. This condition is mainly seen in children with a favorable renal prognosis (2). The diagnosis of TIN or TINU is difficult because of variable and nonspecific clinical manifestations. Studies have reported that urinary α 1-microglobulin and β 2-microglobulin excretion increase in patients with TINU (20,21). The current results indicated that urinary α 1-microglobulin increased significantly (about 100-fold above the upper limit of the normal range) in the 6 patients with ATIN and in the 4 patients with TINU, and the ratio of urinary α 1-microglobulin to microalbumin was greater than 1. This suggests that the ratio of urinary α 1-microglobulin to microalbumin could be used to measure LMWP in urine in patients with TIN or TINU.

Nephronophthisis (NPHP) includes a group of rare autosomal-recessive cystic kidney diseases, characterized by a broad genetic and clinical heterogeneity and accounting for the majority of genetic causes of end-stage renal disease (ESRD) during childhood. NPHP is associated with extra renal manifestations in 10-15% of patients (22,23). The diagnosis of NPHP is difficult because of its genetic and clinical complexity (24). However, the kidneys and liver are involved in most cases, and a low urine specific gravity and low-molecular-weight proteinuria are commonly seen in urinalysis (25). The current results indicated that urinary α 1-microglobulin increased close to 100-fold above the upper limit of the normal range in 2 patients with NPHP, and the ratio of urinary α 1-microglobulin to microalbumin was greater than 1. This suggests that the ratio of urinary α 1-microglobulin to microalbumin could be used to measure LMWP in urine in patients with NPHP. However, albuminuria in the nephrotic range is also seen in a few patients with NPHP (26), and LMWP in urine is not always specific to NPHP.

NS, IgA nephropathy, Henoch-Schonlein purpura nephritis, and lupus nephritis are the most common glomerular diseases that present during childhood. Proteinuria caused by these glomerular diseases mainly involves albumin. Upon diagnosis, urinary microalbumin increased markedly but α 1-microglobulin was almost normal in all 4 control groups, there were almost no LMWP in urine according to urine protein electrophoresis, and the ratio of urinary α 1-microglobulin to microalbumin was near zero. The ratio of urinary α 1-microglobulin to microalbumin differed substantially from that in patients with renal tubular and interstitial diseases.

In conclusion, this study is the first to suggest that a ratio of urinary α 1-microglobulin to microalbumin greater than 1 can be used as a diagnostic criterion for tubuloproteinuria. However, this study has several limitations. The sample size was small, few types of renal tubular and interstitial diseases were examined,

and only pediatric patients were included. Multicenter and larger-scale studies are needed to verify the current results.

References

1. Sekine T, Komoda F, Miura K, Takita J, Shimadzu M, Matsuyama T, Ashida A, Igarashi T. Japanese Dent disease has a wider clinical spectrum than Dent disease in Europe/USA: Genetic and clinical studies of 86 unrelated patients with low-molecular-weight proteinuria. *Nephrol Dial Transplant*. 2014; 29:376-384.
2. Sinnamon KT, Courtney AE, Harron C, O'Rourke DM, Mullan RN. Tubulointerstitial nephritis and uveitis (TINU) syndrome: Epidemiology, diagnosis and management. *NDT Plus*. 2008; 1:112-116.
3. Hoopes RR Jr, Raja KM, Koich A, Hueber P, Reid R, Knohl SJ, Scheinman SJ. Evidence for genetic heterogeneity in Dent's disease. *Kidney Int*. 2004; 65:1615-1620.
4. Grand T, L'Hoste S, Mordasini D, Defontaine N, Keck M, Pennaforte T, Genete M, Laghmani K, Teulon J, Lourdel S. Heterogeneity in the processing of CLCN5 mutants related to Dent disease. *Hum Mutat*. 2011; 32:476-483.
5. Cho HY, Lee BH, Choi HJ, Ha IS, Choi Y, Cheong HI. Renal manifestations of Dent disease and Lowe syndrome. *Pediatr Nephrol*. 2008; 23:243-249.
6. Bockenbauer D, Bokenkamp A, van't Hoff W, Levtschenko E, Kist-van Holthe JE, Tasic V, Ludwig M. Renal phenotype in Lowe Syndrome: A selective proximal tubular dysfunction. *Clin J Am Soc Nephrol*. 2008; 3:1430-1436.
7. Mandeville JT, Levinson RD, Holland GN. The tubulointerstitial nephritis and uveitis syndrome. *Surv Ophthalmol*. 2001; 46:195-208.
8. Saarela V, Nuutinen M, Ala-Houhala M, Arikoski P, Ronnholm K, Jahnukainen T. Tubulointerstitial nephritis and uveitis syndrome in children: A prospective multicenter study. *Ophthalmology*. 2013; 120:1476-1481.
9. Salomon R, Saunier S, Niaudet P. Nephronophthisis. *Pediatr Nephrol*. 2009; 24:2333-2344.
10. Simms RJ, Eley L, Sayer JA. Nephronophthisis. *Eur J Hum Genet*. 2009; 17:406-416.
11. Claverie-Martin F, Ramos-Trujillo E, Garcia-Nieto V. Dent's disease: Clinical features and molecular basis. *Pediatr Nephrol*. 26: 693-704.
12. Devuyst O. Dent's disease: Chloride-proton exchange controls proximal tubule endocytosis. *Nephrol Dial Transplant*. 2010; 25:3832-3835.
13. Li P, Huang JP. Phenotype and genotype of Dent's disease in three Chinese boys. *Nephrology (Carlton)*. 2009; 14:139-142.
14. Jian S, Wei M, He YY, Wang W, Kang YL, Sun ZX. Clinical and genetic analysis of Dent disease in 4 Chinese children. *Zhongguo Dang Dai Er Ke Za Zhi*. 2015; 17:1261-1266. (in Chinese)
15. Frishberg Y, Dinour D, Belostotsky R, Becker-Cohen R, Rinat C, Feinstein S, Navon-Elkan P, Ben-Shalom E. Dent's disease manifesting as focal glomerulosclerosis: Is it the tip of the iceberg? *Pediatr Nephrol*. 2009; 24:2369-2373.
16. Szczepanska M, Zaniew M, Recker F, Mizerska-Wasiak M, Zaluska-Lesniewska I, Kilis-Pstrusinska K, Adamczyk

- P, Zawadzki J, Pawlaczyk K, Ludwig M, Sikora P. Dent disease in children: Diagnostic and therapeutic considerations. *Clin Nephrol.* 2015; 84:222-230.
17. Cramer MT, Charlton JR, Fogo AB, Fathallah-Shaykh SA, Askenazi DJ, Guay-Woodford LM. Expanding the phenotype of proteinuria in Dent disease. A case series. *Pediatr Nephrol.* 2014; 29:2051-2054.
 18. Greising J, Trachtman H, Gauthier B, Valderrama E. Acute interstitial nephritis in adolescents and young adults. *Child Nephrol Urol.* 1990; 10:189-195.
 19. Jones CL, Eddy AA. Tubulointerstitial nephritis. *Pediatr Nephrol.* 1992; 6:572-586.
 20. Li C, Su T, Chu R, Li X, Yang L. Tubulointerstitial nephritis with uveitis in Chinese adults. *Clin J Am Soc Nephrol.* 2014; 9:21-28.
 21. Hettinga YM, Scheerlinck LM, Lilien MR, Rothova A, de Boer JH. The value of measuring urinary β 2-microglobulin and serum creatinine for detecting tubulointerstitial nephritis and uveitis syndrome in young patients with uveitis. *JAMA Ophthalmol.* 2015; 133:140-145.
 22. Wolf MT, Hildebrandt F. Nephronophthisis. *Pediatr Nephrol.* 2011; 26:181-194.
 23. Benzing T, Schermer B. Clinical spectrum and pathogenesis of nephronophthisis. *Curr Opin Nephrol Hypertens.* 2012; 21:272-278.
 24. O'Toole JF, Otto EA, Hoefele J, Helou J, Hildebrandt F. Mutational analysis in 119 families with nephronophthisis. *Pediatr Nephrol.* 2007; 22:366-370.
 25. Sugimoto K, Miyazawa T, Enya T, Nishi H, Miyazaki K, Okada M, Takemura T. Clinical and genetic characteristics of Japanese nephronophthisis patients. *Clin Exp Nephrol.* 2015; 20:637-649.
 26. Zhang H, Su B, Liu X, Xiao H, Ding J, Yao Y. Mutations in TTC21B cause different phenotypes in two childhood cases in China. *Nephrology (Carlton).* 2017. doi: 10.1111/nep.13008.

(Received December 7, 2017; Revised January 28, 2018; Accepted February 1, 2018)

Omental fibromatosis treated by laparoscopic wide surgical resection

David Martin^{1,2,*}, Mirza Muradbegovic¹, Snezana Andrejevic-Blant³, David Petermann¹, Luca Di Mare^{1,2}

¹Department of Visceral Surgery, University Hospital CHUV, Lausanne, Switzerland;

²Department of General and Visceral Surgery, EHC Hospital, Morges, Switzerland;

³Unilabs Pathology, Cypa-Epalinges, Lausanne, Switzerland.

Summary

The current report presents a case of an omental fibromatosis discovered incidentally in a 46-year-old woman with no particular medical history and few symptoms. A surgical biopsy was performed initially, and microscopic examination revealed myofibroblastic proliferation. After additional immunohistochemical and molecular analyses, omental fibromatosis was diagnosed. Omental fibromatosis, also called intra-abdominal desmoid, is a rare and benign tumour but can be locally aggressive. Majority of cases are asymptomatic, and difficult to diagnose based on clinical presentation and radiological investigation. Final diagnosis is usually made on histopathology and immunohistochemistry studies. Surgical wide excision is currently the treatment of choice.

Keywords: Omental fibromatosis, desmoid tumor, surgical resection

1. Introduction

Most intra-abdominal fibromatosis affect small bowel mesentery (1). However, the omentum, transverse or sigmoid mesocolon, or even ligamentum teres may also be affected (2,3). Omental fibromatosis is a rare benign fibroproliferative process but locally aggressive which may infiltrate the adjacent organs or recur, but do not create distant metastatic lesions (2-4). The term "fibromatosis" was first described by a team of American pathologists in the early 1960s (5). Omental fibromatosis is also termed as intra-abdominal desmoids. These tumors occur in a wide age range of patients, and have no gender or race predilection (3). They are typically seen in the third and fourth decades of life and the estimated incidence is 3.7 new cases per million people per year (6,7). Final diagnosis is usually made on histopathology and immunohistochemistry studies. Surgical wide excision is currently the treatment of choice (8).

The current report presents a case of an omental fibromatosis discovered incidentally in a 46-year-old woman with no particular medical history and few symptoms. The Regional Committee for Medical and Health Research Ethics did not require ethical approval for reporting individual cases. Written informed consent was obtained from the patient for the publication of this case report and its accompanying images.

2. Case Report

A 46-year-old woman, with no medical and surgical history, presented electively for an epigastric hernia cure. Due to chronic diffuse abdominal pain, increased fatigue and weight loss of 2 kg in a few months, it was decided to perform a laparoscopic hernia repair with concomitant exploration of the abdominal cavity.

After introduction of the optical trocar in the left flank, exploration revealed greyish-white diffuse nodules of the great omentum, as well as a more localized tumor near the right colonic angle (Figure 1). No mesenteric adenopathy, ascites, or peritoneal implants were identified. The rest of the laparoscopic exploration revealed nothing more. A surgical biopsy was performed. It was decided to stop the procedure in order to obtain anatomopathological results and to provide an

Released online in J-STAGE as advance publication February 26, 2018.

*Address correspondence to:

Dr David Martin, Department of Visceral Surgery, University Hospital CHUV, Lausanne, Switzerland.

E-mail: david.martin@chuv.ch

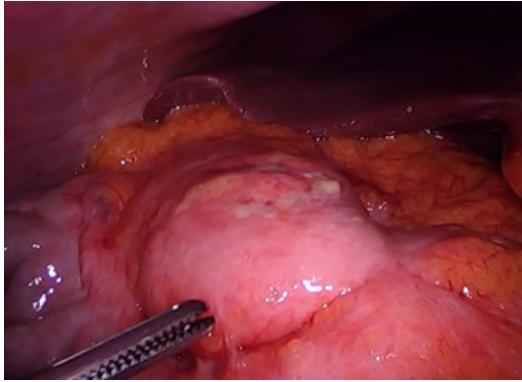


Figure 1. Exploratory laparoscopy: greyish-white nodule of the great omentum.

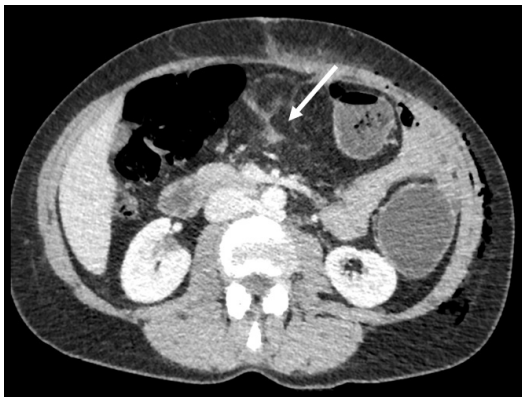


Figure 2. Abdominal CT scan showing a discrete fat infiltration of the greater omentum (white arrow), located above the transverse colon, without individualizable nodule.

oncological assessment.

The retrospective clinical examination was featureless. Tumor markers (CEA, CA 19-9, CA 125) were within the normal range. Thoraco-abdominal CT scan showed only a discrete fat infiltration of the greater omentum, located above the transverse colon, without individualizable nodule (Figure 2).

Macroscopic pathologic examination showed no significant lesions, except for fibrous remodelling (Figure 3a). Microscopic examination revealed adipose tissue with a clearly defined myofibroblastic fusocellular proliferation foci (Figure 3 a, b, and c). After detailed immunohistochemical analysis, fusiform cells expressed smooth muscle actin (SMA), muscle specific actin (MSA) and beta-catenin (Figure 3d), and were negative for S-100 protein and CD-117. The MIB-1 cell proliferation index was very low (< 1%). This myofibroblastic proliferation was morphologically and immunohistochemically consistent with omental fibromatosis. The diagnosis of omental fibromatosis was confirmed by molecular analysis showing that exon 3 of the CTNNB1 gene was present.

After discussion at the local tumor board, it was decided to proceed to a laparoscopic en bloc resection of the greater omentum. Histopathological examination

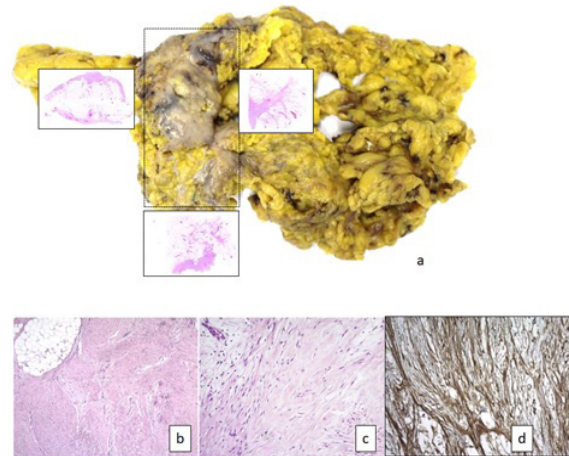


Figure 3. Macroscopic examination showing focal, fibrous remodelling (a). Microscopic examination revealing adipose tissue with a clearly defined myofibroblastic fusocellular proliferation foci (a, b, and c), expressing smooth muscle actin and beta-catenin (d).

confirmed the lesion as omental fibromatosis.

3. Discussion

Omental fibromatosis is a rare and benign disease occurring in a wide age range of patients, and has no gender or race predilection. Patients have few symptoms and its discovery can sometimes be unexpected during radiological imaging or intraoperatively as in this present case.

Fibromatosis have distinct biological behavior, characterized by initial rapid growth, followed by stability or even regression. Majority of fibromatosis occur sporadically, or in association with Gardner syndrome, familial adenomatous polyposis coli (FAP) and bilateral ovarian fibromatosis (2,9). Both males and females are affected with equal frequency based on literature review (5). These tumors are not encapsulated and vary widely in size (8). Most tumors measure between 5 and 10 cm in diameter, but they may be as large as 30 cm (10). Predisposing factors are pregnancy, previous abdominal surgery or trauma, and estrogen therapy (1,11-13).

Patients have few symptoms until the tumor reaches a size large enough to cause pain, abdominal fullness, pressure sensation, constipation, and even weight loss (5,8). Most patients with omental fibromatosis are asymptomatic or may present vague abdominal pain, as in this case (2). Some complications that have been reported include small-bowel obstruction and hydronephrosis from ureteric obstruction (14).

The imaging appearance of these tumors is variable and depends on fibroblastic proliferation, fibrosis, collagen content, and vascularity (1). Ultrasonography or computed tomography may be helpful in diagnosis but ultimately, final diagnosis is made by excision and histological examination (2). On ultrasonography,

desmoid tumors have variable echogenicity, appearing as masses of low, medium, or high echogenicity with smooth defined margins (7). Computed tomography images typically demonstrate tumors as solid, well-circumscribed masses of soft tissue density that do not contain calcium, with homogenous enhancement at the periphery and cystic pattern in the central region (8,15).

On macroscopic examination, desmoid tumors are usually circumscribed lesions, but they may have irregular or infiltrating borders, as in this current case. On the surface, they are white and coarsely trabeculated, resembling scar tissue (1). In 10-15% of cases, they are multiple (1). Histologically, desmoid tumors are lesions composed of bland spindle or stellate fibroblastic cells embedded in a collagenous stroma, without evidence of muscular or neural differentiation and with little or no inflammatory component (1). Differential diagnosis includes cysts, sclerosing mesenteritis, mesenteric panniculitis, or tumours originating from smooth muscle, neuronal tissue, adipose and stromal tissue of gastrointestinal tract (2).

Treatment of choice is surgical resection (8). Radiation therapy and/or chemotherapy demonstrated no benefit (16). Surgical approach includes wide local excision of these tumours as they have tendency toward local recurrence in up to 50% (2,8). Some authors recommend a trial of observation with antioestrogens, nonsteroidal anti-inflammatory drugs with limited role of targeted agents such as Imatinib (2,6). There are no clear guidelines for the treatment and follow-up of omental fibromatosis because of its rarity. Therefore, close long-term follow-up should be performed.

In conclusion, omental fibromatosis is usually a benign tumour but can be locally aggressive. Majority of cases are asymptomatic, and difficult to diagnose based on clinical presentation and radiological investigation. Final diagnosis is usually made on histopathology and immunohistochemistry studies. Currently, surgical excision is the only curative method of treatment.

References

1. Faria SC, Iyer RB, Rashid A, Ellis L, Whitman GJ. Desmoid tumor of the small bowel and the mesentery. *AJR Am J Roentgenol.* 2004; 183:118.
2. Kori C, Singh P, Jain N, Jain J, Kumar V. Giant omental fibromatosis presenting as pelvic mass. *J Clin Diagn Res.* 2015; 9:XD06-XD08.
3. Misiak P, Piskorz L, Wcislo S, Jablonski S, Brocki M. Giant mesentery fibromatosis presenting as acute abdomen – Case report. *Contemp Oncol (Pozn).* 2013; 17:468-469.
4. Osawa H, Nishimura J, Inoue A, *et al.* A case of solitary fibrous tumor from the greater omentum resected via laparoscopic surgery. *Gan To Kagaku Ryoho.* 2014; 41:2493-2495. (in Japanese)
5. Yannopoulos K, Stout AP. Primary solid tumors of the mesentery. *Cancer.* 1963; 16:914-927.
6. Einstein DM, Tagliabue JR, Desai RK. Abdominal desmoids: CT findings in 25 patients. *AJR Am J Roentgenol.* 1991; 157:275-279.
7. Casillas J, Sais GJ, Greve JL, Iparraguirre MC, Morillo G. Imaging of intra- and extraabdominal desmoid tumors. *Radiographics.* 1991; 11:959-968.
8. Disher AC, Biswas M, Miller TQ, Kuvhengahwa A. Atypical desmoid tumor of the abdomen: A case report. *J Natl Med Assoc.* 1993; 85:309-311.
9. Xuereb S, Xuereb R, Buhagiar C, Gauci J, Magri C. A case report of desmoid tumour—a forgotten aspect of FAP? *Int J Surg Case Rep.* 2017; 30:122-125.
10. Sakorafas GH, Nissotakis C, Peros G. Abdominal desmoid tumors. *Surg Oncol.* 2007; 16:131-142.
11. Levy AD, Rimola J, Mehrotra AK, Sobin LH. From the archives of the AFIP: benign fibrous tumors and tumorlike lesions of the mesentery: Radiologic-pathologic correlation. *Radiographics.* 2006; 26:245-264.
12. Gautam A, Khatri AK, Pandey M, Arya NC, Shukla VK. Mesenteric mass in a 28-year-old woman. *Postgrad Med J.* 1997; 73:121-122.
13. Vaswani BA, Shah M, Shah PM, Parikh BJ, Anand AS, Sharma GL. Giant mesenteric fibromatosis in Gardner's syndrome. *Indian J Cancer.* 2011; 48:140-142.
14. Baron RL, Lee JK. Mesenteric desmoid tumors: Sonographic and computed-tomographic appearance. *Radiology.* 1981; 140:777-779.
15. Paksoy Y, Sahin M, Acikgozoglu S, Odev K, Omeroglu E. Omental fibroma: CT and US findings. *Eur Radiol.* 1998; 8:1422-1424.
16. Schwartz RW, Reames M, McGrath PC, Letton RW, Appleby G, Kenady DE. Primary solid neoplasms of the greater omentum. *Surgery.* 1991; 109:543-549.

(Received December 29, 2017; Revised February 17, 2018; Accepted February 19, 2018)

Intracardiac thrombosis in Behçet's Disease successfully treated with immunosuppressive agents: A case of vascular pathergy phenomenon

Francisco Galeano-Valle^{1,2,*}, Pablo Demelo-Rodriguez^{1,2}, Luís Álvarez-Sala-Walther^{2,3}, Blanca Pinilla-Llorente^{2,3}, Miguel Jesús Echenagusia-Boyra⁴, Hugo Rodriguez-Abella⁵, Jorge Del-Toro-Cervera^{1,3}

¹ Venous Thromboembolism Unit, Hospital General Universitario Gregorio Marañón, Madrid, Spain;

² Department of Medicine, School of Medicine, Universidad Complutense Madrid, Spain;

³ Department of Internal Medicine, Hospital General Universitario Gregorio Marañón, Madrid, Spain;

⁴ Department of Vascular Interventional Radiology, Hospital General Universitario Gregorio Marañón, Madrid, Spain;

⁵ Department of Cardiovascular Surgery, Hospital General Universitario Gregorio Marañón, Madrid, Spain.

Summary

Behçet's Disease (BD) is a rare multi-systemic inflammatory disorder classified as a systemic vasculitis of unknown aetiology. Vascular involvement occurs in approximately 5-51.6% cases, affecting venous and arterial vessels. Cardiac involvement is rare in BD (6%). There have been published approximately 93 cases of BD associated with intracardiac thrombosis, with different treatments and courses. We present a case of a 35-year-old spanish male that, after a percutaneous pharmacomechanical thrombectomy with venous stent placement, developed high fever and extensive venous thrombosis despite anticoagulation including intracardiac thrombosis (ICT) in the right ventricle and pulmonary embolism that led to the diagnosis of BD. The patient was successfully treated with immunosuppressants, achieving the complete resolution of ICT. We hypothesize that the endovenous procedure could have acted as a trigger for the posterior acute attack of the disease, representing a 'vascular pathergy phenomenon'. Vascular BD has to be suspected in cases of thrombosis recurrence despite correct anticoagulation, and intense immunosuppressive treatment should be considered.

Keywords: Behçet disease, immunosuppressive agents, intracardiac thrombus, thrombectomy, venous thromboembolism

1. Introduction

Behçet's Disease (BD) is a rare multi-systemic inflammatory disorder classified as a systemic vasculitis of unknown aetiology. Onset occurs usually in the third decade and it affects both genders equally. Diagnosis is mainly clinical with no specific laboratory tests (1). A correlation with human leukocyte antigen (HLA) class I antigens, notably HLA-B51, but also others like A26 has

been observed (2). Clinical course is characterized by frequent relapses and remissions. BD may affect almost all vascularized systems. Prevalence of BD worldwide ranges between 0.12-420/100,000 persons with a significant presence in the Silk Road countries (1-5).

We present a case of Behçet's disease associated with intracardiac thrombosis (ICT) that developed right after pharmacomechanical thrombectomy of a previous deep venous thrombosis (DVT). Venous manipulation acts as a trigger or a vascular attack of Behçet's disease.

2. Case Report

A 35-year-old spanish male had a history of hypercholesterolemia, active smoking and 2 episodes of pericarditis years ago. A year before he had an episode of

Released online in J-STAGE as advance publication February 26, 2018.

*Address correspondence to:

Dr. Francisco Galeano-Valle, Hospital General Universitario Gregorio Marañón, C/. Doctor Esquerdo, 46, 28007, Madrid, Spain.

E-mail: paco.galeano.valle@gmail.com

deep vein thrombosis (DVT) in the left lower extremity that involved the common iliac vein, treated with acenocumarol. Thrombophilia testing was normal. The patient developed a severe post-thrombotic syndrome (PTS) 3 months later. A computerized tomography (CT) showed compression of the left common iliac vein by the right common iliac artery (May-Thurner syndrome). As a severe PTS persisted after one year of anticoagulant treatment, percutaneous rheolytic pharmacomechanical thrombectomy with venous stent placement was performed without complications.

Ten days after the procedure, the patient presented in the emergency department with a 10-day history of high fever, shivers and pain in the left inguinal region. Physical examination revealed: temperature 40°C, blood pressure 120/55 mmHg, heart rate 110 bpm, edema in the left lower extremity, and the remainder was unremarkable. A stent-related infection was suspected. Anticoagulation with low molecular weight heparin and empirical broad spectrum antibiotic therapy were started. Laboratory tests showed 16.850 leucocytes/mm³, 78% neutrophils, C-reactive protein 16.2 mg/dL, international normalized ratio (INR) 3.75, erythrocyte sedimentation rate (ESR) 76 mm 1st hour, and the remainder of the laboratory tests was normal. The blood and urine cultures (6 times) were sterile. The peripheral blood smear showed neutrophil granulation. Proteinogram, autoantibodies, lupus anticoagulant, serologies for human immunodeficiency virus, hepatitis C virus, hepatitis B virus, syphilis, *Rickettsia*, *Mycoplasma*, Rose Bengal agglutination, interferon-gamma release assay and PCR for *Thropheryma whipplei*, *Bartonella sp* and *Coxiella burnetii* were normal. A chest X ray and a transesophageal echocardiogram (TEE) were normal. A transthoracic echocardiogram (TTE) showed dilation of the aortic root (38 mm). An abdominopelvic CT showed a subocclusive thrombosis in the iliac stent.

High fever and daily shivers persisted for 3 weeks despite anticoagulation and antibiotic therapy. A Positron Emission Tomography - Computed Tomography (PET-CT) was performed showing a thrombus in the right ventricle with hyper-metabolic activity, thrombosis in the infrarenal inferior vena cava (IVC) and in both common iliac veins, thrombosis of the stent in the left iliac vein with two areas of hyper-metabolic activity that suggested infection of the stent (Figure 1A, 1B), and a right pulmonary infarction suggesting pulmonary embolism (PE). A TTE showed a rounded moving 30 mm long image stuck on the right ventricle apex with heterogeneous echogenicity, compatible with moving thrombus (Figure 1C), and a TEE showed no valvular damage. At this point, the patient presented three oral aphthous ulcers and papulopustular lesions in the back. Herpes simplex virus culture isolation of an ulcer was negative. The patient acknowledged oral and genital aphtous ulcers

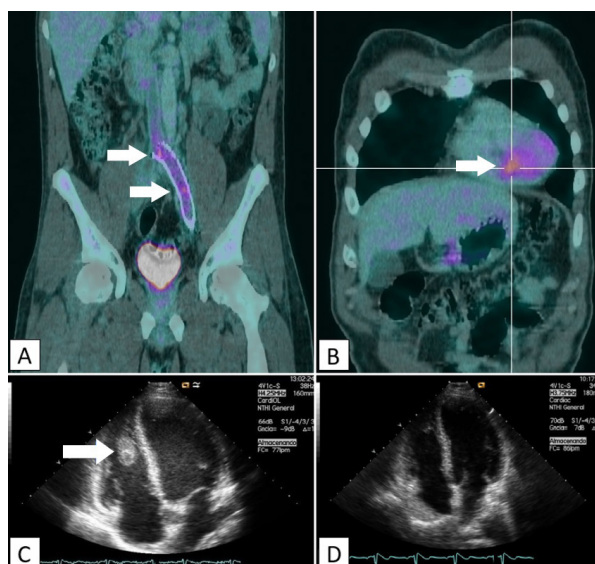


Figure 1. (A), Positron Emission Tomography - Computed Tomography (PET-CT) shows thrombosis of the stent in the left common iliac vein with two areas of hyper-metabolic activity (white arrows); (B), PET-CT reveals a thrombus in the right ventricle with hyper-metabolic activity (white arrow); (C), Transthoracic echocardiogram (TTE) discloses a rounded moving 30 mm long image (white arrow) stuck on the right ventricle apex with heterogeneous echogenicity, compatible with moving thrombus; (D), TTE performed 2 months later showing total resolution of ICT.

occasionally in the past few years. A labeled leukocytes scintigraphy was performed and ruled out intracardiac or stent-related infection. He was finally diagnosed as Behçet's disease associated with extensive venous thromboembolism including intracardiac thrombus (ICT) in the right ventricle and PE. The pathergy test was negative and the phenotype HLA I was A26-A32/B39-B40(B61)/C02-C12/(Bw4-Bw6). Immunosuppressants were started: methylprednisolone bolus, rituximab and cyclophosphamide. Fever disappeared within 48 hours. Acute phase reactants normalized after 1 week. A CT performed 2 weeks later showed partial recanalization of IVC and right iliac vein with persistence of thrombus inside the stent. A TTE performed 2 weeks later showed a reduction of the ICT size from 30 to 21 mm. The patient was discharged with prednisone, cyclophosphamide, colchicine, and acenocumarol. A TTE performed 2 months later showed total resolution of ICT (Figure 1D).

3. Discussion

Vascular system is involved in BD in 5-51.6% including venous and arterial beds and it has a relapsing course (3,4). BD is unique among other vasculitides as it usually affects veins rather than arteries and it has significant thrombotic tendency associated with vascular inflammation, which cannot be explained by thrombophilic factors (3). The most common type of vascular involvement is lower extremity

Table 1. Clinical characteristics and vascular involvement of the previous cases* of Behçet's Disease with intracardiac thrombosis in comparison with our case

Items	Previous cases (n = 93)	Our case
Male to female ratio	81:12	Male
Age at diagnosis (years)	27 (mean)	35
Oral involvement (n, %)	91 (98%)	+
Genital involvement (n, %)	86 (93%)	+
Skin involvement (n, %)	45 (57%)	+ (papulopustular lesions)
Pathergy test (n, %)	41 (61%)	negative
Ocular involvement (n, %)	18 (23%)	-
Pulmonary thromboembolism (n, %)	52 (56%)	+
Venous thrombosis (n, %)	39 (42%)	+
- Lower extremity Deep veins	31 (33%)	+
- Inferior vena cava thrombosis	6 (6%)	+
- Superior vena cava thrombosis	10 (11%)	-
Arterial involvement (n, %)	35 (38%)	+ (dilation of the aortic root)
- Pulmonary artery aneurysm	33 (35%)	-
Thrombosis in the right side of the heart	95%	+
- Thrombosis in the right ventricle	74%	+
- Thrombosis in the right atrium	40 (43%)	-
Sinus thrombosis (n, %)	6 (6%)	-
Budd-Chiari (n, %)	7 (7%)	-

*Adapted from Aksu *et al.* (12).

vein thrombosis, forming 70% of all vascular events (3,4). Pulmonary artery involvement (aneurysms and thrombosis) (PAI) is the most common form of arterial involvement (3,4). Inferior or superior vena cava, hepatic veins, cerebral venous sinuses, PE, and the right-side heart are other described locations of venous involvement (3). PE has been described as a rare complication, and this may be explained because the thrombi in these patients are strongly adherent (3-5) and formed in situ because from an anatomical and physiological point of view, the right-side heart and pulmonary arteries seem to be continuum of the vena cava (3). Vascular involvement is not included in the International Study Group criteria, but it is included in the revised International Criteria for Behçet's Disease (2010) (6,7).

Cardiac involvement is a rare (6%) and life-threatening complication. It may be present as pericarditis, myocarditis, endocarditis with valvular regurgitation, endomyocardial fibrosis, coronary arteritis, Valsalva sinus aneurysms and as intracardiac thrombus (ICT) (8-10). ICT are strongly associated with pulmonary artery involvement and are mostly located on the right side of the heart probably because of the vena cava extension (3,8,11,12). These thrombi contain inflammatory cell infiltrates and are tightly bound to the underlying endocardium or myocardium (3). Relapses are infrequent. Cardiac surgery is not recommended unless there are severe complications such as valve failure or pulmonary hypertension (3). There have been published approximately 93 cases of BD associated with ICT, most of them are case reports and case series, which have been recently reviewed by Aksu and Tufekcioglu (12) with a male to female ratio of 23:2 and a mean age of 27 years. At the time

of detection of ICT, fever, hemoptysis, dyspnea, and cough were the predominant symptoms (11,12). In 40-56% of patients with ICT PAI was detected, 42-56% of them had venous thrombosis, and 52-55% had PE (5,11,12). ICT is uniformly associated with an elevated ESR but it is a poor indicator of disease activity (11,13). Cardiac involvement was the first clinical manifestation of BD in 40-50% of cases (8,10,11). The similarity and difference of the research findings between our case report and that published by other studies are summarized in Table 1.

Immunosuppressants, with or without glucocorticoids, are essential in the management of vascular involvement in BD. It has been shown to reduce the relapse rate and to prolong survival in several retrospective studies (3). Life-threatening conditions such as pulmonary artery involvement, Budd-Chiari syndrome, and peripheral arterial aneurysms/occlusions are managed with aggressive medical treatment, including cyclophosphamide and glucocorticoid pulses. Corticosteroids, azathioprine, cyclosporine A, and cyclophosphamide are recommended in the management of acute DVT (4). In resistant cases, anti-tumor necrosis factor (TNF) agents could be also effective (14). Whether to add anticoagulants to prevent relapses has been an issue of debate. Several retrospective studies showed the inefficacy of anticoagulation alone or added to immunosuppressants in preventing recurrences (3,15). Anticoagulation could increase the risk of aneurysmal rupture (15). Nevertheless, the tolerance of anticoagulation therapy was satisfactory in patients with low-risk of bleeding after ruling out pulmonary artery aneurysms and it could be used in refractory venous thrombosis along with monoclonal TNF-alpha antagonists (16). Rituximab and methotrexate

were found to be more effective than traditional drugs (cyclophosphamide, azathioprine, and prednisone) in improving all the most dreadful ocular manifestations in a single-blind randomized controlled trial (17). When indicated, surgical treatment is not advised in the active phase of the disease. Invasive arterial techniques may cause pseudoaneurysms, especially in the presence of active inflammation (5,18). Unfortunately, there are no randomised controlled trials (RCT) (13).

In our case, ICT developed shortly after venous manipulation with pharmacomechanical thrombectomy and venous stent placement. Quite similar to pathergy phenomenon, this vascular insult could have triggered the acute attack of BD. In a retrospective study, 32.6% of surgeries in patients with BD were complicated by wound dehiscence, infection, or graft failure and they found that glucocorticoids used in conjunction with immunosuppressive agents significantly reduced the risk of postoperative complications (18). There is significant thrombotic tendency that could be triggered even by intravenous needle or cannula insertion (3).

BD can cause substantial morbidity (blindness, physical disability, cognitive impairment) and increased mortality. Vascular manifestations like pulmonary arterial lesions (with a 50% mortality within 3 years) and Budd-Chiari syndrome are the leading causes of mortality in BD patients (3,5,16). In a 25 cases series, the presence of ICT conferred a poor prognosis (44% were treated with surgery, and 28% died from different causes) (11), but in more recent series immunosuppressive agents improved prognosis achieving ICT remission (3,10).

In conclusion, we present a case of ICT associated with BD clinically manifested by prolonged high fever of unknown origin, successfully treated with immunosuppressants. We hypothesize that the endovascular procedure could have acted as a trigger of the acute attack of BD, representing a 'vascular pathergy phenomenon'. Vascular BD has to be considered in cases of thrombosis recurrence despite correct anticoagulation. Different treatment options for ICT in BD have been used including steroids, immunosuppressants, anticoagulation and surgery, with different outcomes. Surgical treatment of ICT is usually not recommended. Further studies are needed to guide the management of vascular involvement and other life-threatening complications of BD.

References

1. Zeidan MJ, Saadoun D, Garrido M, Klatzmann D, Six A, Cacoub P. Behçet's disease pathophysiology: A contemporary review. *Auto Immun Highlights*. 2016; 7:4.
2. Takeuchi M, Kastner DL, Remmers EF. The immunogenetics of Behçet's disease: A comprehensive review. *J Autoimmun*. 2015; 64:137-148.
3. Seyahi E. Behçet's disease: How to diagnose and treat vascular involvement. *Best Pract Res Clin Rheumatol*. 2016; 30:279-295.

4. Calamia KT, Schirmer M, Melikoglu M. Major vessel involvement in Behçet's disease: An update. *Curr Opin Rheumatol*. 2011; 23:24-31.
5. Fei Y, Li X, Lin S, Song X, Wu O, Zhu Y, Gao X, Zhang W, Zhao Y, Zeng X, Zhang F. Major vascular involvement in Behçet's disease: A retrospective study of 796 patients. *Clin Rheumatol*. 2013; 32:845-852.
6. Davatchi F, Assaad-Khalil S, Calamia KT, *et al*. International Study Group for Behçet's Disease. Criteria for diagnosis of Behçet's disease. *Lancet*. 1990; 335:1078-1080.
7. International Team for the Revision of the International Criteria for Behçet's Disease (ITR-ICBD). The International Criteria for Behçet's Disease (ICBD): A collaborative study of 27 countries on the sensitivity and specificity of the new criteria. *J Eur Acad Dermatol Venerol*. 2014; 28:338-347.
8. Emmungil H, Yaşar Bilge NŞ, Küçükşahin O, Kılıç L, Okutucu S, Gücenmez S, Kalyoncu U, Kaşifoğlu T, Turqay M, Aksu K. A rare but serious manifestation of Behçet's disease: Intracardiac thrombus in 22 patients. *Clin Exp Rheumatol*. 2014; 32(Suppl 84):87-92.
9. Desbois AC, Wechsler B, Resche-Rigon M, Piette JC, Huong Dle T, Amoura Z, Koskas F, Desseaux K, Cacoub P, Saadoun D. Immunosuppressants reduce venous thrombosis relapse in Behçet's disease. *Arthritis Rheum*. 2012; 64:2753-2760.
10. Ahn JK, Lee YS, Jeon CH, Koh EM, Cha HS. Treatment of venous thrombosis associated with Behçet's disease: Immunosuppressive therapy alone versus immunosuppressive therapy plus anticoagulation. *Clin Rheumatol*. 2008; 27:201-205.
11. Mogulkoc N, Burgess MI, Bishop PW. Intracardiac thrombus in Behçet's disease: A systematic review. *Chest*. 2000; 118:479-487.
12. Aksu T, Tufekcioglu O. Intracardiac thrombus in Behçet's disease: Four new cases and a comprehensive literature review. *Rheumatol Int*. 2015; 35:1269-1279.
13. Esatoglu SN, Hatemi G, Leccese P, Olivieri I. Highlights of the 17th International Conference on Behçet's syndrome. *Clin Exp Rheumatol*. 2016; 34(Suppl 102):3-9.
14. Caso F, Costa L, Rigante D, *et al*. Biological treatments in Behçet's disease: Beyond anti-TNF therapy. *Mediators Inflamm*. 2014; 2014:107421.
15. Wang H, Guo X, Tian Z, Liu Y, Wang Q, Li M, Zeng X, Fang Q. Intracardiac thrombus in patients with Behçet's disease: Clinical correlates, imaging features, and outcome: A retrospective, single-center experience. *Clin Rheumatol*. 2016; 35:2501-2507.
16. Demirelli S, Degirmenci H, Inci S, Arisoy A. Cardiac manifestations in Behçet's disease. *Intractable Rare Dis Res*. 2015; 4:70-75.
17. Davatchi F, Shams H, Rezaipoor M, Sadeghi-abdollahi B, Shahram F, Nadji A, Chams-Davatchi C, Akhlaghi M, Faezi T, Naderi N. Rituximab in intractable ocular lesions of Behçet's disease; randomized single-blind control study (pilot study). *Int J Rheum Dis*. 2010; 13:246-252.
18. Park MC, Hong BK, Kwon HM, Hong YS. Surgical outcomes and risk factors for postoperative complications in patients with Behçet's disease. *Clin Rheumatol*. 2007; 26:1475-1480.

(Received January 12, 2018; Revised January 27, 2018; Accepted February 19, 2018)

A case of stent thrombosis presenting as acute myocardial infarction related to right coronary artery originating from the left coronary system

Emrah Ermis^{1,*}, Serkan Kahraman², Hakan Ucar¹, Samir Allahverdiyev¹

¹ Department of Cardiology, Biruni University, Faculty of Medicine, Istanbul, Turkey;

² Division of Cardiology, Silivri State Hospital, Istanbul, Turkey.

Summary

Right coronary artery (RCA) originating from the left coronary system is a subtype of single coronary artery (SCA) anomaly, and the origin of RCA as a branch from the left anterior descending artery (LAD) is a very rare variant. A 55-year-old male who had a percutaneous coronary intervention (PCI) history was hospitalized due to acute coronary syndrome. Coronary angiography revealed an aberrant RCA originating from the mid-LAD as well as stent thrombosis. A successful PCI was performed and he was discharged from the hospital three days after the PCI. It is known that there is an increased incidence of atherosclerosis and stent thrombosis in coronary anomaly patients. Therefore, interventional cardiologists should consider the most suitable PCI strategy before stenting and avoid complex techniques.

Keywords: Coronary vessel anomalies, single coronary artery anomaly, percutaneous coronary intervention, stent thrombosis

1. Introduction

The incidence of coronary artery anomaly is about 1.3% in the largest reported series (1). A rare anomaly of the coronary arteries originating from a single coronary ostium in the aorta is called a single coronary artery (SCA) and its incidence ranges from 0.024% to 0.066% in several studies (1,2). Right coronary artery (RCA) originating from the left coronary system is a subtype of this anomaly and the origin of RCA as a branch from the left anterior descending artery (LAD) is a very rare variant of the SCA anomaly. It is known that coronary artery anomalies can be related to coronary ischemia and sudden cardiac death (3).

We herein present a case introducing a patient with a SCA anomaly in which the RCA arose from the LAD mid-segment and percutaneous coronary intervention (PCI) was performed due to stent thrombosis.

2. Case Report

A 67-year-old male having a history of elective PCI two years ago was admitted to our emergency service with chest pain that had been ongoing for three hours. His hemodynamic parameters were stable and he had no property on physical examination. Electrocardiography (ECG) indicated normal sinus rhythm and ST-segment elevation in both the D2-D3-aVF and V1-V3 derivations (Figure 1). At the time he came to the hospital, he had been on clopidogrel for two years because of prior stent implantation. Coronary angiography was performed immediately due to ST-segment elevation acute coronary syndrome (ACS) and following this the LMCA was selectively cannulated with a Judkins Left (JL) 4-6F diagnostic catheter (Medtronic, New York, USA) and the SCA anomaly was demonstrated. It was shown that the RCA arose from the LAD mid-segment and it was seen that the patient had a complex PCI history on the LAD-RCA bifurcation lesion (Figure 2A). There was very late stent thrombosis in the RCA stent, unlike LAD's (Figure 2B). The catheter was changed with a Judkins Left (JL) 4-6F guiding catheter. The LAD and RCA were predilated with 3.0 × 12 mm and 3.0 × 15 mm semi-compliant balloons, respectively (Figure 2C,D). A 3.0 × 23 mm DES (Everolimus eluting coronary stent,

Released online in J-STAGE as advance publication February 26, 2018.

*Address correspondence to:

Dr. Emrah Ermis, Department of Cardiology, Biruni University, Faculty of Medicine, Istanbul, Turkey.

E-mail: emr_ermis@hotmail.com

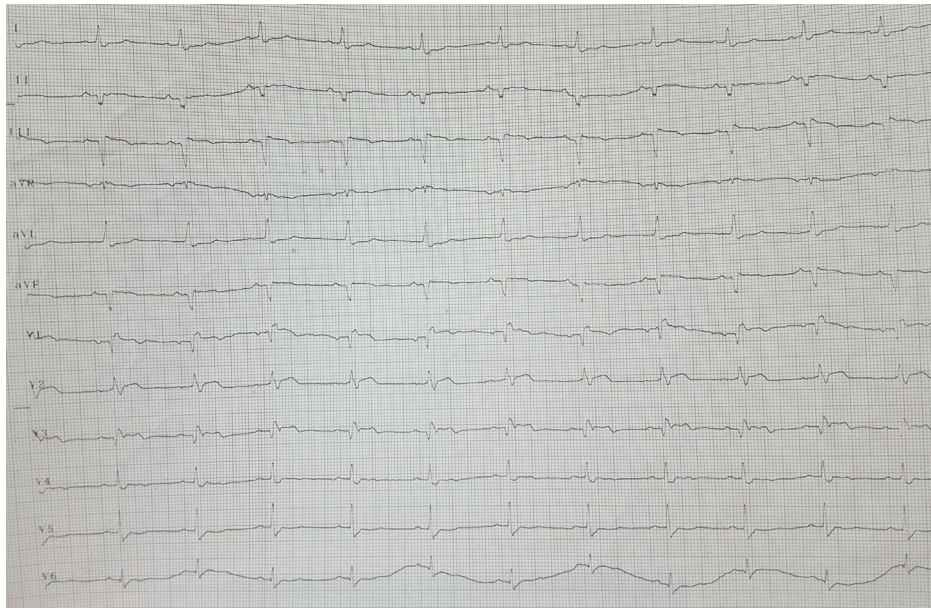


Figure 1. Electrocardiography demonstrates ST-segment elevation.

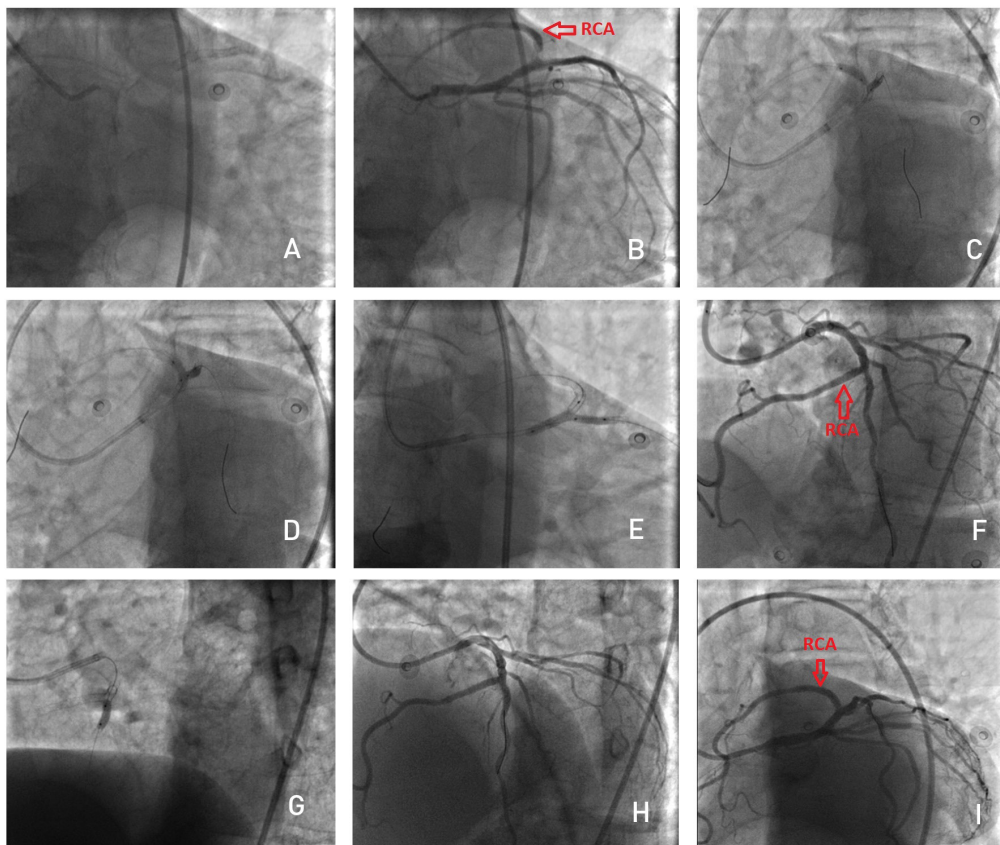


Figure 2. (A) Coronary angiography illustrating the complex coronary intervention on LAD-RCA bifurcation; (B) Appearance of stent thrombosis in RCA stent in caudal position; (C,D) Predilatations before stenting with semi-compliant balloons; (E) Appearance of stent implantation; (F,G) LAD postdilatation with balloon because of a hazy image.

Abbott, CA, USA) was implanted with 18 atm for RCA including pre-stent LAD lesion (Figure 2E). After stent implantation, the procedure was terminated with LAD postdilatation with a 3.5 × 8 mm non-compliant balloon because of a hazy image in LAD after final kissing

(Figure 2F, G). The final angiographic result is illustrated in Figure 2H, I. The patient's hemodynamic parameters were stable after PCI. Antiplatelet treatment changed from clopidogrel to ticagrelor due to ACS on clopidogrel therapy and also 100 mg acetylsalicylic acid treatment

was added to ticagrelor (2×90 mg). He was discharged from the hospital three days later after PCI with no symptom relapse.

3. Discussion

The incidence of congenital coronary anomaly is 0.2-1.4% in the normal population (4). Yamanaka and Hobbs reported that the incidence of coronary artery anomaly was 1.3% in their large coronary angiography series with 126,595 patients (1). However, they did not mention SCA anomaly. SCA refers to coronary arteries originating from a single coronary ostium. It was first described by Hyrtl in 1841 (5) and in a larger series its incidence ranged from 0.024% to 0.066% (2). RCA originating from LAD is a very rare variant of SCA. In light of literature analysis, it is an extremely rare anomaly with an incidence of 0.024% in the general population (6). SCA anomaly can be related to other congenital heart diseases, including transposition of the great vessels, coronary arteriovenous fistula, bicuspid aortic valve, tetralogy of Fallot, truncus arteriosus, ventricular septal defect, patent ductus arteriosus and patent foramen ovale (7). None of these properties was seen in our patient.

Although most of SCA anomaly patients are asymptomatic, it is well known that coronary artery anomalies can be associated with chest pain, dyspnea, palpitations, syncope, ventricular fibrillation, myocardial ischemia and sudden cardiac death, especially following exercise. Suggested mechanisms for ischemia include external compression, acute angulation, kinking, torsion, spasm and atherosclerotic obstruction (8). Despite the mechanism of atherosclerosis in SCA patients not being clear, the incidence of atherosclerosis increases in these patients. It is more difficult to perform PCI in SCA anomaly patients than in patients without coronary anomaly. It is known that the incidence of stent restenosis and thrombosis after PCI is higher in these patients than in the normal population (9). This could be the reason for stent thrombosis in our patient who had an anomalous RCA arising from the mid-LAD. Furthermore, the thrombosis occurred in our patient while he was on clopidogrel treatment. Therefore antiplatelet treatment was changed from clopidogrel to ticagrelor, although we were not able to indicate a possible effect of clopidogrel.

Treatment options are medical, percutaneous and surgical for coronary artery anomalies. PCI for RCA arising from LAD was reported by various authors (9,10). However, stent thrombosis rates are higher in these patients than in patients without coronary anomalies. Surgical treatment is used for osteoplasty, bypass grafting of the RCA and translocation of the RCA to the aorta.

4. Conclusion

RCA arising from LAD is a very rare variant of SCA anomaly and can be related to myocardial ischemia.

Abnormal origin or intramural course of the aberrant artery and compression between the main pulmonary artery and the aorta may be the reasons for atherosclerosis in these patients. It is known that performing PCI in SCA anomaly patients is not usually easy. Periprocedural complications and the incidence of stent restenosis and thrombosis are higher in these patients. The main point in the treatment of bifurcation lesions in patients who have coronary anomalies is determination of the most suitable strategy for each lesion. Interventional cardiologists should avoid a complex technique because of the risk of stent thrombosis.

References

1. Yamanaka O, Hobbs RE. Coronary artery anomalies in 126,595 patients undergoing coronary arteriography. *Cathet Cardiovasc Diagn.* 1990; 21:28-40.
2. Desmet W, Vanhaecke J, Vrolix M, Van de Werf F, Piessens J, Willems J, de Geest H. Isolated single coronary artery: A review of 50,000 consecutive coronary angiographies. *Eur Heart J.* 1992; 13:1637-1640.
3. Schwarz ER, Hager PK, Uebis R, Hanrath P, Klues HG. Myocardial ischaemia in a case of a solitary coronary ostium in the right aortic sinus with retroaortic course of the left coronary artery: Documentation of the underlying pathophysiological mechanisms of ischaemia by intracoronary Doppler and pressure measurements. *Heart.* 1998; 80:307-311.
4. Jacobs ML, Mavroudis C. Anomalies of the coronary arteries: Nomenclature and classification. *Cardiol Young.* 2010; 20(suppl 3):15-19.
5. Hyrtl J. Einige in chirurgischer Hinsicht wichtige Gefassvarieteten. *Med Jahrb Osterr Staats.* 1841; 33:17-38.
6. Xuguang Q, Xiang W, Lu C. The coronary anomaly: Right coronary artery originates from the mid left anterior descending artery. *J Invasive Cardiol.* 2010; 22: E166-167.
7. Poynter JA, Williams WG, McIntyre S, Brothers JA, Jacobs ML; Congenital Heart Surgeons Society AAOCA Working Group. Anomalous aortic origin of a coronary artery: A report from the Congenital Heart Surgeons Society Registry. *World J Pediatr Congenit Heart Surg.* 2014; 5:22-30.
8. Nath A, Kennett JD, Politte LL, Sanfelippo JF, Alpert MA. Anomalous right coronary artery arising from the midportion of the left anterior descending coronary artery – Case reports. *Angiology.* 1987; 38:142-146.
9. Rudan D, Todorovic N, Starcevic B, Raquz M, Bergovec M. Percutaneous coronary intervention of an anomalous right coronary artery originating from the left coronary artery. *Wien Klin Wochenschr.* 2010; 122:508-510.
10. Takano M, Seimiya K, Yokoyama S, Okamatsu K, Ishibashi F, Uemura R, Hata N, Mizuno K. Unique single coronary artery with acute myocardial infarction: Observation of the culprit lesion by intravascular ultrasound and coronary angiography. *Jpn Heart J.* 2003; 44:271-276.

(Received January 5, 2018; Accepted February 21, 2018)

A case of HTLV-1 associated adult T-cell lymphoma presenting with cutaneous lesions and tropical spastic paresis

Purva V Sharma^{1,*}, Michael Witteman¹, Swethika Sundaravel¹, Tulisa Larocca¹, Yuanming Zhang², Harry Goldsztajn³

¹Department of Internal Medicine, University of Miami Palm Beach Regional Consortium, Atlantis, FL, USA;

²Department of Pathology, JFK Medical Center, Atlantis, FL, USA;

³Department of Hematology/Oncology, JFK Medical Center, Atlantis, FL, USA.

Summary

Adult T cell lymphoma (ATL), is a peripheral T cell neoplasm associated with infection by human T-lymphotropic virus (HTLV). This is a case of a 28-year-old lady who presented with back pain for the past month and recent onset weakness in her lower extremities bilaterally. She has a history of T-cell lymphoma secondary to HTLV-1 under remission since 2014 and systemic lupus erythematosus complicated by lupus nephritis. On physical examination patient had hyper-reflexia in both knees, ankle clonus bilaterally and spasticity in both her lower extremities. She also had a diffuse, scaly, macular rash in her upper and lower extremities and ulcer-like lesions on the plantar surface of both feet. Her lumbar puncture showed lymphocyte predominance. The Western Blot test was positive for HTLV antibodies in the CSF. The patient was started on IV Methylprednisone which considerably improved her symptoms. The biopsy of her skin lesions showed an immunophenotype of T-cells similar to the cells in the bone marrow at the time of diagnosis of the lymphoma. HTLV infection is an etiologic agent for ATL as well as for tropical spastic paresis. One should have a high degree of suspicion for tropical spastic paresis in patients with HTLV-1 infection as it can easily go undiagnosed. Indolent forms of ATL can also present in the form of skin lesions in later stages. It is also important to distinguish between skin manifestations of ATL and cutaneous T cell lymphomas, and the importance of skin biopsies for the same cannot be undermined.

Keywords: HTLV infection, T-cell lymphoma, tropical spastic paresis, cutaneous lymphoma

1. Introduction

Adult T cell leukemia-lymphoma (ATL), according to the most recent World Health Organization (WHO) classification of lymphoid neoplasms, is defined as a peripheral T cell neoplasm associated with infection by the human T-lymphotropic virus (HTLV), type I (HTLV-I) (1). Although it is considered as one of the most highly aggressive T cell non-Hodgkin lymphoma (NHL) variants, the disease course is variable and sometimes

quite indolent.

Infection with HTLV-1 is endemic in islands of Japan, Caribbean islands such as Trinidad and Jamaica and some parts of southeastern United States. In the United States as a whole, the incidence of ATL is approximately 0.05 cases per 100,000 people (2). Since ATL is associated with HTLV-I infection, patients with ATL are also at risk for HTLV-I-associated myelopathy, also known as tropical spastic paraparesis.

We present a case of a young lady with known history of Adult T-cell lymphoma presenting with new skin manifestations of ATL as well as tropical spastic paresis.

2. Case Report

A 28-year-old Haitian female patient presented to the

Released online in J-STAGE as advance publication February 26, 2018.

*Address correspondence to:

Dr. Purva V Sharma, Department of Internal Medicine, University of Miami Palm Beach Regional Consortium, Atlantis, FL 33462, USA.

E-mail: purva7sharma@gmail.com

emergency department in March 2017 with complaints of back pain for one month prior to presentation and recent onset weakness in her lower extremities bilaterally.

She has a history of T-cell lymphoma secondary to HTLV-1 infection. This was diagnosed the very first time with a bone marrow biopsy in 2013 in her oncologist's office. She completed 5 cycles of chemotherapy (CHOP), the last one being in March 2014, after which the T-cell lymphoma was under remission. However, she did not maintain follow-up post chemotherapy and her current state of disease during this presentation to the hospital was unknown. On admission, the patient was afebrile, with a heart rate of 88/min and a blood pressure of 110/70 mmHg. Patient's neurological examination revealed hyper-reflexia in both knees, as well as ankle clonus bilaterally. There was also spasticity appreciated in both her lower extremities. On skin examination, the patient was found to have a diffuse, scaly, macular rash in her upper and lower extremities and also in her sub-mammary region. She also had ulcer-like lesions on her soles.

A lumbar spine MRI did not show spinal cord compression and was negative for acute disease process. At this stage, there was concern for tropical spastic paraparesis secondary to HTLV infection and indolent course of the disease. She had a lumbar puncture which revealed 12 white blood cells with lymphocyte predominance, normal protein and glucose (Table 1). The Western Blot test was positive for HTLV antibodies in the CSF. The patient was started on IV Methylprednisone 40 mg every 8 hours which was tapered over the next 2 weeks. The patient experienced gradual improvement in her lower extremity weakness over the next 2-3 weeks, after starting the high-dose steroids. The infectious disease team agreed with this treatment because there is no definitive treatment for tropical spastic paresis.

As the diagnosis of T-cell lymphoma was already established, a repeat bone marrow biopsy was not performed during this admission. However, she had a biopsy of one of the skin lesions on her right lateral thigh which showed atypical T-cells, positive for CD3 and CD8 and showing markedly decreased expression of CD5 and CD7. (Figures 1, 2, and 3).

The immunophenotype of the T-cells in the skin biopsy findings was similar to the cells found in the bone marrow in a repeat bone marrow biopsy in 2016

which showed an atypical T-cell population consistent with a T-cell lymphoproliferative disorder which is the previously diagnosed T-cell lymphoma (Figure 4). The findings raised suspicion of involvement by a mature T-cell lymphoma.

She has a known history of systemic lupus erythematosus (SLE) since 2013, diagnosed by positive ANA as well as ds-DNA and low complement c3 and c4 levels. It was complicated by lupus nephritis and end stage renal disease requiring hemodialysis. Patient also had a history of hyperthyroidism and was diagnosed

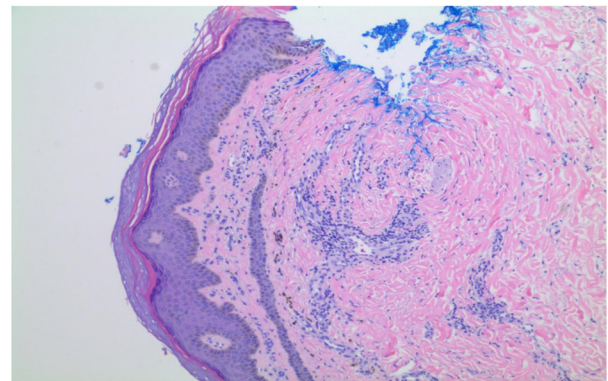


Figure 1. Histopathological slide showing atypical T-cells from biopsy of skin lesion.

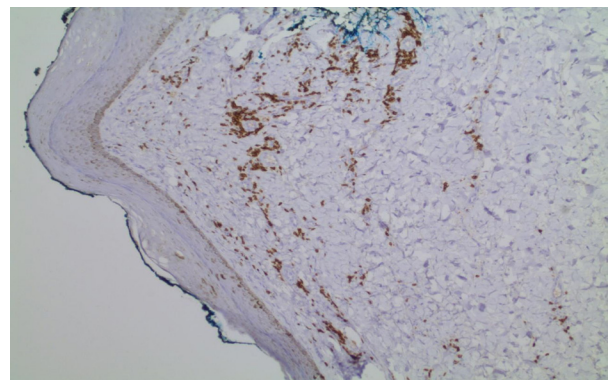


Figure 2. Immunophenotype staining of biopsy from skin lesion showing CD3 positive T-cells.

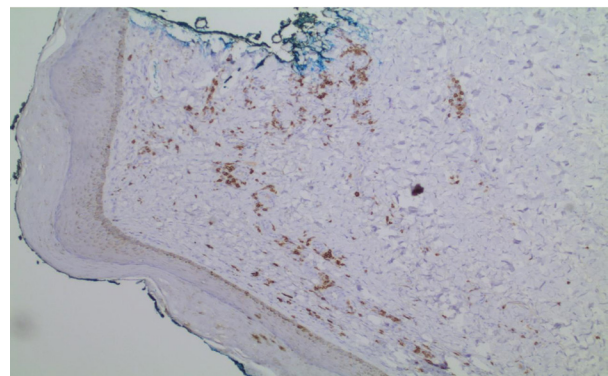


Figure 3. Immunophenotype staining of biopsy from skin lesion showing CD8 positive T-cells.

Table 1. Results of CSF fluid analysis

CSF Appearance	Clear
CSF Color	Colorless
CSF RBC	2 (cells/ μ L)
CSF Lymphocytes %	97 %
CSF Glucose	82 mg/dL (41-75)
CSF Total protein	35.3 mg/dL (15-45)
CSF HTLV 1/2	Positive

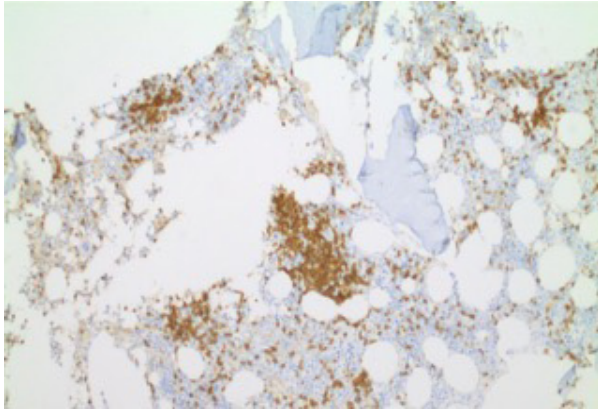


Figure 4. Bone marrow biopsy showing population of atypical T cells with CD8 positivity.

with subacute granulomatous thyroiditis. She was on Methimazole for the same.

3. Discussion

Adult T-cell lymphoma (ATL) is an uncommon neoplasm of the peripheral T lymphocyte cells and it is etiologically associated with HTLV (3). About 5% of the carriers of the HTLV virus can develop adult T-cell lymphoma after a long latent period (4). As per the Shimoyama Classification, Adult T-cell lymphoma can present as different subtypes such as acute, smoldering lymphoma and chronic (5). Among these, the smoldering and chronic forms of ATL follow a more indolent course (6). Our patient's disease course could also be considered indolent as she was in remission for almost 3 years after her last cycle of chemotherapy with no active disease, until her presentation during this hospital admission.

Skin manifestations occur in almost one-third of the patients of ATL (3). They are also seen more commonly in patients with a more indolent course of the disease, as seen in our patient (7). Skin lesions in ATL mimic various other skin conditions, including certain types of cutaneous T-cell lymphomas. Some of these presentations include leukocytoclastic purpura, plaques, erythro-derma and a papulo-squamous eruption (8). Often times it is seen that, when patients present with a skin lesion as the first manifestation of ATL, the diagnosis can be missed. In our patient, however, as her diagnosis of ATL was already established, an immediate biopsy of her skin lesions was done upon presentation. The immunophenotype of the T- cells infiltrating the skin lesions was very similar to the ones in the bone marrow, establishing that the skin lesions are one of the manifestations of the ATL.

A key differentiating feature between skin lesions of ATL and other forms of cutaneous T-cell lymphomas is the presence of HTLV-1 in the malignant cells of ATL, which can be determined by testing for the antibody in the blood.

Another significant finding in our patient was the

positive CSF analysis for HTLV-1 virus. Her medical records showed that she was hospitalized on two occasions in the past for similar complaints of lower extremity weakness. Given the patient's history and the CSF findings, the likely etiology of the weakness and spasticity on examination was thought to be tropical spastic paresis due to infection with HTLV-1. Almost 10% of carriers of HTLV-1 develop HTLV-1 associated myelopathy/tropical spastic paresis (9). Also our patient had antibodies to HTLV-1 in serum as well as CSF, and she could likely be developing a slowly progressive myelopathy defined as 'definite' tropical spastic paresis (10). One of the radiologic findings is diffuse muscle atrophy of the extremities on MRI which was not performed on our patient (11). Other findings include atrophic changes in the spinal cord and multifocal high-signal-intensity lesions in the cerebral white matter on T2-weighted images which were also not seen in our patient (12,13). However, our patient had a positron-emission tomography (PET) scan in 2016 which reported multifocal uptake in thoracic spine, lumbar spine and pelvis, which has been reported in some patients with tropical spastic paresis (14).

Tropical spastic paresis is more common in females than in males, in keeping with the high prevalence of HTLV infection in females. It affects less than 2% of HTLV-1 carriers, so our patient was among the less than 2% population with spastic paresis.

Another important association of HTLV-1 is with autoimmune diseases such as rheumatoid arthritis, Sjogren's syndrome and SLE and has been studied extensively at the molecular level. HTLV-1 virus infects CD4+ T lymphocytes, which can in turn lead to changes in their behavior and can trigger inflammatory reactions that can break immune system tolerance, leading to autoimmunity (15). Our patient has a history of SLE, and the association between SLE and HTLV infection is thought to be based on molecular mimicry. A recent study concluded that there is no real association between SLE and HTLV infection and that geographical and environmental factors should be taken into consideration.

4. Conclusion

HTLV infection is an etiologic agent for ATL as well as for tropical spastic paresis. Indolent forms of the disease can also present in the form of skin lesions in later stages. It is important to distinguish between skin manifestations of ATL and cutaneous T cell lymphomas, and a key feature is the HTLV positivity in the malignant T cells of ATL. HTLV-1 DNA testing in tissues is a useful tool to study T-cell lymphomas.

References

1. Swerdlow SH, Campo E, Pileri SA, Harris NL, Stein H, Siebert R, Advani R, Ghielmini M, Salles GA, Zelenetz

- AD, Jaffe ES. The 2016 revision of the World Health Organization classification of lymphoid neoplasms. *Blood*. 2016;127:2375-2390.
2. Yamamoto JF, Goodman MT. Patterns of leukemia incidence in the United States by subtype and demographic characteristics, 1997-2002. *Cancer Causes Control*. 2008;19:379-390.
 3. Marchetti MA, Pulitzer MP, Myskowski PL, Dusza SW, Lunning MA, Horwitz SM, Moskowitz AJ, Querfeld C. Cutaneous manifestations of human T-cell lymphotropic virus type-1-associated adult T-cell leukemia/lymphoma: A single-center, retrospective study. *J Am Acad Dermatol*. 2015;72:293-301.
 4. Matsuoka M. Human T-cell leukemia virus type I and adult T-cell leukemia. *Oncogene*. 2003; 22:5131-5140.
 5. Shimoyama M. Diagnostic criteria and classification of clinical subtypes of adult T-cell leukaemia-lymphoma. A report from the Lymphoma Study Group (1984-87). *Br J Haematol*. 1991;79:428-437.
 6. Takasaki Y, Iwanaga M, Imaizumi Y, Tawara M, Joh T, Kohno T, Yamada Y, Kamihira S, Ikeda S, Miyazaki Y, Tomonaga M, Tsukasaki K. Long-term study of indolent adult T-cell leukemia-lymphoma. *Blood*. 2010;115:4337-4343.
 7. Levine PH, Manns A, Jaffe ES, Colclough G, Cavallaro A, Reddy G, Blattner WA. The effect of ethnic differences on the pattern of HTLV-I-associated T-cell leukemia/lymphoma (HATL) in the United States. *Int J Cancer*. 1994; 56:177-181.
 8. Sharata HH, Colvin JH, Fujiwara K, Goldman B, Hashimoto K. Cutaneous and neurologic disease associated with HTLV-I infection. *J Am Acad Dermatol*. 1997; 36:869-871.
 9. Oliveira PD, Kachimarek AC, Bittencourt AL. Early Onset of HTLV-1 Associated Myelopathy/Tropical Spastic Paraparesis (HAM/TSP) and Adult T-cell Leukemia/ Lymphoma (ATL): Systematic Search and Review. *J Trop Pediatr*. 2017; doi: 10.1093/tropej/fmx039.
 10. Kaplan JE, Osame M, Kubota H, Igata A, Nishitani H, Maeda Y, Khabbaz RF, Janssen RS. The risk of development of HTLV-I-associated myelopathy/tropical spastic paraparesis among persons infected with HTLV-I. *J Acquir Immune Defic Syndr*. 1990; 3:1096-1101.
 11. Petscavage JM, Mulcahy H, Richardson ML. Human T-cell lymphotropic virus, type 1 (HTLV-1)-associated myelopathy: MR findings. *Radiol Case Rep*. 2015; 6:416.
 12. Yamamoto F, Yamashita S, Yamamura A, Watanabe M, Kimura E, Yamashita T, Hirano T, Uchino M. Abnormal spinal MRI findings in human T-cell lymphotropic virus type I-associated myelopathy. *Clin Neurol Neurosurg*. 2009; 111:624-628.
 13. Alcindor F, Valderrama R, Canavaggio M, Lee H, Katz A, Montesinos C, Madrid RE, Merino RR, Pipia PA. Imaging of human T-lymphotropic virus type I-associated chronic progressive myeloneuropathies. *Neuroradiology*. 1992; 35:69-74.
 14. Umehara F, Hagiwara T, Yoshimura M, Higashi K, Arimura K. Enlarged, multifocal upper limb neuropathy with HTLV-I associated myelopathy in a patient with chronic adult T-cell leukemia. *J Neurol Sci*. 2008; 266:167-170.
 15. Quaresma JA, Yoshikawa GT, Koyama RV, Dias GA, Fujihara S, Fuzii HT. HTLV-1, immune response and autoimmunity. *Viruses*. 2015; 8. pii: E5.

(Received November 20, 2017; Revised January 24, 2018; Accepted February 1, 2018)

Successful ERCP for management of traumatic pancreatic disruption in a patient with situs inversus

Vishal Sharma^{1,*}, Sarthak Malik¹, Harshal S Mandavdhare¹, Harjeet Singh²

¹Department of Gastroenterology, Postgraduate Institute of Medical Education and Research, Chandigarh, India;

²Department of General Surgery, Postgraduate Institute of Medical Education and Research, Chandigarh, India.

Summary Endoscopic retrograde cholangio-pancreatography (ERCP) is an important tool for treatment of pancreaticobiliary diseases. However, ERCP may be difficult in patients who have altered gastrointestinal anatomy due to congenital or surgical reasons. A 40-year-old male with HIV infection presented with abdominal pain following abdominal trauma. The patient was diagnosed to have traumatic pancreatic injury and underlying situs inversus. The pancreatic fluid collection was drained using radiology guided pigtail placement done for the symptoms of abdominal pain and vomiting. The resulting external pancreatic fistula was successfully managed with ERCP and stenting. The patient improved with disappearance of ascites and resolution of pigtail output which was then removed. We report the technique used for ERCP in this patient. We also review the literature on pancreatic endotherapy in patients with situs inversus. The published literature suggests that with modifications in the standard ERCP technique like mirror image technique, 180 degree turn technique, left lateral technique *etc.* these patients can be managed successfully.

Keywords: Pancreatic trauma, pancreatic stent, fistula, situs inversus, ERCP, endoscopy

1. Introduction

Situs inversus viscerum (SIV) is a rare, autosomal recessive genetic abnormality characterised by a left to right transposition of all viscera thereby resembling a mirror image of the usual pattern (*I*). In a complete SIV, there is total transposition of all viscera and dextroversion of the heart. Endoscopic retrograde cholangiopancreatography (ERCP) is a widely used procedure for intervention in pancreatic and biliary tree for various benign and malignant conditions like choledocholithiasis, chronic pancreatitis and malignant extrahepatic biliary obstruction but may not be successful (2-4). Very few reports of endoscopic retrograde pancreatography in patients with SIV have been described in the published literature (5,6). We report here a case of acute pancreatitis with duct

disruption due to trauma and external pancreatic fistula in a patient of SIV which was successfully managed with ERCP.

2. Case Report

A 40-year-old gentleman who was under treatment for human immunodeficiency virus (HIV) infection with highly active anti-retroviral therapy presented with road traffic accident resulting in a fall from a bicycle followed by abdominal pain. He was admitted in March 2017 and the investigations revealed haemoglobin of 14 gm%, total leucocyte count of 18,000 per cubic mm. Liver and renal function tests were within normal limits. Serum amylase and lipase were 3,400 IU/mL and 4,500 IU/mL respectively. Abdominal computed tomography was done for the patient which showed presence of situs inversus with liver to the left and spleen to the right and evidence of pancreatic duct disruption in the head-body junction and presence of fluid collection anterior to the pancreas (Figure 1). The patient underwent percutaneous ultrasound guided pigtail for pain abdomen, fever and vomiting and was discharged after these symptoms settled. However, the patient continued to have a persistent pigtail output

Released online in J-STAGE as advance publication February 26, 2018.

*Address correspondence to:

Dr. Vishal Sharma, Department of Gastroenterology, Postgraduate Institute of Medical Education and Research, Chandigarh 160012, India.

E-mail: docvishalsharma@gmail.com



Figure 1. Computed tomography showing situs inversus with pancreatic disruption and fluid collection.



Figure 2. Endoscopic image of the papilla in the patient.

of 150 to 200 mL/day even a month after the onset of symptoms. At this time, an ERCP was performed for the patient. The procedure was done with the patient in the usual prone position and scope also in the usual position. The scope movements were made in the direction opposite to the usual. After entering the stomach, the scope tip was turned up and stomach insufflated to see the stomach folds and scope was moved to the antrum in this forward viewing position. The duodenum was intubated as usual by keeping the pylorus in setting-sun position and once in first part of duodenum the scope was turned by moving the hand counter-clockwise and turning the scope tip down the junction of D1 and D2 was seen. Now the scope was pushed into second part of duodenum. Further the papilla was brought in the front by moving the right-left knob of the scope to the left and withdrawing the scope (Figure 2). The cannulation of the pancreatic duct was then done by attempting to push the guidewire into the left side of the papilla which is usually the direction of the bile duct. The pancreatogram showed evidence of complete ductal disruption at the neck of the pancreas



Figure 3. Pancreatogram showing duct disruption in the region of pancreatic neck.

and a 5 Fr stent was placed into the disruption (Figure 3). After ERCP, drain output decreased over the next week. Two weeks later, the pigtail catheter was removed. At 2 months of follow-up the patient is doing well and free of symptoms and the ultrasound showed resolution of the collection.

3. Discussion

The index case describes ERCP involving pancreatic system with successful endotherapy. While most of the literature describes use of this procedure in patients with biliary pathology, most common being choledocholithiasis; and there are very few reports of ERCP in patients with SIV in literature (2,4,7). However, to the best of our knowledge, there are only two reports describing pancreatic ERCP in patients with SIV (5,6). Chowdhury *et al* described the procedure in a patient with chronic calcific pancreatitis with pseudocyst. They described the difficulties faced and the modification maneuvers required for doing the procedure (5). Another case was described by Bichard *et al*, a patient with Chronic pancreatitis associated with pancreas divisum with underlying incomplete abdominal situs inversus (6). We searched MEDLINE and Embase for papers published in English till 30 September 2017 using the following terms: ("cholangiopancreatography, endoscopic retrograde" [MeSH Terms] OR ("cholangiopancreatography" [All Fields] AND "endoscopic" [All Fields] AND "retrograde" [All Fields]) OR "endoscopic retrograde cholangiopancreatography" [All Fields] OR "ercp" [All Fields]) AND ("situs inversus" [MeSH Terms] OR ("situs"[All Fields] AND "inversus" [All Fields]) OR "situs inversus" [All Fields]). Of the 38 results, 6

Table 1. Various techniques described for ERCP in patients with situs inversus

Technique	Salient feature	Ref.
Mirror image ERCP	Patient in right lateral position with endoscopist on patients right with all necessary endoscopic maneuvers were performed inversely as per normal procedures.	(8)
180 degree turn technique	Patient in prone position with endoscopist on patients right with duodenoscope has to be turned 180° clockwise in the stomach.	(7,10,11,27)
Left lateral technique	Patient in left lateral position with endoscopist on patients left with minor endoscopic maneuvers.	(5)
1 o' clock papillotomy	Patient prone on his right, endoscopist turned his right side toward the patient and papillotomy is done toward in direction of "1 o'clock".	(12)
Present report	Patient in usual position, and scope in usual position, Turn the scope tip up and inflate the stomach, visualise the body and push to the antrum, cross pylorus and turn counter-clockwise, turn the knob left and withdraw to focus the papilla.	

were in non-English literature and 2 were not relevant. Of the rest 30 results, data about 32 patients with situs inversus was reported (2-5,7-8,10,12-35). To the best of our literature search, this is the first report of successful endoscopic therapy for a case of traumatic pancreatic disruption. In our search, two patients had procedures in surgically altered anatomy for the diagnosis of CBD stone and anastomotic stricture in one patient each (16,20). Of the rest 30 cases, the commonest indication for ERCP in situs inversus was CBD stone (18 patients), malignant biliary obstruction (6 patients), biliary stricture (2 patients) while one patient each had portal biliopathy, ampullary adenoma, chronic calcific pancreatitis and normal CBD (2-5,7-8,10,12-15,17-19,21-35). This suggests that pancreatic endotherapy has been done very infrequently.

ERCP in patients with situs inversus is considered a difficult procedure and has been reported to fail in some cases (21,26,28,32). Various techniques have been described in literature (Table 1). One of the technique involves turning the duodenoscope 180° clockwise when in stomach and then again when the scope reaches second part of the duodenum (4). Another modification of above technique describes 180° clockwise turn of the scope in the gastric lumen and then use of a rotating sphincterotome for cannulation (7). The literature also describes a mirror-image method which places the patient in the right lateral decubitus position. In this technique, the equipment lies behind the patient with all manoeuvres performed inversely during ERCP (8). A different approach involves keeping the patient supine on the table with the endoscopist on the left of patient (9). These reports suggest that repositioning of the patient during the procedure is extremely common in order to obtain a stable position for the procedure. Our technique is similar to the mirror image technique but keeping the patient prone and also the last step is different as we have done the cannulation of the pancreatic duct rather than the bile duct as reported previously. The benefit of the technique reported by us is that the endoscopist is comfortable with maintaining

the usual position of the endoscope and the patient.

In conclusion, ERCP with a few modifications to the standard technique, is feasible and safe in patients with situs inversus. We describe a successfully managed case of traumatic pancreatitis related external pancreatic fistula using pancreatic ductal stenting while maintaining the usual endoscope and patient position.

References

1. Claydon M, McLaughlin S. Gastrointestinal: Situs inversus viscerum. *J Gastroenterol Hepatol.* 2002; 17:1329.
2. Téllez-Ávila FI, Pattel S, Duarte-Medrano G, Seenath M, Herrera-Mora DR, Lopez-Arce G. A challenging case of giant biliary stones in a patient with situs inversus totalis: Conventional ERCP combined with intraductal cholangioscopy and laser lithotripsy. *Endoscopy.* 2017; 49:E248-E249.
3. Hu Y, Zeng H, Pan XL, Lv NH, Liu ZJ, Hu Y. Therapeutic endoscopic retrograde cholangiopancreatography in a patient with situs inversus viscerum. *World J Gastroenterol.* 2015; 21:5744-5748.
4. Morales-Rodríguez JF, Corina Cotillo E, Moreno-Loaiza O. Surgical treatment of choledocholithiasis in a patient with situs inversus totalis: A case report and literature review. *Medwave.* 2017;17:e7002. (in Spanish)
5. Chowdhury A, Chatterjee BK, Das U, Dutta P, Dhali GK, Banerjee PK. ERCP in situs inversus: Do we need to turn the other way? *Indian J Gastroenterol.* 1997; 16:155-156.
6. Bichard P, Rolachon A, Moulin C, Froissart B, Letoublon C, Zarski JP. Chronic pancreatitis associated with pancreas divisum in a patient on incomplete abdominal situs inversus. *Gastroenterol Clin Biol.* 1994; 18: 908-910. (in French)
7. de la Serna-Higuera C, Perez-Miranda M, Flores-Cruz G, Gil-Simón P, Caro-Patón A. Endoscopic retrograde cholangiopancreatography in situs inversus partialis. *Endoscopy.* 2010; 42 Suppl 2: E98.
8. Garcia-Fernandez FJ, Infantes JM, Torres Y, Mendoza FJ, Alcazar FJ. ERCP in complete situs inversus viscerum using a "mirror image" technique. *Endoscopy.* 2010; 42 Suppl 2: E316-E317.
9. Byun JR, Jahng JH, Song JC, Yu JS, Lee DK. Supine position endoscopic retrograde cholangiopancreatography

- in a patient with situs ambiguous with polysplenia. *Dig Endosc.* 2010; 22:322-324.
10. Kamani L, Kumar R, Mahmood S, Jafri S, Siddiqui F. Therapeutic ERCP in patient with situs inversus totalis and ampullary diverticulum. *J Coll Physicians Surg Pak.* 2014; 24: 365-366.
 11. Lee JH, Kang DH, Park JH, Kim MD, Yoon KT, Choi CW, Kim HW, Cho M. Endoscopic removal of a bile-duct stone using sphincterotomy and a large-balloon dilator in a patient with situs inversus totalis. *Gut Liver.* 2010; 4:110-113.
 12. Nordback I, Airo I. ERCP and endoscopic papillotomy in complete abdominal situs inversus. *Gastrointest Endosc.* 1988; 34:150.
 13. Venu RP, Geenen JE, Hogan WJ, Johnson GK, Taylor AJ, Stewart ET, Jackson A. ERCP and endoscopic sphincterotomy in patients with situs inversus. *Gastrointest Endosc.* 1985; 31:338-340.
 14. Lee JM, Lee JM, Hyun JJ, Choi HS, Kim ES, Keum B, Jeon YT, Chun HJ, Lee HS, Kim CD. Successful access to the ampulla for endoscopic retrograde cholangiopancreatography in patients with situs inversus totalis: A case report. *BMC Surg.* 2017;17:112.
 15. El Hajj II, Sherman S, Ceppa EP, Lehman GA. ERCP and Laparoscopic cholecystectomy in a patient with situs inversus totalis. *Dig Liver Dis.* 2017; 49:1374.
 16. Inoue T, Yamamoto T, Ishii N, Kobayashi Y, Ito K, Yoneda M. Double-balloon enteroscopy-assisted ERCP in situs inversus with Roux-en-Y hepaticojejunostomy for complex anastomotic stricture dilated with Soehendra stent retriever. *Endoscopy.* 2017; 49:E46-E47
 17. Sekino Y, Nakajima A, Kubota K. Successful endoscopic papillectomy in a patient with situs inversus. *Dig Endosc.* 2016; 28:616.
 18. Lee JM, Lee HS, Kim CD. Infundibulotomy and endoscopic retrograde cholangiopancreatography in situs inversus totalis combined with choledochocoele. *Dig Endosc.* 2015; 27:776.
 19. Lakhtakia S, Gupta R, Galasso D, Ramchandani M, Reddy PM, Rao GV, Reddy ND. Bleeding from portal biliopathy in situs inversus totalis. *Endoscopy.* 2015; 47:E335-336.
 20. Kim SB, Kim KH, Kim TN. Successful stone removal by endoscopic retrograde cholangiopancreatography in situs inversus totalis with Billroth-II gastrectomy. *Gut Liver.* 2015; 9:118-119.
 21. Giordano G, Bonomo S, Failla G, Luigiano C, Caloggero S, Magnano San Lio V. Percutaneous transhepatic biliary drainage after failed endoscopic approach in patients with pancreatic cancer and situs inversus totalis. *Endoscopy.* 2014; 46:E628-E629.
 22. Tyberg A, Lee T, Karia K, Suresh S, Kim DC, Sharaiha RZ, Kahaleh M. Malignant obstructive jaundice in situs inversus: demonstration of precut and biliary drainage. *Gastrointest Endosc.* 2015; 81:1018-1019.
 23. Patel KS, Patel JN, Mathur S, Moshenyat Y. To twist or not to twist: A case of ERCP in situs inversus totalis. *Endoscopy.* 2014; 46:E304-E305.
 24. Sheikh I, Heard R, Tombazzi C. Technical factors related to endoscopic retrograde cholangiopancreatography in patients with situs inversus. *Gastroenterol Hepatol (NY).* 2014; 10:277-278.
 25. Çoban Ş, Yüksel I, Küçükazman M, Başar Ö. Successful ERCP in a patient with situs inversus. *Endoscopy.* 2014; 46:E222.
 26. Alzahrani HA, Yamani NM. Gallbladder agenesis with a primary choledochal stone in a patient with situs inversus totalis. *Am J Case Rep.* 2014;15:185-188.
 27. Fiocca F, Donatelli G, Ceci V, Cereatti F, Romagnoli F, Simonelli L, Modini C. ERCP in total situs viscerum inversus. *Case Rep Gastroenterol.* 2008; 2:116-120.
 28. Tai CK, Tang CN, Ha JP, Chau CH, Siu WT, Li MK. Laparoscopic exploration of common bile duct in difficult choledocholithiasis. *Surg Endosc.* 2004; 18:910-914.
 29. Sano T, Kamiya J, Nagino M, Kanai M, Uesaka K, Nimura Y. Hepatectomy for proximal bile duct carcinoma in a patient with situs inversus; a case report. *Hepatogastroenterology.* 2003; 50:1266-1268.
 30. Bilimoria MM, Parsons WG, Small W Jr, Talamonti MS. Pancreaticoduodenectomy in a patient with ampullary carcinoma and situs inversus. *Surgery.* 2001; 130:521-524.
 31. McDermott JP, Caushaj PF. ERCP and laparoscopic cholecystectomy for cholangitis in a 66-year-old male with situs inversus. *Surg Endosc.* 1994; 8:1227-1229.
 32. Ibrarullah M, Awasthi S, Choudhuri G, Kapoor VK. Periapillary carcinoma in a young female with situs inversus. *Indian J Gastroenterol.* 1992; 11:91.
 33. Lipschutz JH, Canal DF, Hawes RH, Ruffolo TA, Besold MA, Lehman GA. Laparoscopic cholecystectomy and ERCP with sphincterotomy in an elderly patient with situs inversus. *Am J Gastroenterol.* 1992; 87:218-220.
 34. Mitchell RG, Gilliam JH 3rd, Kerr RM. A new twist to situs inversus. *Gastrointest Endosc.* 1991; 37:590-591.
 35. Organ BC, Skandalakis LJ, Gray SW, Skandalakis JE. Cancer of bile duct with situs inversus. *Arch Surg.* 1991;126:1150-1153.

(Received October 30, 2017; Revised February 17, 2018; Accepted February 19, 2018)

Early electronic screen exposure and autistic-like symptoms

Donna Hermawati¹, Farid Agung Rahmadi², Tanjung Ayu Sumekar³, Tri Indah Winarni^{4,*}

¹ Department of Biology, Faculty of Medicine Diponegoro University/Diponegoro National Hospital. Jl. Prof. H. Soedarto SH, Tembalang, Semarang, Central Java, Indonesia;

² Department of Pediatric, Faculty of Medicine Diponegoro University/Diponegoro National Hospital. Jl. Prof. H. Soedarto SH, Tembalang, Semarang, Central Java, Indonesia;

³ Department of Psychiatry, Faculty of Medicine Diponegoro University/Diponegoro National Hospital. Jl. Prof. H. Soedarto SH, Tembalang, Semarang, Central Java, Indonesia;

⁴ Center for Biomedical Research (CEBIOR), Faculty of Medicine Diponegoro University/Diponegoro National Hospital. Jl. Prof. H. Soedarto SH, Tembalang, Semarang, Central Java, Indonesia.

Summary

Prevalence autism spectrum disorders (ASD) has been on rise, but many studies suggests over-diagnosed. Currently, children have more access to electronic media on the daily basis than those of previous generation. Some studies suggest that increases screen time is associated with melanopsin-expressing neurons and decreasing gamma-aminobutyric acid (GABA) neurotransmitter, and thus results aberrant behavior, decreased cognitive, and language development. Early exposure of electronic media in early life (< 2 years old) gives an impact on language, but it still inconclusive. We made a study aiming at revealing the impact of early exposure of electronic screen on language development and autistic-like behavior. Results showed that children who spent viewing ≤ 3 hours per day had language delay and short attention span, while children who spent viewing ≥ 3 hours per day had language delay, short attention span, and hyperactivity. While, we found that more than a half of children (66.6%) had no parents-child interaction during the exposure, speech delayed and short attention had been reported in all cases, and hyperactivity was found in 66.6% children.

Keywords: Screen exposure, speech delay, short attention span, hyperactivity

Prevalence of using electronic screen media was high among children below 3 years, and tends to increase within a decade. Some studies suggest that increased screen time in young children is associated to negative health outcomes such as decreased cognitive ability, impaired language development, mood, and autistic-like behavior including hyperactivity, short attention span, and irritability (1,2). Currently, children worldwide spend more time with electronic screen media compare to children which previously more socially engage. The first exposure have been found in much younger age and, more overly, parents actively persuade them to use electronic screen media as a companion to entertain and

to keep them occupied, therefore, the parent can freely working on their own. Surprisingly, almost all parents proudly reported that their child aged below 2 years has been able and enjoy electronic media in regular basis.

Early exposure to screen can cause neurochemical and anatomical brain changes. Reduced melatonin concentration has been found significantly in a group of individual who were exposed to screen (3). Neurotransmitter deficiency like dopamin, acetylcholine, gamma aminobutyric acid (GABA), and 5-hydroxytryptamine (5-HT) was observed in study on internet-addicted urban left-behind children which may cause a spectrum of aberrant behavior phenotype (4). Takeuchi *et al.* (5) found that there is a positive effects of screen exposure on regional grey matter volume and white matter volume in the brain that may correlates with verbal competence, aggression, and cognitive abilities.

The disruption of those biological daily light-dark rhythms from environment can increase depression-like behavior and cognitive function through melanopsin-expressing neurons (6). Light input is detected by

Released online in J-STAGE as advance publication February 26, 2018.

*Address correspondence to:

Dr. Tri Indah Winarni, Center for Biomedical Research (CEBIOR), Faculty of Medicine/Diponegoro National Hospital, Diponegoro University, Jl. Prof. H. Soedarto, SH Tembalang, Semarang 50275, Central Java, Indonesia.
E-mail: tri.winarni@fk.undip.ac.id

Table 1. Exposure history of electronic screen media among all cases who were not meet autism criteria

Case	Age (month)	Sex	Chief Complain	Behavioral Phenotype	IQ Score	Time of first exposure	Time spent viewing/day	Parent-child interaction
1	60	Male	Speech delay	short attention span, hyperactivity	108	< 2 years old	≥ 5 hours	No
2	78	Female	Speech delay	short attention span	100	< 2 years old	≤ 3 hours	No
3	55	Female	Non-verbal	short attention span, hyperactivity	83	< 2 years old	≥ 5 hours	Yes
4	56	Male	Speech delay	short attention span, hyperactivity	70	< 2 years old	3-5 hours	Yes
5	51	Female	Speech delay	short attention span	75	< 2 years old	3-5 hours	No
6	44	Male	Speech delay	short attention span, hyperactivity	72	< 2 years old	3-5 hours	Yes
7	68	Male	Speech delay	short attention span, hyperactivity	70	< 2 years old	3-5 hours	No
8	70	Male	Speech delay	short attention span, hyperactivity	83	< 2 years old	3-5 hours	No
9	57	Male	Speech delay	short attention span	82	< 2 years old	≤ 3 hours	No

and signaled to relevant brain regions through retinal ganglion cells (RGCs). The majority of RGCs signal light to thalamic nuclei and visual cortex for image visual function, the minority, called intrinsically photosensitive retinal ganglion cells (ipRGCs) for non-image visual function expresses the photopigment melanopsin. Melanopsin expression ipRGCs distribute to multiple brain regions including suprachiasmatic nucleus (SCN), ventrolateral preoptic area (VLPO), and limbic regions in order to regulate circadian rhythms, sleep, cognitive function, and mood (7).

Brain and behavioral studies indicate a very complex set of interacting brain systems in the initial acquisition of language. Attention and social interaction will activate brain mechanisms that raise up a sense of relationship between the self and other, and social understanding systems that connect the perception and action (8). Media screen exposure is electronic screen media as a source of information and entertainment for children that can contribute to children's language development, however, learning at an early age including language extremely depends mainly on the influence of the context of linguistic directly from social interactions.

In Indonesia, young children are commonly found bounding with various electronic screen media in both higher socio-economic level and lower socio-economic level society. This phenomenon can easily be seen in public places such as restaurant, shopping mall, playing ground, and school.

We made an autism risk factor study in special school for autism children in Probolinggo, East-Java, Indonesia in 2016. Diagnostic and Statistical Manual of Mental Disorders (DSM)-5 had been administered by experienced Pediatricians to diagnosed Autism Spectrum Disorders (ASD). Children who met criteria of ASD, had an IQ under 70, and had syndromic intellectual disabilities (ID) were excluded, only Children who had autistic-like behavior were included. Intellectual Quotient (IQ) was measured in 2016 using Wechsler. Parents of children who had scored above 70 who signed the consent form was administered structured interview of electronic screen media exposure questionnaires to access time of first exposure, spent time viewing, and parent-child interaction. Chief complaint was obtained during

interview and confirmed by experienced pediatricians. Risk factors of language delayed *i.e* family history of language delayed, low birth weight, neurological disorders, ear problems, severe toxic exposure, chronic medical illness, severe infectious diseases were obtained using questionnaire. Ethical Clearance was obtained from Komite Etik Penelitian Kesehatan (KEPK), Faculty of Medicine Diponegoro University/dr. Kariadi Hospital, Semarang, Central-java.

Nine children who met criteria with autistic-like behavior were included (6 males, 3 females; aged 44-78 months). All children had speech delay as a chief complain, and among those one case was non-verbal. The time of first exposure was very early, all had exposure before 2 years old, more overly, two cases had been exposed before the age of first. Parents reported having interaction with children during the exposure only in three cases, while the majority of cases (66.6%) there was no interaction during the exposure. Aberrant behavioral phenotypes were observed including short attention span was found in all cases and hyperactivity in the majority of cases (66.6%). Children who spent viewing ≤ 3 hours per day had language delay and short attention span, while children who spent viewing ≥ 3 hours per day had language delay, short attention span, and hyperactivity (Table 1).

In all cases, the first exposure was started before 2 years old and the intention of exposure was very high in the majority of cases (≥ 3 hours/day). Chonchaiya et al. found that children who started watching television before 12 months and watched more than 2 hours a day were six times more likely to have language delays (2). Electronic screen stimulation in early stage leads dysregulation and disorganization of various biological systems. Escalation of stimulation especially in early stage, will also influence other function, and language is the function that mostly affected (9). Recently, Fisher introduce a new term of electronic screen syndrome (ESS), an unrecognized disorders associated with exposure of electronic media and mental health symptoms *i.e* mood, anxiety, cognition, behavior, and social interaction due to hyperarousal. (Unpublished data, Martin H Fisher, Electronic Screen Syndrome: An unrecognized disorder)

This study found that more than a half of children (66.6%) had no parents-child interaction during the exposure, speech delayed and short attention had been reported in all cases, and hyperactivity was found in 66.6% children. Previous studies shown negative associations between times spent viewing TV and the range of cognitive outcomes in young children including attention, intelligence and future educational attainment. A longitudinal study in 2004 found that the more TV watched by infants (aged 1-3), the more likely they were to have attention problems (9). In addition, poor quality of interactions with parents combine with screen excessive use may have negative effects on children's health and development, parent-child interactions was found had positive impact on language development especially word learning and retention (10). Studies in rodent revealed the behavioral changes occurred because ipRGCs project to the brain regions involved in mood. Bedrosian TA and Nelson RJ summarizing the effect of aberrant light and mood disorders through ipRGC projections to brain regions involved in emotions (1), and also an effective sources for suppressing nocturnal melatonin that can lead sleep disruption (3).

Study Limitation: An important limitation is the lack of a control group that would help us evaluate the effect of screen exposure and whether autistic-like behavior is indeed increased in children due to excessive screen exposure.

Acknowledgements

This work was supported by Riset Dasar dan Penerapan PNB Faculty of Medicine Diponegoro University: 834/UN7.P/HK/2016. We thank the family who participated in this study. We all address our appreciation to all the school committee who were involved in this study for their help in this study.

References

1. Bedrosian TA, Nelson RJ. Timing of light exposure affects mood and brain circuits. *Transl Psychiatry*. 2017; 7:e1017.
2. Chonchaiya W, Pruksananonda C. Television viewing associates with delayed language development. *Acta Paediatr*. 2008; 97:977-982.
3. Figueiro MG, Wood B, Plitnick B, Rea MS. The impact of light from computer monitors on melatonin levels in college students. *Neuro Endocrinol Lett*. 2011; 32:158-163.
4. Ge Y, Liu J. Psychometric analysis on neurotransmitter deficiency of internet addicted urban left-behind children. *J Alcohol Drug Depend*. 2015; 3:221.
5. Takeuchi H, Taki Y, Hashizume H, Asano K, Asano M, Sassa Y, Yokota S, Kotozaki Y, Nouchi R, Kawashima R. The impact of television viewing on brain structures: Cross-sectional and longitudinal analyses. *Cereb Cortex*. 2015; 25:1188-1197.
6. LeGates TA, Altimus CM, Wang H, Lee H-K, Yang S, Zhao H, Kirkwood A, Weber ET, Hattar S. Aberrant light directly impairs mood and learning through melanopsin-expressing neurons. *Nature*. 2012; 491:594-598.
7. Hattar S, Liao HW, Takao M, Berson DM, Yau KW. Melanopsin-containing retinal ganglion cells: Architecture, projections, and intrinsic photosensitivity. *Science*. 2002; 295:1065-1070.
8. Hari R, Kujala MV. Brain basis of human social interaction: From concepts to brain imaging. *Physiol Rev*. 2009; 89:453-479.
9. Christakis DA, Zimmerman FJ, DiGiuseppe DL, McCarty CA. Early television exposure and subsequent attentional problems in children. *Pediatrics*. 2004; 113:708-713.
10. Tanimura M, Okuma K, Kyoshima K. Television viewing, reduced parental utterance, and delayed speech development in infants and young children. *Arch Pediatr Adolesc Med*. 2007; 161:618.

(Received January 12, 2018; Revised February 3, 2018; Accepted February 19, 2018)

Guide for Authors

1. Scope of Articles

Intractable & Rare Diseases Research is an international peer-reviewed journal. Intractable & Rare Diseases Research devotes to publishing the latest and most significant research in intractable and rare diseases. Articles cover all aspects of intractable and rare diseases research such as molecular biology, genetics, clinical diagnosis, prevention and treatment, epidemiology, health economics, health management, medical care system, and social science in order to encourage cooperation and exchange among scientists and clinical researchers.

2. Submission Types

Original Articles should be well-documented, novel, and significant to the field as a whole. An Original Article should be arranged into the following sections: Title page, Abstract, Introduction, Materials and Methods, Results, Discussion, Acknowledgments, and References. Original articles should not exceed 5,000 words in length (excluding references) and should be limited to a maximum of 50 references. Articles may contain a maximum of 10 figures and/or tables.

Brief Reports definitively documenting either experimental results or informative clinical observations will be considered for publication in this category. Brief Reports are not intended for publication of incomplete or preliminary findings. Brief Reports should not exceed 3,000 words in length (excluding references) and should be limited to a maximum of 4 figures and/or tables and 30 references. A Brief Report contains the same sections as an Original Article, but the Results and Discussion sections should be combined.

Reviews should present a full and up-to-date account of recent developments within an area of research. Normally, reviews should not exceed 8,000 words in length (excluding references) and should be limited to a maximum of 100 references. Mini reviews are also accepted.

Policy Forum articles discuss research and policy issues in areas related to life science such as public health, the medical care system, and social science and may address governmental issues at district, national, and international levels of discourse. Policy Forum articles should not exceed 2,000 words in length (excluding references).

Case Reports should be detailed reports of the symptoms, signs, diagnosis, treatment, and follow-up of an individual patient. Case reports may contain a demographic profile of the patient but usually describe an unusual

or novel occurrence. Unreported or unusual side effects or adverse interactions involving medications will also be considered. Case Reports should not exceed 3,000 words in length (excluding references).

News articles should report the latest events in health sciences and medical research from around the world. News should not exceed 500 words in length.

Letters should present considered opinions in response to articles published in Intractable & Rare Diseases Research in the last 6 months or issues of general interest. Letters should not exceed 800 words in length and may contain a maximum of 10 references.

3. Editorial Policies

Ethics: Intractable & Rare Diseases Research requires that authors of reports of investigations in humans or animals indicate that those studies were formally approved by a relevant ethics committee or review board.

Conflict of Interest: All authors are required to disclose any actual or potential conflict of interest including financial interests or relationships with other people or organizations that might raise questions of bias in the work reported. If no conflict of interest exists for each author, please state "There is no conflict of interest to disclose".

Submission Declaration: When a manuscript is considered for submission to Intractable & Rare Diseases Research, the authors should confirm that 1) no part of this manuscript is currently under consideration for publication elsewhere; 2) this manuscript does not contain the same information in whole or in part as manuscripts that have been published, accepted, or are under review elsewhere, except in the form of an abstract, a letter to the editor, or part of a published lecture or academic thesis; 3) authorization for publication has been obtained from the authors' employer or institution; and 4) all contributing authors have agreed to submit this manuscript.

Cover Letter: The manuscript must be accompanied by a cover letter signed by the corresponding author on behalf of all authors. The letter should indicate the basic findings of the work and their significance. The letter should also include a statement affirming that all authors concur with the submission and that the material submitted for publication has not been published previously or is not under consideration for publication elsewhere. The cover letter should be submitted in PDF format. For example of Cover Letter, please visit <http://www.irdrjournal.com/downcentre.php> (Download Centre).

Copyright: A signed JOURNAL PUBLISHING AGREEMENT (JPA) form must be provided by post, fax, or as a scanned file before acceptance of the article. Only forms with a hand-written signature are accepted. This copyright will ensure the widest possible dissemination of information.

A form facilitating transfer of copyright can be downloaded by clicking the appropriate link and can be returned to the e-mail address or fax number noted on the form (Please visit [Download Centre](#)). Please note that your manuscript will not proceed to the next step in publication until the JPA Form is received. In addition, if excerpts from other copyrighted works are included, the author(s) must obtain written permission from the copyright owners and credit the source(s) in the article.

Suggested Reviewers: A list of up to 3 reviewers who are qualified to assess the scientific merit of the study is welcomed. Reviewer information including names, affiliations, addresses, and e-mail should be provided at the same time the manuscript is submitted online. Please do not suggest reviewers with known conflicts of interest, including participants or anyone with a stake in the proposed research; anyone from the same institution; former students, advisors, or research collaborators (within the last three years); or close personal contacts. Please note that the Editor-in-Chief may accept one or more of the proposed reviewers or may request a review by other qualified persons.

Language Editing: Manuscripts prepared by authors whose native language is not English should have their work proofread by a native English speaker before submission. If not, this might delay the publication of your manuscript in Intractable & Rare Diseases Research.

The Editing Support Organization can provide English proofreading, Japanese-English translation, and Chinese-English translation services to authors who want to publish in Intractable & Rare Diseases Research and need assistance before submitting a manuscript. Authors can visit this organization directly at <http://www.iacmhr.com/iac-eso/support.php?lang=en>. IAC-ESO was established to facilitate manuscript preparation by researchers whose native language is not English and to help edit works intended for international academic journals.

4. Manuscript Preparation

Manuscripts should be written in clear, grammatically correct English and submitted as a Microsoft Word file in a single-column format. Manuscripts must be paginated and typed in 12-point Times New Roman font with 24-point line spacing. Please do not embed figures in the text. Abbreviations should be used as little as possible and should be explained at first mention unless the term is a well-known abbreviation (e.g. DNA). Single words should not be abbreviated.

Title page: The title page must include 1) the title of the paper (Please note the title should be short, informative, and contain the major key words); 2) full name(s) and affiliation(s) of the author(s), 3) abbreviated names of the author(s), 4) full name, mailing address, telephone/fax numbers, and e-mail address of the corresponding author; and 5) conflicts of interest (if you have an actual or potential conflict of interest to disclose, it must be included as a footnote on the title page of the

manuscript; if no conflict of interest exists for each author, please state "There is no conflict of interest to disclose"). Please visit [Download Centre](#) and refer to the title page of the manuscript sample.

Abstract: The abstract should briefly state the purpose of the study, methods, main findings, and conclusions. For article types including Original Article, Brief Report, Review, Policy Forum, and Case Report, a one-paragraph abstract consisting of no more than 250 words must be included in the manuscript. For News and Letters, a brief summary of main content in 150 words or fewer should be included in the manuscript. Abbreviations must be kept to a minimum and non-standard abbreviations explained in brackets at first mention. References should be avoided in the abstract. Key words or phrases that do not occur in the title should be included in the Abstract page.

Introduction: The introduction should be a concise statement of the basis for the study and its scientific context.

Materials and Methods: The description should be brief but with sufficient detail to enable others to reproduce the experiments. Procedures that have been published previously should not be described in detail but appropriate references should simply be cited. Only new and significant modifications of previously published procedures require complete description. Names of products and manufacturers with their locations (city and state/country) should be given and sources of animals and cell lines should always be indicated. All clinical investigations must have been conducted in accordance with Declaration of Helsinki principles. All human and animal studies must have been approved by the appropriate institutional review board(s) and a specific declaration of approval must be made within this section.

Results: The description of the experimental results should be succinct but in sufficient detail to allow the experiments to be analyzed and interpreted by an independent reader. If necessary, subheadings may be used for an orderly presentation. All figures and tables must be referred to in the text.

Discussion: The data should be interpreted concisely without repeating material already presented in the Results section. Speculation is permissible, but it must be well-founded, and discussion of the wider implications of the findings is encouraged. Conclusions derived from the study should be included in this section.

Acknowledgments: All funding sources should be credited in the Acknowledgments section. In addition, people who contributed to the work but who do not meet the criteria for authors should be listed along with their contributions.

References: References should be numbered in the order in which they appear in the text. Citing of unpublished results, personal

communications, conference abstracts, and theses in the reference list is not recommended but these sources may be mentioned in the text. In the reference list, cite the names of all authors when there are fifteen or fewer authors; if there are sixteen or more authors, list the first three followed by *et al.* Names of journals should be abbreviated in the style used in PubMed. Authors are responsible for the accuracy of the references. Examples are given below:

Example 1 (Sample journal reference):
Inagaki Y, Tang W, Zhang L, Du GH, Xu WF, Kokudo N. Novel aminopeptidase N (APN/CD13) inhibitor 24F can suppress invasion of hepatocellular carcinoma cells as well as angiogenesis. *Biosci Trends*. 2010; 4:56-60.

Example 2 (Sample journal reference with more than 15 authors):
Darby S, Hill D, Auvinen A, *et al.* Radon in homes and risk of lung cancer: Collaborative analysis of individual data from 13 European case-control studies. *BMJ*. 2005; 330:223.

Example 3 (Sample book reference):
Shalev AY. Post-traumatic stress disorder: Diagnosis, history and life course. In: *Post-traumatic Stress Disorder, Diagnosis, Management and Treatment* (Nutt DJ, Davidson JR, Zohar J, eds.). Martin Dunitz, London, UK, 2000; pp. 1-15.

Example 4 (Sample web page reference):
World Health Organization. The World Health Report 2008 – primary health care: Now more than ever. http://www.who.int/whr/2008/whr08_en.pdf (accessed September 23, 2010).

Tables: All tables should be prepared in Microsoft Word or Excel and should be arranged at the end of the manuscript after the References section. Please note that tables should not in image format. All tables should have a concise title and should be numbered consecutively with Arabic numerals. If necessary, additional information should be given below the table.

Figure Legend: The figure legend should be typed on a separate page of the main manuscript and should include a short title and explanation. The legend should be concise but comprehensive and should be understood without referring to the text. Symbols used in figures must be explained.

Figure Preparation: All figures should be clear and cited in numerical order in the text. Figures must fit a one- or two-column format on the journal page: 8.3 cm (3.3 in.) wide for a single column, 17.3 cm (6.8 in.) wide for a double column; maximum height: 24.0 cm (9.5 in.). Please make sure that artwork files are in an acceptable format (TIFF or JPEG) at minimum resolution (600 dpi for illustrations, graphs, and annotated artwork, and 300 dpi for micrographs and photographs). Please provide all figures as separate files. Please note that low-resolution images are one of the leading causes of article resubmission and schedule delays. All color figures will be reproduced in full color in the online edition of the journal at no cost to authors.

Units and Symbols: Units and symbols conforming to the International System of Units (SI) should be used for physicochemical quantities. Solidus notation (*e.g.* mg/kg, mg/mL, mol/mm²/min) should be used. Please refer to the SI Guide www.bipm.org/en/si/ for standard units.

Supplemental data: Supplemental data might be useful for supporting and enhancing your scientific research and Intractable & Rare Diseases Research accepts the submission of these materials which will be only published online alongside the electronic version of your article. Supplemental files (figures, tables, and other text materials) should be prepared according to the above guidelines, numbered in Arabic numerals (*e.g.*, Figure S1, Figure S2, and Table S1, Table S2) and referred to in the text. All figures and tables should have titles and legends. All figure legends, tables and supplemental text materials should be placed at the end of the paper. Please note all of these supplemental data should be provided at the time of initial submission and note that the editors reserve the right to limit the size and length of Supplemental Data.

5. Submission Checklist

The Submission Checklist will be useful during the final checking of a manuscript prior to sending it to Intractable & Rare Diseases Research for review. Please visit [Download Centre](#) and download the Submission Checklist file.

6. Online submission

Manuscripts should be submitted to Intractable & Rare Diseases Research online at <http://www.irdjournal.com>. The manuscript file should be smaller than 5 MB in size. If for any reason you are unable to submit a file online, please contact the Editorial Office by e-mail at office@irdjournal.com

7. Accepted manuscripts

Proofs: Galley proofs in PDF format will be sent to the corresponding author *via* e-mail. Corrections must be returned to the editor (office@irdjournal.com) within 3 working days.

Offprints: Authors will be provided with electronic offprints of their article. Paper offprints can be ordered at prices quoted on the order form that accompanies the proofs.

Page Charge: No page charges will be levied to author for the publication of their article except for reprints.

(As of February 2013)

Editorial and Head Office:

Pearl City Koishikawa 603
2-4-5 Kasuga, Bunkyo-ku
Tokyo 112-0003, Japan
Tel: +81-3-5840-9968
Fax: +81-3-5840-9969
E-mail: office@irdjournal.com

IRD R

Intractable & Rare Diseases Research



JOURNAL PUBLISHING AGREEMENT (JPA)

Manuscript No.:

Title:

Corresponding Author:

The International Advancement Center for Medicine & Health Research Co., Ltd. (IACMHR Co., Ltd.) is pleased to accept the above article for publication in Intractable & Rare Diseases Research. The International Research and Cooperation Association for Bio & Socio-Sciences Advancement (IRCA-BSSA) reserves all rights to the published article. Your written acceptance of this JOURNAL PUBLISHING AGREEMENT is required before the article can be published. Please read this form carefully and sign it if you agree to its terms. The signed JOURNAL PUBLISHING AGREEMENT should be sent to the Intractable & Rare Diseases Research office (Pearl City Koishikawa 603, 2-4-5 Kasuga, Bunkyo-ku, Tokyo 112-0003, Japan; E-mail: office@irdrjournal.com; Tel: +81-3-5840-9968; Fax: +81-3-5840-9969).

1. Authorship Criteria

As the corresponding author, I certify on behalf of all of the authors that:

- 1) The article is an original work and does not involve fraud, fabrication, or plagiarism.
- 2) The article has not been published previously and is not currently under consideration for publication elsewhere. If accepted by Intractable & Rare Diseases Research, the article will not be submitted for publication to any other journal.
- 3) The article contains no libelous or other unlawful statements and does not contain any materials that infringes upon individual privacy or proprietary rights or any statutory copyright.
- 4) I have obtained written permission from copyright owners for any excerpts from copyrighted works that are included and have credited the sources in my article.
- 5) All authors have made significant contributions to the study including the conception and design of this work, the analysis of the data, and the writing of the manuscript.
- 6) All authors have reviewed this manuscript and take responsibility for its content and approve its publication.
- 7) I have informed all of the authors of the terms of this publishing agreement and I am signing on their behalf as their agent.

2. Copyright Transfer Agreement

I hereby assign and transfer to IACMHR Co., Ltd. all exclusive rights of copyright ownership to the above work in the journal Intractable & Rare Diseases Research, including but not limited to the right 1) to publish, republish, derivate, distribute, transmit, sell, and otherwise use the work and other related material worldwide, in whole or in part, in all languages, in electronic, printed, or any other forms of media now known or hereafter developed and the right 2) to authorize or license third parties to do any of the above.

I understand that these exclusive rights will become the property of IACMHR Co., Ltd., from the date the article is accepted for publication in the journal Intractable & Rare Diseases Research. I also understand that IACMHR Co., Ltd. as a copyright owner has sole authority to license and permit reproductions of the article.

I understand that except for copyright, other proprietary rights related to the Work (e.g. patent or other rights to any process or procedure) shall be retained by the authors. To reproduce any text, figures, tables, or illustrations from this Work in future works of their own, the authors must obtain written permission from IACMHR Co., Ltd.; such permission cannot be unreasonably withheld by IACMHR Co., Ltd.

3. Conflict of Interest Disclosure

I confirm that all funding sources supporting the work and all institutions or people who contributed to the work but who do not meet the criteria for authors are acknowledged. I also confirm that all commercial affiliations, stock ownership, equity interests, or patent-licensing arrangements that could be considered to pose a financial conflict of interest in connection with the article have been disclosed.

Corresponding Author's Name (Signature):

Date:

Intractable & Rare Diseases Research (www.irdrjournal.com)

Pearl City Koishikawa 603, 2-4-5 Kasuga, Bunkyo-ku, Tokyo 112-0003, Japan; E-mail: office@irdrjournal.com; Tel: +81-3-5840-9968; Fax: +81-3-5840-9969

